Author:
Archer, Leanne

Title:
Suitability of TanDEM-X Data for Flood Inundation Modelling in Small Island Developing States

Suitability of TanDEM-X Data for Flood Inundation Modelling in Small Island Developing States

Leanne Archer

A dissertation submitted to the University of Bristol in accordance with the requirements for award of the degree of Master of Science by Research in Geographical Sciences in the Faculty of Science

School of Geographical Sciences

2018

Word count: 24,844

Abstract

Recent disastrous flood events across Small Island Developing States (SIDS) have reaffirmed the extraordinary risk of flooding in SIDS following extreme rainfall and tropical storms. Estimating flood hazard for disaster risk reduction policy requires simulations of flood extent and water depths from hydrodynamic models. In many SIDS these models have relied upon coarse, global spaceborne Digital Elevation Models (DEMs) such as the ~90m Shuttle Radar Topography Mission data. This has limited the capacity to adequately estimate flood hazard at the localised scale (~10m) suited to many SIDS catchments. Following the release of the global TanDEM-X DEM with a horizontal resolution of ~12m, there is an opportunity to assess whether the finer-resolution TanDEM-X can be utilised to improve flood hazard estimates in SIDS.

The first section of this thesis synthesises the relevant literature on flood risk in SIDS and how flood hazard has been simulated using previous DEMs. The results of this literature review indicate that there is a mismatch between flood risk and capacity to estimate flood hazard in SIDS. A key reason for this is a lack of adequate topographic data for input into a hydrodynamic model used to estimate flood hazard.

The second section of this thesis details and compares methods to process vegetation surface artefacts from the TanDEM-X DSM for input to a hydrodynamic model using the Ba catchment in Fiji as a test case. Seven TanDEM-X DTMs were generated by combining three methods that remove vegetation: Progressive Morphological Filtering and Image Classification of two TanDEM-X auxiliary datasets (Height Error Map and Amplitude). The seven TanDEM-X DTMs were input into the hydrodynamic model LISFLOOD-FP to compare modelled flood extent and water surface elevation with those simulated using the SRTM (v4) and Multi Error-Removed Improved-Terrain (MERIT) DEMs. A model based on an airborne LiDAR DTM was used as a benchmark. The results show that the unprocessed TanDEM-X DSM does not improve flood estimates over the MERIT DTM, but does improve flood estimates over the unprocessed SRTM DSM. The method to remove vegetation that combines Progressive Morphological Filtering with Image Classification of the TanDEM-X Amplitude map has the best fit to the LiDAR model flood extent and water surface elevation estimates in comparison to all other models. The findings indicate the potential for TanDEM-X to improve flood hazard estimates in SIDS when processed using the method developed in this thesis, which should be applied to other SIDS catchments and used to improve flood hazard estimates in flood risk estimations by policy makers.

Acknowledgements

I would like to thank my supervisors Jeff Neal, Paul Bates and Jo House for all their support this year, and to Laurence Hawker for comments on my publication and for your advice throughout the year. Thank you to Sarah Hemstock for helping with contacts in the appropriate Fijian organisations to access Fiji-specific datasets, Nicholas Rollings for providing the LiDAR data, and the Fiji Meteorological Office for access to the rainfall data and other useful information on the hydrology of Fiji. I received the MSc Studentship Award supported by the British Hydrological Society, JBA Trust and the Environment Agency, and funding by the University of Bristol Alumni Fund.

Author’s Declaration

I declare that the work in this dissertation was carried out in accordance with the requirements of the University's Regulations and Code of Practice for Research Degree Programmes and that it has not been submitted for any other academic award. Except where indicated by specific reference in the text, the work is the candidate's own work. Work done in collaboration with, or with the assistance of, others, is indicated as such. Any views expressed in the dissertation are those of the author.

SIGNED: .....DATE:

Contents Page

List of Figures

List of Tables

Chapter 1 –Introduction

Flood risk is a key concern for policy makers globally (Merz *et al*., 2010a), with global insured losses caused by flooding reaching 2.14 billion USD in 2017 (SwissRe, 2018). Flood risk is comprised of the probability of a hazard and the exposure and vulnerability of a population (UNISDR, 2015a). Modelling of flood risk has proliferated due to an improvement in the quality and resolution of relevant datasets (Ward *et al*., 2015), such that, numerous local and global initiatives have developed methodologies to model flood risk across different scales (e.g. Ward *et al*., 2015; EU Floods Directive, 2017) for current and future conditions (Alfieri *et al*., 2017). Flood hazard is often estimated using a hydrodynamic model and topographic data, mathematically approximating the propagation of a flood wave downstream, calculating water flow in-channel and across the floodplain when water flows out of bank (Bates *et al.,* 2005). Specifically, the estimation of flood hazard has become a data-rich science over the last two decades due to the dramatically increased availability of high-quality terrain data such as LiDAR - collected using airborne altimetry (Bates, 2012). LiDAR has improved the precision with which flood predictions can be made, due to a high vertical accuracy (5-20cm: Baltsavias, 1999) and horizontal resolution (1-2m), although acquisition incurs high economic cost (Sampson *et al*., 2016). Near-global openly-accessible datasets collected using spaceborne technologies such as the ~90m resolution Shuttle Radar Topography Mission (SRTM) have also unlocked the capacity to provide predictions of flood hazard globally where LiDAR data are unavailable (e.g. Sampson *et al*., 2015). SRTM is a ~90m DEM initially released in 2000, following acquisition using single-pass interferometry (Rabus *et al*., 2003), and was the most complete high-resolution DEM available until the release of the ~30m Advanced Spaceborne Thermal Emission and Reflection Radiometer (ASTER) DEM in 2009, offering coverage from 60°N-54°S (Sampson *et al*., 2016). SRTM has improved flood hazard information for insurance, disaster risk management, local authorities and planning in regions where open-access high resolution topographic data was previously unavailable at the global scale (Bates, 2012). Nonetheless, SRTM is

a Digital Surface Model (DSM), measuring surface objects such as buildings and vegetation, and so the data must be processed to a Digital Terrain Model (DTM) measuring the 'bare earth' surface before input into a hydrodynamic model. Surface artefacts, as well as other errors such as striping and speckle, mean SRTM has a high vertical error (~10m: Rodriguez *et al*., 2006), and many scholars have identified the need for a higher accuracy global DEM for the future improvement of global flood modelling (Schumann *et al*., 2014; Sampson *et al*., 2016).

1.1 The Case of Small Island Developing States

SIDS – a 37 island nation grouping identified at the 1992 UNFCCC Rio Conference – share a unique risk to hydro-meteorological hazards such as hurricanes and flooding, with a high relative exposure and vulnerability (Hay and Mimura, 2013). Reinforcing the formidability of risk experienced by SIDS, in 2017 the Caribbean experienced the worst hurricane season in recorded history and disaster aid relief provided by the Caribbean Catastrophe Risk Insurance Facility topped 54 million USD (NASA, 2017; SwissRe, 2018). In 2017, Hurricane Maria was the largest insured-loss event (32 billion USD) reported by SwissRe (2018), devastating several Caribbean SIDS. In 2016, Fiji - a Pacific SIDS that is the focus of this thesis - experienced the Southern Hemisphere's strongest ever-recorded cyclone, Cyclone Winston, resulting in losses equivalent to 20% of GDP and affecting 62% of the population (Government of Fiji, 2016).

Despite advances in global flood modelling, assessing flood risk in SIDS is critically disadvantaged by a lack of adequate data for detailed and accurate flood hazard assessments (UN, 2015). SIDS are typically data-sparse locations with a lack of accurate topographic data such as LiDAR, meaning coarser-scale (~90m) global datasets such as SRTM are relied upon (Gesch, 2009). This has limited the capacity to accurately model flood hazard in SIDS (see Simpson *et al*., 2009; Gesch, 2009; Albert *et al*., 2013), for three key reasons:

a) The scale of catchments and rivers in SIDS are small meaning a localised analysis is required.

b) Small-scale features important for accurate flow routing are not well-resolved by ~90m SRTM.

c) The vertical accuracy of SRTM (~10m) inhibits accurate model prediction in relation to the elevation range of many low-lying SIDS catchments.

Most SIDS catchments and rivers are small in comparison to catchments in other locations. Chandler *et al.,* (2014) define a catchment as 'small' if <1000km^2, meaning that most drainage basins in SIDS will be categorised as small as often whole islands are smaller than 1000km^2 – although Fiji's main island of Viti Levu has a total land surface of 10,389km^2 (Fiji Bureau of Statistics, 2018). For example, the estimated drainage area of the Ba River – the study site selected in this thesis on Fiji's main island Viti Levu - is 930km^2 (McGree *et al*., 2010). This is the fourth largest catchment in Viti Levu, with the largest catchment 2920km^2 (McGree et al., 2010). In comparison, the estimated drainage area of the River Po in Italy, defined as a 'large river' by (Schumann *et al*., 2010) and used as a study site for a number of published hydrology papers using remotely sensed data (e.g. Di Baldasserre *et al*., 2009) is 71,000km^2 (Montenari, 2012). River channels in SIDS also typically have a width less than 90m in many places, meaning SRTM is not able to resolve the river channel with a 90m resolution (Neal *et al*., 2012a). Furthermore, Sanders (2007) suggests no DEM can resolve a river channel smaller than twice the grid resolution. 69% of the Ba river in Fiji has a width <90m based on measurement using Google Earth™ imagery and 48% of Ba river has a width less than twice the resolution of SRTM at 90m, demonstrating the likelihood of a poorly-resolved river for the Ba catchment. Most river reaches in Viti Levu are also undetected by Yamazaki *et al*.'s (2014) width database for rivers, which uses the 90m SRTM and USGS Hydrosheds data (hydrographic data derived from SRTM: see Lehner *et al.,* 2008) as river reaches with a width <183m are not well represented, further demonstrating the inability to accurately resolve smaller river reaches using coarser (~90m) datasets. As river width is a basic geometric indicator used to estimate flow conveyance in hydrodynamic models, poorly-represented channel width will reduce flow calculation accuracy in the model (Yamazaki *et al*., 2014) and likely result in inaccurate flood extent and flow

velocity in-channel (Sanders, 2007). As a result, coarser datasets such as SRTM are unable to fully resolve the necessary information for accurate flood simulation in small catchments (<1000km^2).

When modelling at the local scale (<1000km^2), as is typically required in SIDS catchments, the representation of small-scale features (<10.5m: US Department of Agriculture, 1971) such as dykes and ditches in the DEM will also have an influence on floodplain flow (Horritt and Bates, 2001). Sanders (2007) demonstrates simulation differences due to the resolution of bridges between datasets in their study site, whereby a bridge between two roads is relatively well-resolved in the USGS National Elevation Dataset (NED) dataset up to 30m resolution, but best resolved in the LiDAR at 3m resolution. The bridge in the SRTM data at 30m and 90m is not visible, highlighting potential inability to resolve small-scale features which are likely to affect flow routing in the hydrodynamic model. Horritt and Bates (2001) suggest that the inclusion of small-scale (<10.5m) features improves calculation of floodplain water storage adjacent to the channel and flood wave travel times, thus improving flood extent accuracy.

Furthermore, the vertical accuracy of SRTM (~6.2m for islands: Rodriguez *et al*., 2006) and ASTER (10-25m: Fujisada *et al*., 2012) is larger than the elevation range of many SIDS floodplains. Vertical accuracy refers to the difference in observed and modelled elevation height (Rizzoli *et al*., 2017). For example, the elevation range of the study site in this thesis - Ba catchment, Fiji - is 127m, and the majority of the floodplain has an elevation range <3m. Furthermore, the vertical error of SRTM and ASTER is greater than the amplitude of most flood waves (typically <2m for SIDS), particularly for rivers in Fiji where average flood wave amplitudes range from 1-4m (Yeo *et al*., 2007). Mason *et al*., (2015) suggest that the more accurate a DEM, the more accurate the flood estimation, highlighting the importance of a DEM with a high vertical accuracy. Therefore, these key reasons demonstrate why SRTM at ~90m is unsuitably matched with the scale of analysis necessary for SIDS. It is clear that

a DEM with higher spatial resolution and vertical accuracy than SRTM is required to provide improved flood estimates for SIDS.

1.2 The TanDEM-X Mission: An Opportunity?

Following the release of Digital Elevation Model TanDEM-X by the German Aerospace Center in 2016, this thesis aims to provide the first application of TanDEM-X into a hydrodynamic model, and specifically in a SIDS context. The TanDEM-X DEM has a ~12m resolution and a reported vertical error of <2m (Wessel *et al*., 2018), following acquisition using an X-band bistatic Interferometric Synthetic Aperture Radar from 2010-2015 (Rizzoli *et al*., 2017). Scholars such as Yan *et al*., (2015) and Mason *et al*., (2015; 2016) have suggested that the finer resolution and lower vertical error is likely to improve flood estimates, although no published research has yet tested this hypothesis. As this is a critical issue for SIDS, it is important to determine the potential for TanDEM-X in this context. However, because TanDEM-X is a DSM, pre-processing TanDEM-X to a Digital Terrain Model (DTM) is necessary for input into a hydrodynamic model. Therefore, this thesis also aims to identify a suitable methodology for processing TanDEM-X to a DTM.

1.3 Thesis structure

The structure of this thesis is as follows. In Chapter 2, a succinct review of the literature regarding the concept of flood risk and flood risk specific to SIDS is conducted, providing a justification for the focus on SIDS in this thesis. Literature on hydrodynamic models and the use of DEMs in hydrodynamic modelling is outlined, followed by the key research describing processing methods for DEM error reduction and DTM processing. This literature review will inform the reasons for conducting this research, as well as providing an understanding of the key assumptions made throughout Chapter 2 and informing the development of the methodology used in this thesis. In Chapter 3 (a paper chapter published by *Water Resources Research*) two key research questions are investigated:

1) How can artefacts be removed from TanDEM-X to create a suitable Digital Terrain Model for input into a hydrodynamic model?
2) Are flood estimates improved using TanDEM-X in comparison to SRTM and MERIT?

Chapter 3 outlines the methodology developed to process TanDEM-X from a DSM to a DTM, as well as discussing the key hydrodynamic model results comparing unprocessed TanDEM-X DSM and the resultant DTMs with LiDAR, SRTM and MERIT models. The results determine the candidate closest to the LiDAR model as the most suitable – as the LiDAR model is considered as an appropriate benchmark for this study in absence of ground truth information. Finally, the thesis concludes in Chapter 4 by relating the work detailed in Chapter 3 to the wider context, noting the limitations of the research and outlining the potential for further research within the scientific community and SIDS.

Chapter 2 – Literature Review

In this thesis, a newly-released DEM TanDEM-X is applied in a hydrodynamic modelling test case, with the aim of identifying the potential to improve flood hazard estimates in a SIDS context in comparison to existing datasets LiDAR, SRTM and MERIT. To inform this analysis, and to justify and understand the importance of the results in this thesis, there must be a wider understanding of the context in which this thesis is situated within the literature and wider risk management community. Resultantly, the purpose of this literature review is to synthesise and identify the key themes within the literature, starting with the overarching topic of flood risk, and the assumptions made when defining risk as outlined by the UNISDR (2015a) and its individual components. This chapter acknowledges this widely-encompassing topic, before narrowing the lens on one key component of flood risk – flood hazard. Furthermore, as one of the research questions addressed in this thesis aims to understand how TanDEM-X might be processed for input into a hydrodynamic model for such flood hazard estimation, this literature review will evaluate how DEMs have been utilised in flood hazard estimation, as well as associated errors and pre-processing methods. This synthesis of information is used to inform and justify the methodology for TanDEM-X vegetation processing outlined in Chapter 3.

In Section 2.1 research regarding risk, and specifically flood risk is discussed, considering the three key components: hazard, exposure and vulnerability. Following this, flood risk is specifically described in the context of SIDS, providing a justification for the focus on these territories in this thesis. Section 2.1 concludes that improving estimation of flood hazard is an important first step for improving flood risk assessment in SIDS. Accordingly, Section 2.2 focuses on the key methodology used to estimate flood hazard in the literature and this thesis: hydrodynamic modelling. Hydrodynamic modelling, model types and the hydrodynamic model used in this thesis (LISFLOOD-FP are described. As topographic data is a key hydrodynamic model input (Bates, 2012) and the focus of this thesis, Section 2.3 discusses how the proliferation of DEMs has improved the

capabilities of hydrodynamic modelling, and outlines the key DEM products used in the literature. Section 2.4 outlines key errors in DEMs, and how DEMs have previously been processed from a Digital Surface Model to a Digital Terrain Model for suitable use in a hydrodynamic model, before identifying potential methods for developing a suitable method for processing vegetation artefacts in TanDEM-X.

2.1 Flood Risk

Flooding is generally defined by Smith (2013:309) as 'a temporary state existing when a body of water rises to inundate land not normally submerged'. Flooding is one of the world's most widespread hazards, affecting most countries worldwide (Blaikie *et al*., 1994). Globally, flood events accounted for 50.5% of disasters between 2006-2015, affecting 36.8% of the average annual population affected by disasters in the same period (Guha-Sapir *et al*., 2017). Different types of floods including riverine, coastal and flash floods (Kron, 2005) affect areas with differing frequencies and magnitudes.

The UNISDR (2015a:26) describes disaster risk as 'a function of the severity and frequency of the hazard, of the numbers of people and assets exposed to the hazard, and of their vulnerability or susceptibility to damage'. A disaster refers to an event whereby a hazard adversely affects a vulnerable population, resulting in loss of life and excessive damage to buildings and infrastructure (Smith, 2013). A succinct visualisation adopted by the UNISDR (2015a) and the IPCC (2012) Special Report on Managing the Risks of Extreme Events and Disasters to Advance Climate Change Adaptation to understand disaster and climate change risk is:

Risk = Probability of a hazard x Vulnerability x Exposure

Apel *et al*., (2009) specifically define flood risk as the hazard (expressed as the return period, flood extent and inundation depth) combined with human and asset exposure, and vulnerability as

susceptibility to flood damage. Jonkman *et al*., (2008) and Thieken *et al*., (2005) reiterate this by suggesting that to understand flood risk, one must determine both the probability of the flood hazard and the consequences. Two key models have been used to describe disaster risk, notably the Pressure and Release model first outlined by Blaikie *et al*., (1994), which demonstrates the interaction between the hazard, and several socially-constructed drivers leading to the underlying vulnerability of a population and the Source-Pathway-Receptor model, created by DETR (2000), which models how a hazard (source) meets the vulnerable population (receptor) through a pathway of exposure (Sayers *et al*., 2002).

2.1.1 The Changing Discourse on Flood Risk

In recent years, the discourse on flood risk has changed in two key ways. Firstly, scholars have suggested that flood risk is increasing as the climate changes and human populations grow, become wealthier and migrate to zones with higher flood hazard (Merz et al., 2010a). Secondly, in tandem with the increasing number of flood disasters, the discourse on how to assess and manage flood risk has changed from a focus on technocratic modification approaches to an emphasis on preparedness and holistic management (Apel *et al*., 2009).

Regarding the issue of increasing flood risk, it is apparent in the literature that flood risk is changing, and in most regions increasing (Merz *et al*., 2010a). Of the 3455 floods reported from 1980-2011 globally, there is an upward trend in the number of flood disasters reported (Munich Re, 2016). As well as an increase in disaster reporting, two main explanatory variables are presented. Firstly, anthropogenic warming is identified as a potential reason for an increase and future acceleration in the number of extreme events, although the IPCC expresses low confidence in the attribution of anthropogenic climate change to flood events or trends (Cisneros *et al*., 2014). To attribute this trend to climate change would require the detection of all the drivers of this trend and their contributions. This is not usually possible due to the number of potential human and climatic

influences. Secondly, it is widely accepted that an increase in exposure of people and infrastructure to floods has increased the number of flood disasters, particularly in low-lying floodplains in developing countries (Merz *et al*., 2010a; Hallegatte *et al*., 2016; Eckstein *et al*., 2017). For example, in Fiji – the SIDS study site selected in this thesis - 54% of the population are urban residents, and the flood-prone, low-lying town of Nadi is growing by 2.5% per annum due to tourism sector growth (Government of Fiji, 2017), directly increasing the exposure of persons and assets and increasing the propensity for loss.

Disaster management follows two main pathways: the modification of an at-risk area to a specific hazard as a management tool or the holistic management of the overall flood risk by addressing the underlying stressors which increase the propensity of a population to be adversely affected by the hazard (Blaikie *et al*., 1994). Previously, especially in developed countries, emphasis on modifying the hazard has dominated, investing in hard engineering solutions such as levees which facilitate the continuation of floodplain development (Jonkman *et al*., 2003). However, a paradigm shift in emphasis from modification to holistic management of the hazard has been observed, partly out of critique for the over-emphasis on the hazard with the modification approach, and the acknowledgement that the modification strategy is not reducing disaster loss trends (Merz *et al*., 2010a). The successor to the Hyogo Framework - the Sendai Framework 2015-2030 - identifies the need to understand risk as a multi-dimensional factor of the hazard, vulnerability, exposure of assets and people and the capacity to cope (UNISDR, 2015b). Preparedness is emphasised as a key component of this risk management strategy and a key motivation for the move from a focus on modification to holistic management. Preparedness includes the presence of adequate early warning and risk identification systems that enhance response and protection measures to a flood hazard (UNISDR, 2012). Furthermore, there is a prominent need to address the underlying factors that increase vulnerability to stressors within society, by facilitating sustainable and inclusive

development which leads to improved resilience to the flood hazard (Mileti and Gailus, 2005; Egorova *et al.,* 2008).

To better understand the concept of flood risk, trends and management, it is important to also consider the individual components that influence risk. As one main objective of this thesis is to identify whether improved estimates of flood hazard can be attained in SIDS using TanDEM-X, flood hazard is considered in detail, before briefly summarising exposure and vulnerability.

2.1.2 Hazard

Fluvial hazards are demarcated by the magnitude of the event for a given probability (Kron, 2005). The probability of an event occurring in a year is often described as a 'return-period' (Smith, 2013), for example the depth of the flood water in metres for a given return period. A return period event refers to the inverse probability that an event with be exceeded in a given year (Bates, 2005). For example, a 100-year return period event will have a 1% probability of occurrence in a year. It is widely acknowledged that inundation depth influences risk, as the greater the depth, the greater the damage potential (Thieken *et al*., 2005). Less often considered however, are the velocity, duration, lag time and quality of the floodwater. This is largely because flood policies do not specify them in their directives, as these variables are more difficult to simulate and are therefore less certain. For example, the EU Floods Directive (2017) requires the depths of medium-likelihood and extreme-likelihood events. Yet it is logical that all these characteristics of an event will influence the damage potential (Merz *et al*., 2010b).

2.1.2.1 Estimating the Flood Hazard

Policy makers are often interested in extreme flood events that pose the largest threat to the population (Blaikie *et al*., 1994). Extreme event analysis calculates the return period of a flood event by analysing the statistical spread of past events (Smith, 2013). Data on extreme events are usually

taken from flow gauge data along a river. A distribution is then fitted to the annual maximum flows from the gauge data to generate peak flows for a specified return period. However, using gauge data can be problematic, and gauge networks are in decline globally (Buchele *et al*., 2006). Extreme magnitude events, e.g. a 100-year return period, are unlikely to have been recorded as gauge data often has a limited time coverage (typically 40-50 years) meaning an extreme event with a low probability of return may not have occurred within the recorded time (Reed, 2002). Data for high-flow events may also not be available due to equipment failure or inadequate capture, and incomplete time-series are especially common in data-sparse catchments such as in Fiji (Buchele *et al*., 2006). For example, Yeo *et al*., (2007) report that flow gauges along Fijian rivers have been known to wash away at high flows, and information on flood height or extent were not recorded during recent events (McAneney *et al*., 2017). Limited information on these extreme events due to incomplete or missed data thus skew the statistical distribution of events to lower-flow events, making return period calculation more uncertain (Salinas *et al*., 2013). Extreme flows of interest for flood event simulation are also often less accurate because an extrapolation from the observed flows is required. Thus, estimating flood discharges in ungauged or poorly-gauged basins is a fundamental challenge for measuring flood hazard (Salinas *et al*., 2013: Smith *et al*., 2015). Where inadequate gauge data exists, key methods for peak flow simulation include: Regional Flood Frequency Analysis and rainfall-runoff models whereby rainfall data is cascaded through a model to estimate flow (Blöschl *et al*., 2013). Methods to conduct a Regional Flood Frequency Analysis are summarised here.

A Regional Flood Frequency Analysis is often conducted to determine the probability of an event with a particular peak flow discharge in comparison to the mean annual flood for hydrologically-similar catchments (Smith *et al*., 2015). This technique assumes that catchments can be 'grouped' based on similar characteristics such as topography, climate, geology and land use, whereby these

conditions create a similar hydrological response (Salinas *et al*., 2013). Typically, catchments are grouped statistically using methods such as cluster analysis (Rao and Srinivas, 2006), regression (Laaha and Blöschl, 2006) and regions of influence (Burn, 1990). Smith *et al*., (2015) pools catchments using a hybrid-clustering approach, distributing Global Runoff Data Centre flow data by Koppen-Geiger classification to create homogenously-pooled regions. Once regions have been created, a number of methods can be utilised to determine the flood size, based on the flow information in the area of interest (Salinas *et al*., 2013). Peak flow information for a particular return period flood event can be calculated using the index flood method (Dalrymple, 1960; Meigh *et al*., 1997; Zaman *et al*., 2012), regression (Gupta et al., 1994) and geostatistical methods (Merz and Blöschl, 2005). Smith *et al*., (2015) use the index flood method, whereby the Mean Annual Flood is calculated using flow data within the region of interest, before scaling the flood to a specified return period using a growth curve. The Regional Flood Frequency Analysis method detailed in Smith *et al*., (2015) was adopted in this thesis, as the author had access to the underlying code and the method was utilised in the most recent flood risk assessment for Fiji (see Government of Fiji, 2017).

To date, hydrodynamic modelling has been the most useful and widely-used method for simulating flood inundation, taking available or predicted extreme event information and modelling how the flood event translates across space (Takeuchi, 2001). Plate (2002) suggests that the creation of flood hazard maps, identifying regions potentially affected by a flood, is the most appropriate first step in identifying flood risk. However, Buchele *et al*., (2006) and Merz *et al*., (2010b) have suggested that this may not give a complete identification of flood hazard, as other factors that will affect the flood are not considered such as water quality. As a main tool used in this thesis, flood modelling is discussed in more detail in Section 2.2.

2.1.3 Exposure and Vulnerability

Although flood hazard is of particular interest to this thesis, it is important to understand the other key factors influencing flood risk: exposure and vulnerability. Both are complex concepts, with bodies of literature dedicated to the discussion and definition of the concepts within disaster risk and climate change discourse (UNISDR, 2015a). The generally accepted definitions and key points regarding both topics are broadly summarised.

Exposure is often defined as the presence of people or assets located in a hazardous area (UNISDR, 2017), and is sometimes categorised within the concept of vulnerability (Blaikie *et al*., 1994; Smith, 2013). However, it is considered separately in this thesis following the widely-adopted definition of disaster risk by the UNISDR (2015a) which presents exposure as a defining feature. The UNISDR (2015a) argue that exposure and vulnerability are not synonymous, as exposure to a hazard does not mean you are vulnerable (Cardona *et al*., 2012). Exposure and hazard are also distinct because if there is no exposed population or assets, there is no risk.

Broadly, there are two approaches to estimating exposure: population and asset exposure (Cardona *et al*., 2012). To quantify population exposure, population density data are often used to estimate the number of people exposed to an event (Apel *et al*., 2009). The estimated population exposed is then divided by the country population to create an exposure index value for each country. For example, exposure is calculated as an indicator in the global risk index 'WorldRiskIndex' compiled by Bündis Entwicklung Hilft, (2017) by calculating the probability of population exposure based on the population exposed and the probability and frequency of a particular hazard. Asset exposure estimates the value or number of assets, such as buildings and infrastructure, that are exposed to an event (Jonkman *et al*., 2003). Asset exposure is the more commonly-used metric because it can be

easily quantified and is regularly collected by insurance companies. Merz *et al*., (2010b) suggests that to fully assess exposure, ideally several variables would be assessed in conjunction to holistically estimate exposure. It is recognised that these methods of defining exposure are not necessarily robust for all types of hazards, and that the scale and resolution of available datasets can significantly limit detailed exposure estimates (Apel *et al*., 2009; Merz *et al*., 2010b).

Vulnerability is a concept that has been widely debated in the literature (Cutter, 1996). Disciplines in engineering, disaster management, climate science, ecology and sociology all have differing criteria as to what vulnerability encompasses (Adger, 2006). In the field of disaster management, it is generally agreed that vulnerability broadly describes a set of physical, social, economic or environmental factors or conditions which increase the propensity of an individual to be negatively impacted by a hazard (UNISDR, 2017). The IPCC (2012) also underline the importance of viewing the concept of vulnerability as dynamic over space and time, being both hazard-specific and representative of the underlying social system. The complexity of vulnerability has been discussed by many scholars to better categorise and understand vulnerability to hazards and is frequently conceptualised as a product of a mix of 'physical' and 'social' factors that encompass the conditions outlined in the UNISDR (2017) definition (Cutter, 1996; Brooks, 2003; Adger, 2006; Füssell and Klein, 2006; Cardona *et al*., 2012). These categorisations can be useful when trying to understand how different factors drive vulnerability in a place-specific capacity (Cardona *et al*., 2012). Cutter (1996) notably distinguish 'biophysical' and 'social' vulnerability. Biophysical vulnerability is usually described as both the nature of the hazard and the physical features of a place or environment that increase vulnerability, including geographic location and the built environment (Brooks, 2003). Social vulnerability aims to describe how the population vulnerability in these environments are further differentiated by demographics, social status and individual conditions (Cutter, 1996).

Vulnerability is perhaps the most difficult variable of risk to estimate (Adger, 2006). Social vulnerability is difficult to quantify, and data is not always available, so often proxy indicators may be used to infer a population's vulnerability (UNISDR, 2012). One widely-used example is Cutter *et al*.'s (2003) Social Vulnerability Index which combines a number of social and demographic indicators in an attempt to describe the social vulnerability of a place, considering the underlying social systems as well as individual conditions.

It is beyond doubt that all three interlinking and complex concepts hazard, exposure and vulnerability, as well as the overarching risk, could be discussed in far greater detail than in the capacity of this thesis, dominating the scope in many IPCC and UNISDR reports. Yet, it is also important to contextualise these broad encompassing theories in the frame of SIDS, to provide a more holistic understanding of why SIDS have such a high flood risk, justifying the focus in this thesis.

2.1.4 Flood Risk in Small Island Developing States

SIDS are unduly affected by flood risk in comparison to the rest of the world (UN, 2015). Specifically, the combination of high hazard frequency and intensity, large exposure in relation to size, and underlying vulnerability propel disaster risk (UNISDR, 2015a).

Firstly, SIDS are disproportionately exposed to hydro-meteorological hazards, accounting for 75% of all reported disasters between 1970-2006 (Julca and Paddison, 2010). Within the top fifteen countries most exposed to natural disasters worldwide, eight are SIDS because of the high hazard frequency and exposure in relation to population size and geographical area (Radtke *et al*., 2017). This suggests SIDS are frequently affected by flood hazards. The formidable hurricane season

experienced by Caribbean SIDS in 2017 reinforces this premise, as well as underlining key exposure and vulnerabilities within the region (NASA, 2017).

The small size of SIDS also means that cyclone storm tracks leading to heavy rainfall can span entire islands, so a large percentage of the total population and assets are exposed to each event (Barnett and Adger, 2003). This is reflected in Annual Average Losses for all hazards globally which are highest in SIDS as a percentage of GDP (UNISDR, 2015a). Annual Average Losses for all hazards across SIDS (of which the majority are associated with extreme rainfall and cyclones/hurricanes) are equivalent to 10% of capital investment and 20% of government social spending, in comparison to 1.2% and 1% in Europe. This depicts the high exposure of assets as a proportion of the total capital stock in SIDS (Barnett, 2001).

Moreover, SIDS such as Fiji have complex and widespread vulnerabilities that make flood risk greater than areas with similar flood hazard probabilities (Nurse *et al*., 2014). Perhaps most notably, Briguglio (1995) provided an explanation for this vulnerability which encompasses a range of biophysical and social factors that give rise to vulnerability. As well as their high exposure to flood events, SIDS have several qualities, labelled as 'Small Island Handicaps' that are conducive to the increased vulnerability to flooding. Biophysical 'handicaps' include their isolated location, small size and low-lying elevations. Limited access to international markets, narrow economic base and large urban populations can be classed as social 'handicaps' (Pelling and Uitto, 2001). This is echoed by Nurse *et al*.'s (2014) IPCC AR4 'Small Islands' chapter, outlining the complex interaction between a high hazard exposure and a unique set of vulnerabilities which cannot be easily explained by simply combining one hazard and one particular vulnerability.

These features of SIDS thus give rise to an extraordinarily high risk to flooding (UNISDR, 2015a; UN, 2015; Hallegatte *et al*., 2016; Eckstein *et al*., 2017). Most recently, Bündis Entwicklung Hilft's (2017) WorldRiskIndex report identifies the need to focus on disaster risk and the future impacts of climate change with particular reference to small island nations. They recognise the overwhelming exposure SIDS face to both quick-onset extreme events, and slow-onset hazards (e.g. ocean acidification or rising sea levels) which combine with underlying vulnerabilities to further exacerbate risk in these locations. Nevertheless, there is little research that provides quantitative flood risk assessments because of the lack of appropriate data (Bettencourt *et al.,* 2006). SIDS are predominantly data-sparse locations, meaning flood risk assessment has relied upon use of global datasets for risk assessment. As Plate (2002) and Cardona *et al*., (2012) suggest, estimating flood hazard is a useful first step in determining the risk. Thus, if flood hazard estimation can be improved, a key element of flood risk assessment can be improved. DEM quality is a key step to improving flood hazard estimation, so this thesis focuses on the application of a new DEM TanDEM-X, to determine whether this dataset has the potential to improve flood hazard estimates in a SIDS catchment.

The next section of this chapter will focus on synthesising the literature on how flood hazard will be estimated in this thesis – using the hydrodynamic model LISFLOOD-FP - before summarising the literature on using DEMs in hydrodynamic modelling and how these datasets can be appropriately processed. This literature is used to inform the methodology for processing TanDEM-X in Chapter 3.

2.2 Flood Modelling

As highlighted in Section 2.1, a key component in estimating flood risk is estimating the flood hazard (Bates *et al*., 2000). This section of the literature review aims to broadly outline how hydrodynamic models are used to estimate flood hazard, providing an overview of the different model approaches before narrowing the focus to the LISFLOOD-FP model used in this thesis.

Flood models, often termed hydrodynamic models, are defined as predictive models used to mathematically estimate flood flows, inundation extents and depths based on a set of parameters (Bates and De Roo, 2000).

Hydrodynamic models primarily need three key inputs (Hunter *et al*., 2007):

1) A grid representing the topographic relief of the channel and the floodplain e.g. a Digital Terrain Model.
2) A value of resistance to flow for each grid cell e.g. Manning's coefficient value.
3) Boundary flow or level data in and out of the model domain e.g. flow time-series.

However, in many data-sparse regions such as SIDS, detailed and accurate information on these inputs are not available (Komi *et al*., 2017). Data-sparse areas are typically defined as areas whereby a lack of detailed topographic data, flow data or ground truth information exists (Schumann et al., 2014). Methods have been created to overcome issues with data-sparsity that are fundamentally useful for this thesis and are discussed further in Section 2.2.5.

Hydrodynamic models use a set of mathematical functions to calculate fluid flows. Most hydrodynamic models solve either the complete set, or a variation of, the Saint Venant equations, depending on the number of dimensions modelled (Bates *et al*., 2005). Discussed in more detail in Section 2.2.2, one-dimensional (1D) approaches model flow of water longitudinally. Two-dimensional (2D) approaches model flow longitudinally, as well as calculating lateral flows. Three-dimensional (3D) approaches simulate water longitudinally, laterally and vertically. Only in the event of simulating 3D turbulent flow in a hydrodynamic model does the entire Reynolds-Averaged Navier-Stokes equation need solving. For a full mathematical explanation, see Ingham and Ma (2005) or Shaw *et al*., (2011). More often however, either the 1D or 2D Saint Venant equations are used to

simulate 1D or 2D flows (Bates *et al*., 2005). Sometimes referred to as Shallow Water Equations (SWE), these equations act as a numerical representation of a flood wave attenuating downstream, following the basic premise that flood waves are a few metres high, and are therefore a 'shallow water phenomenon' (Bates *et al*., 2014:840).

2.2.1 The Saint Venant Equations

The 1D Saint Venant equations consider the conservation of mass and momentum on a 1D channel flow (Ingham and Ma, 2005). Equation 1 below represents the continuity equation which ensures the conservation of water volume, and Equation 2 represents the conservation of momentum. These equations can be used to calculate the velocity and depth at any cross-section along a river channel, flowing in a single direction (*x*) (Bates *et al*., 2005). Often, to reduce computational demand, three simpler versions of the momentum equation are implemented, ignoring components of the second equation. Kinematic waves only include the friction and bed slopes, meaning it is difficult to simulate backwatering adequately (Bates *et al*., 2013). Diffusive waves ignore local and convection acceleration, and local inertial waves ignore convective acceleration.

$$\frac{\partial A}{\partial t} = -\frac{\partial Q}{\partial x} \qquad \textit{Equation 1}$$

$$\underbrace{\frac{\partial Q}{\partial t}}_{\text{Local acceleration}} + \underbrace{\frac{\partial\left(\frac{Q^2}{A}\right)}{\partial x}}_{\text{Convective acceleration}} + \underbrace{gA\frac{\partial h}{\partial x}}_{\text{Bed slope term}} - \underbrace{gA\left(S_f - S_o\right)}_{\text{Friction term}} = 0 \quad \textit{Equation 2}$$

Q is the volumetric flow rate, *A* the area of the cross section, *h* the water depth, *z* the bed elevation, *g* is gravity, *n* the Manning's coefficient, S_f is the water slope, S_o is the channel bed slope, and *t* is time. *x* is the distance in the *x* Cartesian direction, where *y* can be substituted when calculating the *y*-distance in the 2D equations. When considering 2D flood flows, the 2D Saint Venant Equation is applied (Bates *et al*., 2005). The 2D Saint Venant equations calculate depth-averaged velocities in the *x* and *y* Cartesian directions also considering local acceleration, convective acceleration, slope,

pressure and friction. Equation 2 is constructed of: local acceleration, convective acceleration, water slope or pressure term and friction term respectively.

1D and 2D models have been the most widely-applied models, as 3D models have a high computational demand (Horritt and Bates, 2001). Although computational capacity has dramatically increased in the last two decades, 3D model computations are still intensive relative to computational power and are not significantly more skilful based on typical input and validation data uncertainties (Hunter *et al*., 2007). Often when considering which model type is most suitable, the user must determine the scale, computational power and the information required to determine which model produces the most suitable outputs for the intended purpose against available validation data using the least computational power (Bates *et al*., 2005). There are many different commercial hydrodynamic modelling packages (see Neelz and Pender, 2013). As this thesis uses LISFLOOD-FP, other packages are briefly mentioned, but LISFLOOD-FP is described in more detail in Section 2.2.5.

2.2.2 1D Models

Bates and De Roo (2000) describe 1D models as the minimum required to simulate the propagation of a flood wave along the cross-section of a river, as more simplistic planar surface approximations do not capture dynamic flood wave behaviour adequately. 1D models are primarily useful for in-bank flow as they provide a one-dimensional representation of a flood wave attenuating downstream. However, most 1D packages solve floodplain flow by using an extended cross section to represent the floodplain and channel together, or by treating the floodplain as a separate storage volume when water flows out of bank, whereby during each time-step water flows in and out of a floodplain reservoir based on surface height gradients between cells (Bates *et al*., 2010). Despite the relative simplicity of the 1D model, Horritt and Bates (2002) detail similar flood event simulations when comparing the 1D HEC-RAS model with the 2D TELEMAC-2D model on the River Severn, indicating that 1D models can provide a similar level of simulation skill in certain cases.

Due to their low computational requirements 1D models have been the most operationalised to date, providing a framework for several flood modelling packages such as HEC-RAS and MIKE11 (Castellarin *et al*., 2009). The 1D HEC-RAS model has been used to estimate inundation extents for the Waidina tributary on the Rewa river in Fiji (Rathnayake *et al*., 2015); one of two published journal papers outlining flood modelling in Fiji (Yeo *et al*., 2007).

2.2.3 2D Models

Although they are more computationally intensive, studies that are particularly interested in floodplain water depths, or areas where there are extensive floodplain flows, are best suited to 2D models such as TELEMAC, LISFLOOD-FP and TUFLOW (Neelz and Pender, 2013). This is because 2D models include the calculation of depth-averaged velocities in the 2D SWE which allows the consideration of changing inundation extents across a floodplain over time (Horritt and Bates, 2001). For example, Wilson *et al*., (2007) conduct the first large-scale 2D model of seasonal flooding in the Amazon, which although computationally expensive, was justified because an in-depth view of the dynamic flood processes over time was required.

2.2.4 3D Models

Despite the strengths of reduced-complexity hydrodynamic models such as the 1D and 2D approximations outlined, if the aim of the model is to accurately simulate a flood event, then 3D may have the most realistic flow simulation; although this is difficult to demonstrate conclusively in practice (Lane *et al*., 1999). Flood flows are inherently a three-dimensional phenomenon, variable over time and dominated by turbulence (Ingham and Ma, 2005). Thus, the models producing the most valid flow estimations are likely those that include these factors. A small number of studies have used full 3D derivations of the Reynold's-Averaged Navier-Stokes equation, including Stoesser *et al*., (2003) whom model a 3.5km stretch of the Rhine River, Germany. Dye tracing experiments

showed that the model could simulate turbulent flows and varying velocity in the channel. Other examples of 3D model codes implemented in studies include CFX, FLUENT and PHOENIX (Castellarin *et al*., 2009).

Several factors currently constrain the widespread application of 3D modelling (Bates *et al*., 2005). As well as the computational power required which inhibits most users, data used to parameterise and validate the models are not often detailed enough to justify the use of 3D models, with no additional benefit over 2D models unless flume data is available (Lane *et al*., 1999). 3D models may become more feasible in the future as computational power and the quality of boundary condition and validation data improves (Bates *et al*., 2005). Still, Bates and De Roo (2000) and Bates *et al*., (2005) highlight that the most suitable hydrodynamic models are those that provide the required flood information in the simplest form, so it will be important to consider whether 3D models can provide more information than the current models to justify the increased complexity.

2.2.5 LISFLOOD-FP

Developed from the viewpoint that a model providing the required flood information in the simplest form is preferable as is described in Occam's Razor, LISFLOOD-FP was created to provide accurate flood inundation simulations using a simple and logical process (Bates and De Roo, 2000). This section reviews the functionality of 1D-2D models with particular reference to LISFLOOD-FP, as well as providing a justification for choosing this model. This thesis uses the 1D-2D subgrid variant of the LISFLOOD-FP model (Neal *et al*., 2012a), whereby both a 1D and 2D solver are used to simulate channel and floodplain flow (Bates *et al*., 2006).

First developed and described by Bates and De Roo (2000), LISFLOOD-FP is a raster-based hydrodynamic model that has been continuously developed since its original simple storage model

(Bates *et al*., 2010). 1D, 2D and 1D-2D solvers have been developed for use within the model, dependent on the needs of the user. The user-manual gives details on the different solvers, including the kinematic, adaptive, diffusive and sub-grid solvers, which solve various simplifications of the SWE and have been developed over time since the Bates and De Roo's (2000) initial release (see Bates *et al*., 2013). The LISFLOOD-FP model solvers have been widely implemented and validated in the flood modelling community (Hunter *et al*., 2008; Neal et al., 2012b). Most recently, the inertial formulation of LISFLOOD-FP has been used as the base model for the global flood model developed by Sampson *et al*., (2015).

LISFLOOD-FP is predominantly implemented as a 1D-2D model (Bates *et al*., 2013). First described by Cunge *et al*., (1980), the strengths of 1D and 2D models are combined to improve inundation prediction, whilst still prioritising the simplest method. In-bank flows are calculated using the 1D equations. Once bankfull height is exceeded, a 2D model solver is used to calculate floodplain flow (Bates *et al*., 2006). This model structure has the benefit of the reduced computational power needed to solve the 1D component when water flow is in-bank, whilst utilising the strengths of the 2D model for areas of the river that exceed the channel confines, allowing a more accurate simulation of floodplain flows in comparison to the storage-volume approach (Neal *et al*., 2012a).

Within LISFLOOD-FP, a solver of relevance to this thesis is the 'sub-grid' model, developed by Neal *et al*., (2012a). This solver takes a 1D-2D approach and is useful for modelling in data-sparse catchments where most input datasets are derived from global-scale DEMs discussed in Section 2.3. The key feature of this solver is that river channels smaller than the DEM resolution can be included in the model simulation (Komi *et al*., 2017), and is adopted in the global flood model described in Sampson *et al*., (2015) to account for data-sparse catchments without detailed channel information. In Neal *et al*.'s (2012a) comparison of four solvers to simulate flows along the River Niger, Mali, the

sub-grid model significantly improved the accuracy of simulated water depths, flood wave timings and inundation extents. The main assumption is that increased connectivity of small river channels over floodplains provides an improved representation of the flow dynamics. Fernández *et al*., (2016) used the sub-grid LISFLOOD-FP solver to simulate flooding on the data-sparse Logone floodplain, Cameroon, and found agreement with Neal *et al*.'s (2012a) conclusion.

There are four key justifications for the use of the subgrid LISFLOOD-FP solver in this thesis. Firstly, SIDS are inherently data-sparse, lacking channel information such as bed elevation and widths meaning remotely-sensed data is relied upon. Areas of the river cross-section modelled in this thesis are also smaller than the grid size at 90m, meaning connectivity would be reduced if the sub-grid solver was not used (Yeo, 2015). Thus far, of the two published studies detailing flood inundation in Fiji, Rathnayake *et al*., (2015) use the 1D HEC-RAS model, and Nawai *et al*., (2015) use a 2D rainfall-runoff-inundation model, and both models have grid cell sizes larger than the smaller river channels. Moreover, based on benchmarking studies of different model types such as Hunter *et al*., (2008) and Horritt and Bates (2002), there are only subtle differences between the numerical simplifications of the shallow water equations made by the models, which means the choice of model does not dictate the representation of the flood wave. This thesis has access to the model source code, meaning the representation of the underlying processes can be better understood. Finally, the model is inherently fast, making it methodologically advantageous (Fernández *et al*., 2016).

Overall, the range of approaches to modelling the flood hazard as a component of a flood risk assessment are diverse, based on a number of different mathematical representations of flow, user needs and computational demand (Bates *et al*., 2005). The formation, improvement and implementation of hydrodynamic models has proliferated over the last two decades, and one key reason for this is the substantial increase in remote sensing technology (Bates, 2012).

2.3 Digital Elevation Models

Despite the numerous processes involved in simulating river flows, adding highly-accurate topography data into a hydrodynamic model is paramount for the valid simulation of flooding (Marks and Bates, 2000). A DEM is defined by Sanders (2007:1831) as a 'grid of elevation data', whereby each elevation assigned to a cell is an average of all elevation values recorded within that cell. Most DEMs are Digital Surface Models (DSM), measuring surface objects such as vegetation and buildings. However, a Digital Terrain Model (DTM) is required for input into a hydrodynamic model, representing 'bare earth' topography (Sanders, 2007).

Two key features of a DEM are their horizontal resolution - or grid cell size – and their vertical accuracy (Sanders, 2007). Vertical accuracy can be reported as either absolute or relative (Rodriguez *et al*., 2006). Absolute vertical accuracy refers to the difference in elevation height between DEM height and the assigned ellipsoid or geoid depending on the DEM's vertical coordinate system (Rizzoli *et al*., 2017). Relative vertical accuracy refers to the difference in elevation heights between the modelled and the observed heights and is more commonly used to describe DEM error than absolute vertical accuracy (Wise, 2000).

2.3.1 Types of Digital Elevation Model

Many methods can be used to collect elevation data using remote sensing, including Airborne Laser Altimetry (LiDAR), Interferometric Synthetic Aperture Radar (InSAR) and photogrammetry (Bates *et al*., 2014). Each method varies in cost, accuracy, resolution and coverage, and thus the needs of the user and availability of data often determine which method is used (Smith *et al*., 2006).

2.3.1.1 LiDAR

Light Detecting and Ranging (LiDAR) data are collected using an airborne laser altimeter. A series of laser pulses are transmitted from an aircraft to measure the ground surface, and an elevation value is determined by the triangulation of the time taken for the pulse to return and instrument GPS location (Baltsavias, 1999; French, 2003). LiDAR data has greatly advanced the application of remotely-sensed data in flood modelling (Bates, 2004; 2012). There are four key reasons for this, including: high horizontal and vertical accuracy, high density (typically >5 points per m^2: Pirotti and Tarolli, 2010) of elevation points from multiple pulse returns, reduced noise from radar scatter in comparison to radar systems and swift data-collection (Marks and Bates, 2000). LiDAR datasets provide an accurate representation of the surface because of the average relative vertical accuracy between 5-20 centimetres and the density of multiple returns (Baltsavias, 1999; Di Baldassarre and Uhlenbrook, 2012). These multiple returns include the first and last returns, which are often used to distinguish 'bare earth' and 'object' heights (Bates, 2004).

LiDAR data are suitable for flood estimation at the local scale (10-1000km^2); heralded as particularly useful in areas with fine-scale (<10m) topographic variability such as SIDS and urban areas (Gesch, 2009). As the vertical accuracy of LiDAR measurements is high (5-20cm: Baltsavias, 1999), predictions are improved in comparison to use of spaceborne DEMs with lower relative vertical accuracy (e.g. SRTM ~10m: Rodriguez *et al*., 2006). However, high accuracy incurs a high cost (Simpson *et al*., 2009). This is a key limitation in the context of SIDS, whereby collection of LiDAR for a small community in the Pacific (10-100km^2) is estimated to cost AUS$500,000-1,000,000 (Albert *et al*., 2013). SIDS have few local technical specialists able to collect and process the data, leading to a reliance on external analysis of the data, reducing community participation and increasing cost. As a result, InSAR datasets such as SRTM are relied upon in this context as they are open access and therefore freely-available to use (Gesch, 2009). Nonetheless, recent calls for improved LiDAR

coverage in developing regions for adequate flood risk assessment have led to increasing investment in LiDAR acquisition of localised floodplains in developing regions (World Bank, 2017).

2.3.1.2 Interferometric Synthetic Aperture Radar (InSAR)

Airborne and spaceborne Interferometric Synthetic Aperture Radar (InSAR) systems are based on the same interferometric physical principles and create DSMs (Sanders, 2007). Two signal pulses backscattered from the Earth's surface to two SAR antennae are used to calculate the interferometric phase difference between the two signals to produce a surface elevation height (Rodriguez *et al*., 2006). A prominent example of airborne InSAR application is TOPSAR, a C-band radar used to create airborne DSMs, with a RMSE of ~1m (Zebker *et al*., 1992). Airborne DEMS have limited application in SIDS (Gesch, 2009), and thus this thesis focuses on the spaceborne InSAR applications.

Regarding spaceborne InSAR, the greater altitude to which the pulses must travel leads to a decrease in RMSE vertical accuracy in comparison to airborne InSAR, with relative vertical accuracies of ~10m for C-band radar SRTM (Rodriguez *et al*., 2006). Nonetheless, this system can measure elevation at a global scale in a much smaller timeframe (11 days for SRTM; Rabus *et al*., 2003) due to the velocity of the satellite orbit (Rosen *et al*., 2000), making it a comparatively 'low-cost' dataset per kilometre (Yan *et al*., 2015). Spaceborne InSAR is conducted using two methods: repeat-pass and single-pass interferometry (Rabus *et al*., 2003). Repeat-pass interferometry emits the radar pulses using the same system at two different intervals, whereas single-pass interferometry utilises two Synthetic Aperture Radar systems operated in tandem (Rosen *et al*., 2000). Spaceborne DEMs over the last decade have received widespread attention in flood modelling, primarily due to their global coverage and increased resolution in comparison to earlier DEMs such as ACE GDEM and GTOP30 (Yan *et al*., 2015).

2.3.1.3 Photogrammetry

Previously, photogrammetry has been a main method used to acquire elevation data for DEM production (Lane, 2000; Hohle, 2009). Photogrammetry uses aerial or spaceborne images collected of the Earth's surface to produce DEMs (Pulighe and Fava, 2013). DEMs are produced in a two-step process (Toutin, 2008). Firstly, aerial images are captured, using digital (and previously analogue) cameras. Secondly, through manual or automated stereoscopic pairings and image matching, images taken from different angles are matched using area-based matching, feature-based matching or relational matching to produce a DEM (Fabris and Pesci, 2005). Matched images are known as stereo pairs, and images are matched from the same date using along-track stereo pairs or from multiple dates using across-track stereo pairs (Toutin, 2008). The accuracy of DEMs produced using photogrammetric techniques are highly dependent on several factors, including: flying altitude, camera-object distance, image resolution, shadow and vegetation (Pulighe and Fava, 2013). Best practice for image acquisition suggests images should be captured in off-leaf conditions if possible, considering the sun angle and other atmospheric conditions, meaning a number of factors must be considered to ensure good quality image capture (Hohle, 2009). As a result, photogrammetric techniques are weather-dependent and influenced by cloud cover and shadow, often reducing accuracy of the resultant DEM. The Advanced Spaceborne Thermal Emission and Reflection Radiometer (ASTER) DEM is the most widely-applied photogrammetric DEM applied in hydrodynamic modelling (Sampson *et al*., 2016), and is discussed in Section 2.3.2.2. Another example of a photogrammetric DEM is AW3D. The Advanced Land Observing Satellite with the Panchromatic Remote-Sensing Instrument for Stereo Mapping (ALOS/PRISM) was a mission launched in partnership with the Japan Aerospace Exploration Agency (JAXA), NTT DATA Corp. and the Remote Sensing Technology Centre of Japan in 2006 (Tadono *et al*., 2015). A DSM known as AW3D was generated using optical PRISM data, created using over 3 million satellite orthorectified images to produce a DSM with a ~5m horizontal resolution, and 5m height accuracy. The AW3D

dataset was released commercially in 2014, although the AW3D30 (~30m version) was made publicly available from JAXA in 2015.

2.3.2 Key Global Datasets in Flood Model Applications

Spaceborne datasets have provided particularly useful for applications in data-sparse locations such as SIDS, whereby previously the cost of using topographic data were too great (Farr *et al*., 2007). The two most widely-applied global datasets in flood modelling studies are discussed and compared below, before outlining the research suggesting the potential of the most recently-released TanDEM-X DEM.

2.3.2.1 Shuttle Radar Topography Mission (SRTM)

The Shuttle Radar Topography Mission (SRTM) DEM is a global single-pass spaceborne Interferometric Synthetic Aperture Radar (InSAR) C and X-band system, flown between February 11th-22nd, 2000, in a joint mission performed by NASA, the German Aerospace Center (DLR) and Italian Space Agency (Rabus *et al*., 2003). The goal of the mission was to create the first globally consistent DEM between 60°N-54°S (Rodriguez *et al*., 2006). This mission was the first global single-pass InSAR operation, initially released as a 3-arc second (~90m) product (Farr *et al*., 2007) and re-released at 1-arc second (~30m) in 2015. It has a quoted relative vertical accuracy of <6m for the X-band SAR and <10m for the C-band SAR and an absolute vertical accuracy of <16m (Farr *et al*., 2007).

The SRTM DEM is the most widely-used global DEM in flood modelling applications, despite the argument that a 6m relative vertical accuracy at 90m resolution is greater than most flood waves (<2m) (Wilson *et al*., 2007). Benchmark comparisons such as Sanders *et al*., (2007) identify 25% difference in flooded area between models using LiDAR, USGS National Elevation Dataset (NED) and SRTM data, despite stark differences in vertical accuracy (ranging from 0.15m for LiDAR to 15m for SRTM). Furthermore, Berry *et al*., (2007) show concordance between SRTM elevation heights and 'ground truth' altimeter heights, and Jarvis *et al*., (2004) demonstrates an improvement of 12m in

absolute vertical accuracy in comparison to the coarser GTOPO30 DEM. However, there are several limitations of the SRTM including: noise and 'speckle', presence of vegetation and building artefacts, striping and absolute bias (Rodriguez *et al*., 2006; Sampson *et al*., 2016; Yamazaki *et al*., 2012).

2.3.2.2 Advanced Spaceborne Thermal Emission and Reflection Radiometer (ASTER)

ASTER is an example of a spaceborne DEM often compared with SRTM (Sanders, 2007; Rexer and Hirt, 2014). In collaboration with the Japanese Ministry of Economy, Trade and Industry and NASA, the ASTER DEM was created for all areas covering 83°N-83°s with a horizontal resolution of 30m, improving both coverage and resolution over the SRTM (Fujisada *et al*., 2012). A multispectral imaging sensor was used aboard the NASA Terra spacecraft, capturing a series of stereoscopic images that are stacked and correlated to process a DEM. Version 1 (ASTERv1) was released in 2009 with an overall relative vertical accuracy of 10-25m, followed by an upgraded version in 2011 (ASTERv2).

Although ASTER has a finer horizontal resolution than SRTM, SRTM has been more widely-implemented in flood modelling studies than ASTER (Sampson *et al*., 2016). Benchmarking studies comparing the accuracy and usefulness of the two datasets, found vertical accuracies over Australia of 5m for SRTM compared to 9m for ASTER, thus providing justification for the greater implementation of SRTM (Hirt *et al*., 2010; Rexer and Hirt, 2014). However, Jing *et al*., (2013) suggest that ASTERv2 can be useful in areas where SRTM artefacts such as voids are widespread, although artefacts such as cloud cover in the ASTER are also a limiting factor (Chirico, 2004).

As SIDS rely on global datasets such as SRTM and ASTER, it is important to consider how these datasets have been applied in this context. Bannari *et al*., (2017) concluded that for Bahrain,

ASTERv2 was superior to SRTM 90m, but inferior to SRTM 30m, showing the importance of horizontal resolution in areas where the resolution of smaller-scale features is necessary for accurate simulation. Furthermore, in the Caribbean context, and echoed by Simpson *et al*., (2009), Chirico (2004) found a lower RMSE of 16m for the SRTM in comparison to 22.46m for ASTER, thus identifying SRTM as more applicable to Caribbean SIDS, despite the argument that even 16m is much larger than the range of floodplain elevations in many of these low-lying areas.

2.3.2.3 TanDEM-X - The Future of Global DEMs?

The TanDEM-X mission provides a potential opportunity to meet the need for a high-accuracy, global-scale DEM for flood inundation modelling, as well as specifically in SIDS. TanDEM-X is a global, spaceborne DEM, acquired at least twice between December 2010 and January 2015 using an X-band bistatic single-pass Interferometric Synthetic Aperture Radar (InSAR) system in a public-private partnership between the German Aerospace Center (DLR) and Airbus (Rizzoli *et al*., 2017). Two SAR systems, TerraSAR-X and TanDEM-X were flown in close helix orbit, between 300-500m apart, producing a high-precision, globally-consistent DEM product (Borla-Tridon *et al*., 2016). The DEM has a posting of 0.4 arc-seconds (~12m), and a relative vertical accuracy of 2m in low slope (<20%) areas and 4m in steep slope areas (>20%), providing substantial promise of improved accuracy in comparison to previous global spaceborne DEMs (Krieger *et al*., 2007; Rizzoli et al., 2017).

Nonetheless, to the best of our knowledge, no published research has yet applied TanDEM-X in a hydrodynamic modelling test case. Hence, a key objective of this thesis is to benchmark the capacity of TanDEM-X to simulate flood extents in comparison to SRTM and LiDAR datasets. SRTM was chosen as the most widely used spaceborne DEM in flood modelling in SIDS (Albert *et al*., 2013). LiDAR was chosen because it is the most accurate DEM available in the study site. TanDEM-X is a DSM, measuring surface objects (Wessel *et al.,* 2018). The X-band SAR system has a limited capacity to penetrate vegetation, leading to volume decorrelation over densely-forested areas and reduced

vertical accuracy (Martone *et al*., 2012). To date, a limited number of studies have validated the TanDEM-X DEM (Gruber et al., 2012; Baade and Schmillius, 2016; Rexer and Hirt, 2016). Most recently, Wessel *et al*., (2018) validated the TanDEM-X DEM against GPS data, calculating the absolute vertical error as the Root Mean Square Error (RMSE) between GPS and DEM heights. They reported an absolute height error of <2m for the TanDEM-X in the test cases they examined. Thus far, results indicate a superior accuracy in comparison to SRTM and ASTER, giving the promise of an improved global DEM for a variety of geoscience applications. As a DTM is required for flood inundation models, a suitable method for TanDEM-X processing is necessary, and potential processing methods used to guide the methodology developed in this thesis are discussed in Section 2.4.2.

2.4 DEM Error and Processing

As Bates (2012) argues DEM quality is an important factor in hydrodynamic model skill, the errors present in these global datasets - and how to remove or process them – are a key discussion point in the literature surrounding terrain data in flood modelling. This section outlines the key error sources in DEMs, with particular reference to spaceborne InSAR DEMs, as well as synthesising the literature detailing numerous methods used to process SRTM and LiDAR, as these are the main datasets used in the literature. The methodologies are significantly different, largely due to the difference in horizontal resolution of the DEM used, and thus this must be considered when determining an appropriate method for TanDEM-X, in which horizontal resolution is different again. For these purposes, methods are described as coarse-scale if suited to a DEM with a horizontal resolution of ~90m typically used for SRTM processing, and fine-scale if suited to a DEM with a horizontal resolution of <5m which are typical of LiDAR processing methods.

2.4.1 DEM Error

When comparing global DEM products, the limitations are dictated by the error (Yan *et al*., 2015). Error can be both vertical and horizontal, although vertical error is more widely reported. Wise (2000) categorises error as data-based, whereby error resides in the data itself, and model-based, whereby error is introduced to the DEM through processing and creation of the DEM. Often, error is categorised as random, systematic or a blunder (Wise, 2002; Weschler, 2007). Random errors are unpredictable disparities in the data (Smith *et al*., 2006). Systematic error is generated during the DEM process and often follows fixed patterns e.g. striping error. Blunders are associated with human error or equipment failure and can be easily removed if identified (Weschler, 2007). Error in a DEM is most commonly reported as a RMSE, bias, standard deviation or mean error statistic (Smith *et al*., 2006). These statistics provide a singular assessment across the whole dataset, assuming that error is random and normally distributed (Carlisle, 2005). Nonetheless, a number of scholars have indicated that error would be better reported with consideration of the spatial distribution (Carlisle, 2005; Weschler, 2007; Fisher and Tate, 2006).

Key examples of DEM error such as speckle noise, voids, sinks and striping (Yamazaki *et al*., 2012) are summarised in Table 1. Error often introduces artefacts into the DEM surface, affecting vertical accuracy (Weschler, 2007). Hirt (2018:5) describes an 'artefact' as a 'step-like disruption' that is not representative of actual terrain. It is necessary to remove such artefacts to successfully process a DSM product to a DTM for input into a hydrodynamic model.

2.4.2 Processing a Digital Surface Model to a Digital Terrain Model

Due in part to the widespread use of SRTM, several limitations have been outlined with processing SRTM to a DTM (Sampson *et al*., 2016). Many methods have been described to increase the suitability of SRTM for flood models, including vegetation removal (Baugh *et al*., 2013; O'Loughlin *et al.,* 2016), speckle and noise filtering (Yamazaki *et al*., 2017), hydrological corrections (Yamazaki *et*

al., 2012; Jarihani *et al*., 2015) and void-filling processes (Jarvis *et al*., 2008; Lehner *et al*., 2008). These methods aim to process the DSM model to a model better-representing 'bare earth' or a DTM. The most common errors and processing methods are summarised in Table 1, and vegetation removal is discussed further as this is the key processing technique of interest in this thesis.

Table 1 - Table outlining the key errors found in Digital Elevation Models and the processing methods detailed in the literature.

Artefact	**Explanation**	**Processing methods**
Striping error	Medium wavelength (500m – 50km) undulation present in the DEM (Rodriguez *et al*., 2006).	Two-dimensional Fourier transform filter (Gallant *et al.,* 2012; Tarakegn and Savama, 2013; Yamazaki *et al*., 2017); simple cut filter (Arrell *et al*., 2008)
Absolute bias	Average elevation shift or bias across the domain (Yamazaki *et al*., 2017).	Reference to ICESat centroid elevations (Yamazaki *et al*., 2017)
Voids	Areas of 'no data' (Jarvis *et al*., 2008).	Void interpolation (Jarvis *et al*., 2008); Iterative neighbourhood analysis (Lehner *et al*., 2008)
Sinks	Spurious or artificial depressions in elevation (Wise, 2000).	Fill (Lehner *et al*., 2008); Lift (Jenson and Domingue, 1988); Priority-flood algorithm (Barnes *et al*., 2014); Simplified erosion model (Grimaldi *et al*., 2007)
Speckle	Surface reflectance leads to random pixel variation (Yamazaki *et al*., 2017).	Adaptive smoothing filter (Gallant, 2011; Yamazaki *et al*., 2017); aggregating DEM resolution (Neal *et al*., 2012b); wavelet filter (Falorni *et al*., 2015)
Hydrological corrections	Unresolved channel identification or hydrologically-disconnected surfaces (Lehner *et al*., 2008).	Stream burning; carving (Soille *et al*., 2003; Lehner *et al*., 2008); surface reconditioning (Callow *et al*., 2007)
Vegetation	Peaks in elevation in locations where vegetation is present.	Uniform height removal (Coe *et al*., 2008; Paiva *et al*., 2011); spatially-distributed height removal (Baugh *et al*., 2013); least squares estimation of vegetation patch edges (Gallant *et al.,* 2012); Vegetation height removal related to canopy density (O'Loughlin *et al*., 2016).

2.4.3 Artefact Removal

Over time, SRTM and ASTER products have been improved to reduce error. For example, the original release of SRTM (Rabus *et al*., 2003) included several pits, spikes and voids, whereas SRTM (v2) had

pits, spikes and minor voids removed (Slater *et al*., 2006) and SRTM (v3) used the ASTER DEM to further remove voids (Abrams *et al*., 2016). The most widely-used SRTM (v4) released by Jarvis *et al*., (2008) has undergone void-removal processes but still contains surface artefacts such as buildings and vegetation. ASTER (v2) was released in 2011, following initial release in 2009, adding more than 260,000 stereo pairs to the DEM to improve coverage and accuracy (Fujisada *et al*., 2012).

Most recently, Yamazaki *et al*., (2017) presented the first global, multiple error-reduced SRTM product, known as Multi-Error-Removed Improved-Terrain (MERIT) DEM. The key vertical errors present in SRTM, such as absolute bias, stripe error, speckle noise and tree height bias are reduced using an iterative method to create a DTM from SRTM. Firstly, stripe noise was removed using a two-dimensional Fourier transform filter, followed by absolute bias correction using ICESat centroid elevations. Tree height was estimated using a function of tree density and height using Simard *et al*., (2011). Finally, speckle noise was removed using Gallant's (2011) adaptive smoothing filter. The dataset is freely available at the global scale for non-commercial purposes and global validation against ICESat and SRTM datasets suggests MERIT improves relative vertical accuracy (proportion of points with error <2m) from 39% to 58% of the globe over SRTM (Yamazaki *et al*., 2017), although building artefacts have yet to be removed from the data. Hirt (2018) most recently reported greatly reduced artefact presence in the MERIT DEM (108 artefacts) in comparison to SRTM (v4.1) (1341 artefacts) based on a 0.1° x 0.1° DEM tile comparison.

2.4.4 Vegetation Removal

The presence of vegetation artefacts in DSMs is a well-known problem, and a number of processing methods have been developed (Bates, 2012). Of specific importance to flood modelling, vegetation artefacts in the DSM creates areas of higher elevation on a floodplain or along a river channel which impact the simulation of flooding (Baugh *et al*., 2013; Jarihani *et al*., 2015). Bank-lined vegetation artificially elevates the channel bank and reduces overbank flow, whilst elevation peaks on the floodplain can block key flow pathways along the surface, as well as increasing surface roughness

(Jarihani *et al*., 2015). Manual methods to vegetation removal are sometimes used, particularly in the commercial setting, but fully automated methods are preferable at the large scale due to lower user expense in comparison to manual methods (Gallant *et al.,* 2012).

Vegetation processing methods differ substantially between SRTM and LiDAR processing, due to difference in DEM acquisition, horizontal resolution and vertical accuracy. Methods used to remove vegetation for each method are summarised below, before identifying potential methods suitable for TanDEM-X vegetation removal.

2.4.4.1 SRTM Processing

The SRTM C-band radar signal partially penetrates the vegetation canopy (Bates, 2012). The radar has a short operating wavelength (5.6cm) - a similar length to vegetation scattering elements e.g. leaves and branches (Hofton *et al*., 2006) - and thus the height of the SRTM elevation over a vegetated area represents a height in between the ground surface and the top of the canopy (Baugh *et al*., 2013). Brown *et al*., (2010) refer to this as the scattering phase centre height. As a result, studies have tried to determine the penetration capability of the radar to determine how much vegetation height to remove from the DSM when processing to a DTM. Wilson *et al*., (2007) conducted vegetation height surveys for a reach of the Amazon basin and applied a 50% canopy penetration depth in accordance with the author's personal communication with SRTM developer Ernesto Rodriguez. Kellndorfer *et al*., (2004) critically identified that canopy density directly affects penetrative capacity, and thus different tree types will produce different scattering phase centre heights. Specifically, Kenyi *et al*., (2009) suggests the SRTM scattering phase centre is 60% for red fir, 53% for Sierra mixed conifer and 50% for montane hardwood-conifer tree species.

Many methods include the use of additive datasets such as a forest cover or height maps. Several global datasets have been produced to indicate land cover and vegetation, including Hansen *et al*.'s (2013) map of forest change between 2000 and 2012 at 30m resolution and Shimada *et al*.'s (2014)

global forest cover map derived using Advanced Land Observing Satellite (ALOS) Phased Arrayed L-band Synthetic Aperture Radar. Gallant *et al.,* (2012) used the Landsat Thematic Mapper dataset at 30m to remove tree heights from SRTM. Two key global height datasets available on forest cover are Lefsky's (2010) global forest canopy height map produced by segmenting MODIS data to identify forest patches, followed by Simard *et al*.'s (2011) global forest canopy map which has been most widely-utilised for SRTM processing, derived using spaceborne ICESat Geoscience Laser Altimeter System LiDAR data (e.g. Baugh *et al*., 2013; O'Loughlin *et al*., 2016; Yamazaki *et al*., 2017).

Using a uniform height removal methodology, Coe *et al*., (2008) removed a standardised height of 23m from the SRTM DEM to estimate 'bare earth'. Recognising the problem with removing a uniform height, Baugh *et al*., (2013) subtracted an optimised fixed percentage (60%) of the spatially-distributed vegetation height from the SRTM DEM to remove vegetation artefacts over the Amazon basin, using Simard *et al*.'s (2011) vegetation height map to indicate spatial distribution in vegetation height. The optimised percentage was determined by producing ten DEMs with between 10 – 100% of the vegetation height identified in Simard *et al*.'s (2011) forest canopy map, before filtering random noise and optimising floodplain friction values in the model setup. The flood outputs were assessed for all 10 DEMs to determine which percentage height subtraction improved simulation accuracy the most. This methodology improved model accuracy of the water surface elevation with a RMSE of 1.84m in comparison to 6.61m with no vegetation removal, indicating a significant improvement. Although O'Loughlin *et al*., (2016) suggest that any vegetation correction improves the SRTM DEM at the global scale, removing a spatially uniform percentage height from SRTM does not account for spatial variability in vegetation height based on varying penetrability (e.g. Coe *et al*., 2008; Paiva *et al*., 2011; Baugh *et al*., 2013). Pinel *et al*., (2015) suggest that removing a uniform height leads to inconsistent elevations across a floodplain whereby vegetation is likely to vary in height, leading to under or over-estimated elevations in areas whereby vegetation varies above or below the uniform height. As a result, O'Loughlin *et al*., (2016) validate a global methodology to remove vegetation heights from the SRTM, by relating vegetation height (using Simard *et al*., 2011)

to canopy density to determine the percentage of vegetation height to remove from the DEM on a pixel-by-pixel basis. Yamazaki *et al*., (2017) utilise this concept in vegetation removal for the MERIT product. Other methods have included Jarihani *et al*.'s (2015) adoption of Gallant's (2011) adaptive smoothing method for 'vegetation smoothing', reduces the RMSE from 3.25m in SRTM (v4) to 1.55m in the study areas: Diamantina River and Cooper Creek catchments of the Lake Eyre basin in Australia.

In summary, vegetation removal methods for SRTM are often conducted by removing a uniform or spatially-distributed height from the SRTM data to identify 'bare earth', using >90m resolution datasets to aid the identification of vegetation (e.g. Simard *et al*., 2011).

2.4.4.2 LiDAR Processing

LiDAR is typically a Digital Surface Model, but several methods have been developed to process the DSM to a DTM with high vertical accuracy (<20cm) (Liu, 2008). Four key steps are often conducted to produce a LiDAR DTM from the returns (Meng *et al*., 2010). First, outlier points are identified and removed, before interpolating all points to create a DSM surface. Then a filtering algorithm is selected by classifying ground and non-ground points before creating the final DTM.

Most simply, a DTM can be created by taking the last ground return for each laser pulse as the ground measurement (Bates, 2004). When a LiDAR pulse hits an object surface, multiple returns will be captured as the pulse continues to penetrate further towards the ground e.g. through gaps in the canopy if the object is vegetation (Harding *et al*., 2001). Generally, the first return represents the object height and the last return the ground height. As common practice, the last return is often used to create a LiDAR 'bare earth DTM', assuming that the last return represents ground elevation (French, 2003; Bates, 2004; Mason *et al*., 2007).

Several filter algorithms have also been produced to classify ground and non-ground returns. Meng *et al*., (2010) provided a good summary of the different types of filters commonly adopted, suggesting that four key assumptions guide the various algorithms when separating ground and non-ground points:

1) The lowest points within an area are often ground points.
2) The surface slope gradient between two ground points is often lesser than between a ground and non-ground point.
3) The terrain of an area does not change dramatically.
4) Terrain is a smooth, continuous surface.

Liu (2008) classifies LiDAR ground filters into three types based on the methodology adopted: interpolation-based, slope-based and morphological-based.

Interpolation-based methods calculate the 'bare earth' surface by approximating a surface based on all LiDAR points, before calculating the distance from the surface to each point. The process is then repeated until the surface represents the ground points (Lohmann *et al*., 2000). Kraus and Pfeifer (1998) introduced this method as a linear prediction, and Lee and Younan (2003) introduced a combined modified linear prediction which can accommodate steep-sloped areas. Slope-based methods classify ground and non-ground points based on the slope between two points, whereby slope values above a defined threshold are indicative of a non-ground point, assuming terrain changes slowly and smoothly, and objects show steep gradients. Vosselman (2000) first detailed this method to produce a LiDAR DTM, and Sithole (2001) improved the method by introducing a varying threshold to produce a method better-suited to varying terrain.

Morphology-based methods build upon the principles of mathematical morphology, often used in image processing (Zhang *et al*., 2003). Two key operators – erosion and dilation – are used to perform an opening operation on an image, whereby ground and non-ground points are identified within a specified window across the entire image. The lowest points identified within the window are then considered ground points and used to create a DTM. Zhang *et al*., (2003) detail a popular method known as a Progressive Morphological Filter, whereby the window is iteratively increased in size to identify objects of different sizes. This method has been adopted for Intermediate-TanDEM-X processing by Geiß *et al*., (2015) and Schreyer *et al*., (2016) and will be discussed further within this thesis as a potential processing method for TanDEM-X vegetation removal. Chen *et al*., (2007) also detail a morphology-based approach whereby the assumption is that a sharp boundary between non-ground and ground points can be used in classification.

Other filters used to process LiDAR data include segmentation, directional-scanning, contour-based and TIN-based (Meng *et al*., 2010). For example, Cobby *et al*., (2001) separate ground and non-ground points using a segmentation algorithm, classifying non-ground points as short or tall vegetation (see also Mason *et al*., 2003). Overall, the most commonly-used LiDAR ground filters work on a fine scale, as the horizontal resolution of LiDAR data is extremely high (often ~1m: Bates, 2012), and so objects are clearly-defined in the DSM model.

2.4.4.3 TanDEM-X processing

As the resolution of TanDEM-X is significantly different to LiDAR (~1-2m) and SRTM (~90m), application of current DTM-processing methods is likely to be unsuitable for TanDEM-X processing in isolation (Geiß *et al*., 2015). Schreyer *et al*., (2016) show that the Progressive Morphological Filtering method was most successful when Intermediate-TanDEM-X was disaggregated to 4m in comparison

to analysis at ~12m, suggesting that the method works best at a finer LiDAR-typical resolution. Geiß *et al*., (2015) also suggest that TanDEM-X is still too coarse for use of LiDAR processing methods, as the minimum window size (3x3 pixels) used in the Progressive Morphological Filter is still too large to identify small vegetation or individual buildings. On the other hand, the coarse-scale (>90m) methods applied to SRTM (e.g. Baugh *et al*., (2013) and Yamazaki *et al*., (2017)) are also likely unsuitable, as the global vegetation map used to remove vegetation has a resolution of 90m (see Simard *et al*., 2011), and thus does not have a high-enough resolution to identify areas of vegetation smaller than 90m that are well-resolved in the TanDEM-X DEM. Vegetation correction of the SRTM C-band radar is also likely to differ in comparison to the TanDEM-X, as X-band radar has a limited ability to penetrate canopy, and thus removing a percentage of vegetation height from the DEM may not be suitable as the scattering phase centre height is likely closer to the top (or at the top) of the canopy. Further investigation is required to understand the scattering phase centre height of TanDEM-X under different land covers.

Thus far, a limited number of studies have been released detailing possible processing methods for TanDEM-X error. Mason *et al*., (2016) describe a method to use flood extent SAR images to improve the Intermediate-TanDEM-X error against LiDAR data for the potential input to a hydrodynamic model, reducing relative vertical error to 60% of the original TanDEM-X error in the study area. The standard deviation between the original Intermediate-TanDEM-X heights and the LiDAR heights was 2.05m, reduced to 0.74m after correction. Geiß *et al*., (2015) and Schreyer *et al*., (2016) adopt a LiDAR-style ground filtering approach to identifying buildings and vegetation using Progressive Morphological Filtering. Gallant *et al.,* (2012) suggest that the least squares estimation at a vegetation patch edge method utilised in their study could likely be applied to TanDEM-X with some adaptation, but no further study applying this methodology has been published. As a result, it will be important in this thesis to thoroughly understand whether information can be utilised from previous

processing methods of both SRTM and LiDAR, whilst considering the limitations of using datasets that are both too coarse or too fine for the ~12m resolution of TanDEM-X. The map shown in Figure 1 demonstrates the spatial distribution of height differences between the LiDAR DTM and TanDEM-X. Large areas of vegetation along the channel and downstream boundary are identified, as well as smaller isolated regions, indicating the importance of a method that considers a range of artefact sizes.

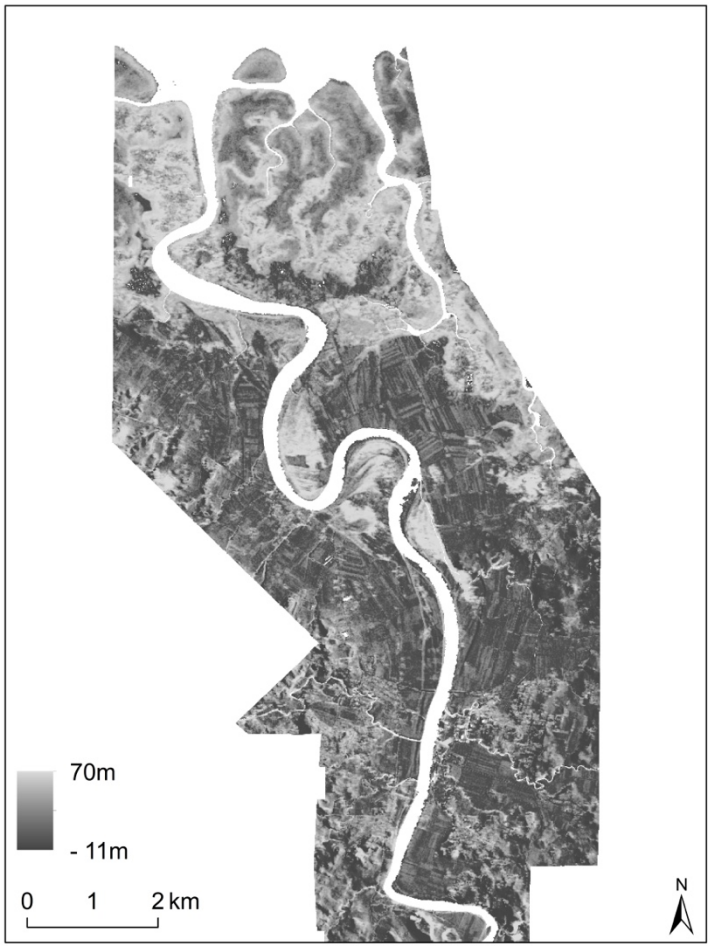

Figure 1 - Map showing the difference in heights between the LiDAR DTM and TanDEM-X DSM in the Ba study area

On the other hand, a number of studies have been published outlining how vegetation artefacts may be detected in the TanDEM-X DEM. Martone *et al*., (2012) suggest the pairing of polarimetric and interferometric measurements to infer volume scattering information collected by the TanDEM-X mission should allow inference of vegetation height in the TanDEM-X DSM. Based on analysis by

Schlund *et al*., (2014) and Martone *et al*., (2012; 2018), a key signifier of vegetation artefacts in the TanDEM-X DEM is interferometric coherence. Interferometric coherence signifies the normalised complex correlation coefficient between two acquisitions, indicating the amount of noise or decorrelation in the interferogram (Martone *et al*., 2012). In areas of vegetation, volume scattering of the signal increases (Kellndorfer *et al*., 2014), leading to a higher presence of interferometric decorrelation and thus lower interferometric coherence. Although L and P-band SARs are considered more appropriate for forest classification than X-band SARs, higher volume decorrelation was observed in areas whereby vegetation structure was denser, as the X-band signal interacts with a higher vegetation volume, thus increasing volume decorrelation (Schlund *et al*., 2014). Interferometric coherence and the volume correlation in the TanDEM-X was the main indicator used by Martone *et al*., (2018) in the classification of forested areas to produce the Global Forest/Non-Forest Classification map at 50m resolution, using a fuzzy multi-clustering classification method. Although the map is stated to be available for scientific purposes, it is not yet accessible and thus could not be utilised in this thesis as an indicator of vegetation artefact.

Breidenbach *et al*., (2010) suggest that the backscatter values for TerraSAR-X images are higher for vegetation than agricultural land, outlining the potential use to separate land cover classes. Because the TerraSAR-X and TanDEM-X SARs were flown as a bistatic acquisition (one SAR transmits and receives the signal and the other SAR only receives the signal: Willis, 2005), the presence of multiple scattering coefficients can be calculated, allows increased object detection than in monostatic mode (one SAR transmits and receives the signal). Schlund *et al*., (2014) suggest that calculating the amplitude (backscatter) of the signal from each SAR can be used to classify forest areas, although better classification is observed using interferometric coherence than amplitude.

Accompanying the TanDEM-X DEM data are a number of auxiliary datasets which report height error and artefacts in the DEM, including: Height Error Map, amplitude, Water Indication Mask, coverage,

consistency and a shadow mask (see Wessel, 2016). Of specific interest in this thesis, the Height Error Map represents the standard deviation of height error for each pixel within the DEM based on the interferometric coherence estimates derived between signal returns. The Amplitude map represents radar backscatter as a mean value for all the calibrated amplitudes between SAR images (Ferretti *et al*., 2000; Wessel, 2016). To the best of our knowledge, no published study has utilised these auxiliary variables to process the TanDEM-X DSM to a DTM thus far, although on visual inspection the pattern between surface artefacts in Google Earth imagery and the Height Error Map and Amplitude map provide promise for artefact identification. As a result, the Amplitude map and Height Error Map may provide some capacity to determine vegetation presence in the DEM. Figure 2a and 2b demonstrate the pattern for the Height Error Map and Amplitude map in the study area in

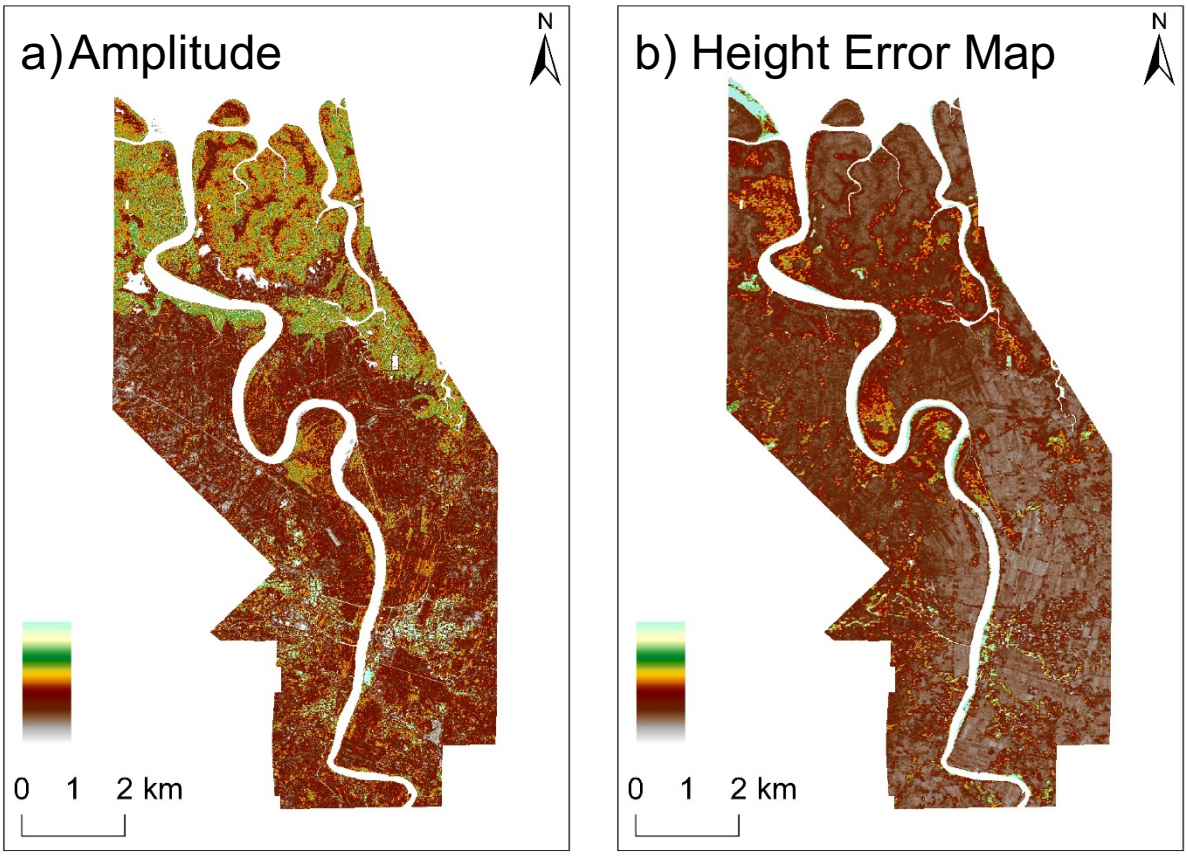

Figure 2 - Maps showing the identification of vegetation artefact in the TanDEM-X auxiliary datasets a) Amplitude and b) Height Error Map.

2.5 Chapter Conclusion

In this literature review, the concepts of flood risk, flood models and DEMs have been discussed separately to categorise and synthesise the relevant literature in each. Flood risk was discussed as a multi-factorial concept in Section 2.1, constructed of several interactions between the flood hazard, asset and human exposure, and the vulnerability of the population (Apel *et al*., 2009). Flood risk specifically in SIDS was identified, justifying the focus on SIDS in this thesis and emphasising the need for improved flood risk assessment. A number of different hydrodynamic models, with particular reference to LISFLOOD-FP, were identified as a key method to estimating the flood hazard in Section 2.2. As topography is a key input into a hydrodynamic model, the use of DEMs undoubtedly influences the capacity to accurately estimate flood hazard. The proliferation of DEMs over time was discussed in Section 2.3, identifying the key types of DEM and the main DEM products used in flood modelling, before outlining the key characteristics of the DEM of focus in this thesis: TanDEM-X. A thorough investigation into the different methods utilised to process DEMs from a DSM to a DTM was also conducted in Section 2.4, as a DTM is a key requirement for input into a hydrodynamic model. Critically, this literature review emphasised that a method for processing TanDEM-X from a DSM to a DTM that has been tested in a hydrodynamic model has not been published, providing the key justification for conducting this project. By understanding how other DEM products have been processed, these methods are used to inform the development of a suitability methodology for processing TanDEM-X in this thesis.

In reality, the three fields of research are intrinsically related, whereby flood modelling and the use of a DEM are smaller dolls stacking inside the largest Russian nesting doll that is measuring flood risk. There is an emphasis on the estimation of flood hazard in this thesis, although flood risk is composed equally of the three key components (UNISDR, 2015a). Nonetheless, as the methods detailed in this thesis focus on improving the simulation of flood hazard through the appropriate

vegetation processing of TanDEM-X for input into LISFLOOD-FP, the emphasis on flood hazard is justified.

Chapter 3 will outline the methodology, results and discussion sections of this thesis, outlining and comparing three methods to processing vegetation in the TanDEM-X data to create seven DTMs. The seven DTMs will be input in to hydrodynamic model LISFLOOD-FP and the flood output extent and water surface elevation will be compared with LiDAR, SRTM and MERIT models to determine a) which vegetation processing method is the most suitable for input into a hydrodynamic model, and b) whether the TanDEM-X DSM and DTMs have a better fit to the LiDAR model simulation in comparison to SRTM and MERIT models.

Chapter 3 – Paper titled: Comparing TanDEM-X data with frequently-used DEMs for flood inundation modelling

3 Chapter Introduction

Framed within the synthesis of literature in Chapter 2 regarding flood hazard estimation in SIDS using DEMs in hydrodynamic models, this chapter aims to answer the two key research questions first posed in Section 1.3:

1) How can artefacts be removed from TanDEM-X to create a suitable Digital Terrain Model for input into a hydrodynamic model?
2) Are flood estimates improved using TanDEM-X in comparison to SRTM and MERIT?

With reference to the first research question, as TanDEM-X is a DSM a suitable method will be required to process TanDEM-X to a DTM for input into a hydrodynamic model. Fine and coarse scale methods developed to process LiDAR and SRTM were identified in Section 2.4.4, although Geiß *et al*., (2015) suggest that these are unlikely to be appropriate in isolation for TanDEM-X processing. However, several authors have identified potential vegetation detectors in the TanDEM-X data (e.g. Martone *et al*., 2018). This chapter will therefore detail three key processing methods for TanDEM-X: Progressive Morphological Filtering and Image Classification of the Amplitude and Height Error Maps shown in Figure 6 in the methodology section of this chapter (Section 3.1). Hydrodynamic modelling outputs given the seven resulting TanDEM-X DTMs will indicate whether the methods used to process the TanDEM-X DSM produce flood extents and water surface elevation with a better fit to the LiDAR model, informing the most appropriate method for TanDEM-X DSM processing for input into a hydrodynamic model. Following this, the model outputs of the TanDEM-X DSM and DTMs are compared to the SRTM and MERIT models to identify whether the TanDEM-X DSM and DTMs simulate flood extent and water surface elevations closer to those produced by the LiDAR model. These results, calculated using binary pattern matching performance metrics, will be used to identify

whether the TanDEM-X models improve flood estimates against the LiDAR model in comparison to SRTM and MERIT, answering the second research question.

This paper chapter details the methodology (Section 3.1), results (Section 3.2) and discussion (Section 3.3) sections of the thesis, whereby methods for processing the TanDEM-X DSM to a DTM are compared and input into hydrodynamic model LISFLOOD-FP, before comparing the flood extent and water surface elevation of the model outputs with SRTM and MERIT models.

This chapter is largely based on a publication published by Water Resources Research:

Archer, L., Neal, J.C., Bates, P.D., House, J., (2018), 'Comparing TanDEM-X data with frequently used DEMs for flood inundation modeling', *Water Resources Research*, vol. 54, no. 10, 10205-10222

Figures and tables as part of the Supporting Information for the publication are included within the main body of the thesis. The paper introduction is omitted and is instead incorporated into the literature review in Chapter 2 whereby a background of the topics covered in this paper are discussed. Collaboration with other authors on this paper include the review of the publication and the role as supervisors.

3.1 Methods

3.1.1 Study Area

The study was conducted in Fiji – an upper-middle income SIDS located in the South Pacific (see Figure 3a). The archipelago is made up of 330 islands, of which approximately 100 are inhabited (Brown *et al*., 2014). The largest island, Viti Levu (see Figure 3b) has an area of approximately 10,389km^2 and is home to ~60% of the total population (Fiji Bureau of Statistics, 2018). Fiji has a tropical maritime climate driven by trade winds, the South Pacific Convergence Zone and the El Niño Southern Oscillation, with 70% of annual rainfall falling between November and April during the cyclone season (Mataki *et al*., 2006). The island has many small rivers with a high flood frequency

(McAneney *et al*., 2017), experiencing on average two flood events and one cyclone per year, with 97% of disasters reported between 1983-2012 attributable to extreme rainfall (Holland, 2014). Nonetheless, little research has estimated current or future flood hazard in Fiji using hydrodynamic modelling (Yeo *et al*., 2007). The most recent flood assessment for Fiji relies on MERIT data at 90m resolution, which is relatively coarse in comparison to the scale of Fijian catchments (see Government of Fiji, 2017).

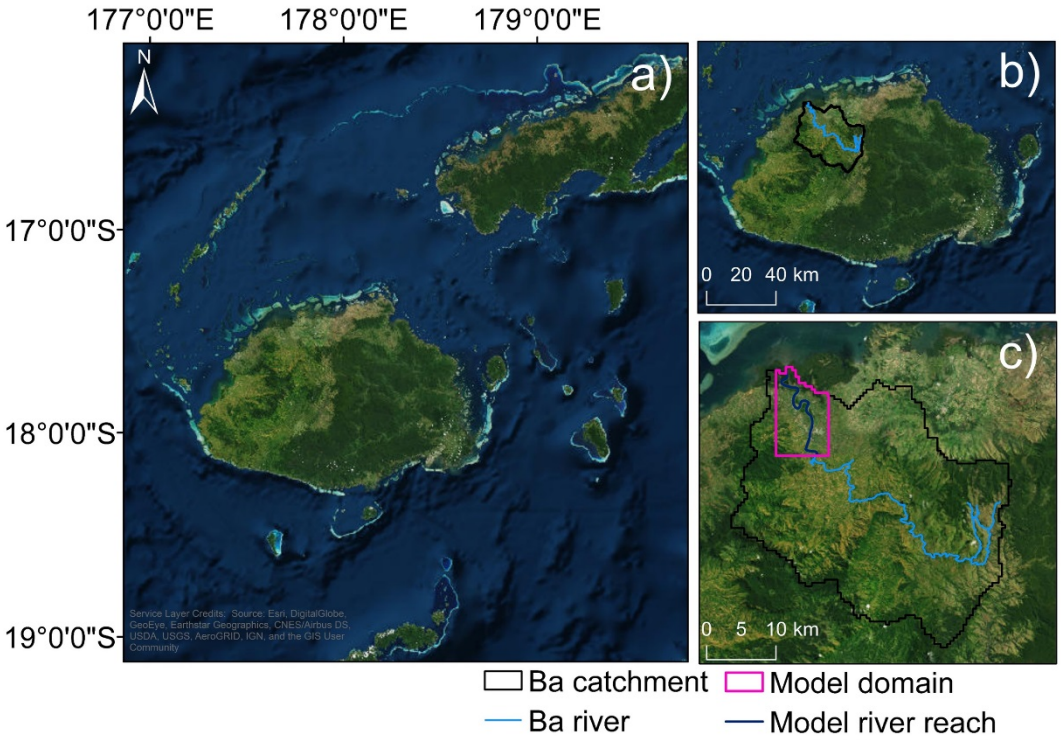

Figure 3 - Map of the study site a) Map of Fiji b) Map of the Ba Catchment on the main island of Viti Levu c) Map showing the model domain within the Ba catchment, including Ba town

The Ba catchment on the island of Viti Levu (Figure 3c) was chosen as the test site for three key reasons: high flood frequency, representative floodplain characteristics and availability of LiDAR data. Recent disastrous flood events in Fiji (January 2009; 2012; March 2012; April 2018), in which the Ba catchment was worst affected, resulted in Fiji ranking 3rd in the 2018 Global Climate Risk Index (Eckstein *et al*., 2017). In 2016, Fiji experienced the strongest cyclone ever recorded in the Southern Hemisphere – Cyclone Winston – affecting 62% of the population and causing damage equivalent to 20% of the nation's GDP (Government of Fiji, 2016). The floodplain along the Ba river is dominated by cropland (63.85%: Fiji Bureau of Statistics, 2010), with isolated areas of vegetation and buildings, representative of most floodplains in SIDS and many other floodplains globally. It is therefore expected that the study results are likely to be replicable in other floodplains. The 21.72km river reach in Figure 3c was chosen for the model domain as LiDAR data were available. The LiDAR data shown in Figure 4 was collected and pre-processed to a DTM using the last returns method in 2012 through collaboration with the Secretariat of the South Pacific and the World Bank (Thomas, 2012), and was obtained for this study by Dr Nicholas Rollings at the University of the South Pacific. Access to LiDAR data provides a good validation data source in the absence of ground truth information, as the LiDAR has a much superior vertical accuracy than the satellite DEM products (see Table 2). The LiDAR was validated against ground truth data by Thomas (2012) for 27 locations, reporting an average absolute vertical error of 73.6mm. As a result, the Ba catchment provides a good SIDS test case whereby TanDEM-X can be adequately validated against a benchmark.

In data-sparse areas, ground truth validation data are often unavailable and so LiDAR data has been used as a proxy (Yamazaki *et al*., 2012). The LiDAR model is not necessarily an exact representation of floodplain topography as the LiDAR sensor also returns canopy height measurements and has been processed (LaLonde *et al*., 2010). Yet, for the purposes of DEM comparison, this was

considered an acceptable limitation as the LiDAR data is likely to provide the most reliable benchmark available (Yamazaki *et al*., 2012). Comparative studies have concluded that LiDAR datasets have the lowest vertical error in comparison to other available DEMs due to density of signal returns (Liu, 2008; Saksena and Merwade, 2015). Using LiDAR as a benchmark when comparing spaceborne DEMs is common practice within flood modelling, providing justification for the adoption of this approach for validation purposes (LaLonde *et al*., 2010; Mason *et al*., 2016).

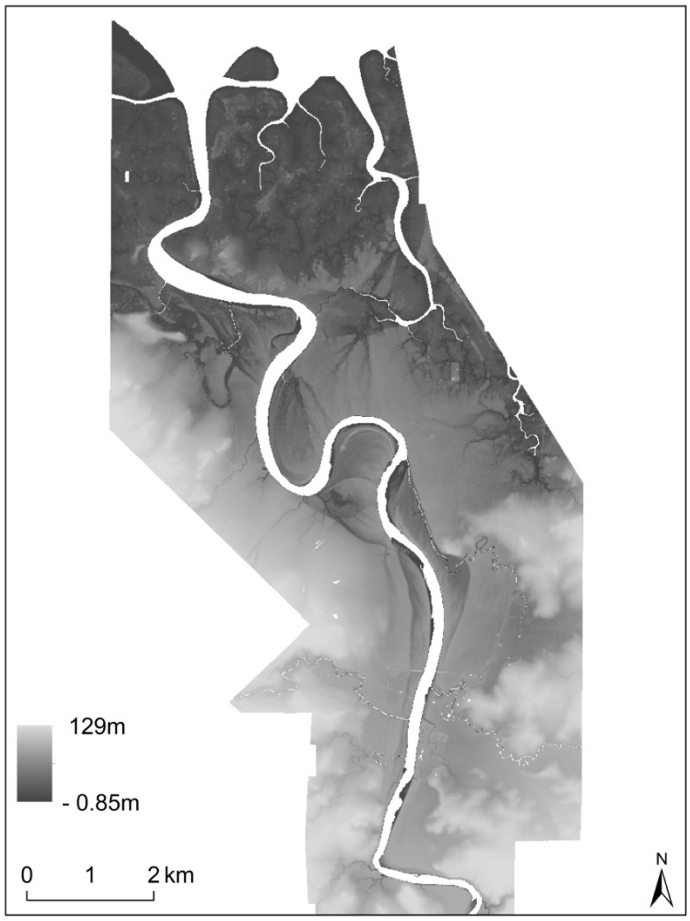

Figure 4 - Map showing LiDAR DTM for the Ba study area

3.1.2 Datasets and Pre-processing

The key DEM datasets used in this study to compare against TanDEM-X DSM and DTMs are listed in Table 2, highlighting the variation in resolution and vertical accuracy. The difference in resolution between the datasets is shown in Figure 5.

Three modifications to TanDEM-X were conducted before processing from a DSM to a DTM. As water bodies in the TanDEM-X were incoherent with high signal disturbance, a water mask was created to exclude these pixels from further analysis, using the auxiliary dataset Water Indication Mask included with the TanDEM-X data (Wessel, 2016) and a rasterized OpenStreetMap™ river network. The vertical coordinate system was converted from the WGS Ellipsoid to the EGM96 Geoid, aligning with the other DEMs using the open-source conversion software NOAA VDatum™ (v3.8). Finally, a block elevation offset of -0.5542m was applied to the TanDEM-X, SRTM and MERIT datasets to correspond with the local mean sea level used in the LiDAR dataset (Thomas, 2012).

Table 2 - Summary characteristics of DEMs used in this study.

DEM	Horizontal resolution	Global relative vertical height error	Reported relative vertical height error in SIDS	Acquisition dates
TanDEM-X	~12m	<2m for low slope areas (<20%) and 4m for high slope areas (>20%) (mission specification) (Rizzoli *et al.*, 2017); 90% linear absolute error <2m (Wessel *et al.*, 2018)	Unknown	2010-2015
SRTM v4.1	~90m and ~30m	16m (mission specification) Rodriguez *et al.*, 2006); <10m (Farr *et al.*, 2007); 3.6m (Berry *et al.*, 2007)	6.2m for 'islands' (Farr *et al.*, 2007); 5-10m Solomon Islands (Albert *et al.*, 2013); 3m Bahrain (Bannari *et al.*, 2017); 25.53m Grenada (Chirico, 2004)	2000
MERIT	~90m	58% <2m (Yamazaki *et al.*, 2017)	Unknown	2000
LiDAR	1m	5-25cm (Baltsavias, 1999)	73.6mm (Thomas, 2012)	2012

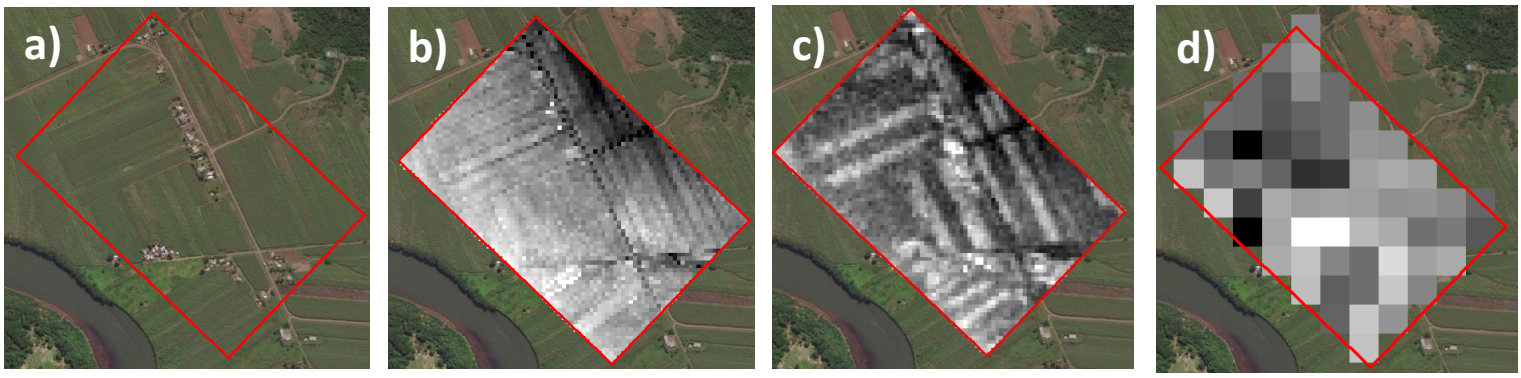

Figure 5 - Comparison between DEMs on a section of floodplain in Ba catchment. a) satellite imagery b) LiDAR c) TanDEM-X DSM d) SRTM

Section 3.1.3 describes the Progressive Morphological Filtering approach for isolated vegetation removal, and Section 3.1.4 details the Image Classification approach used to remove large areas of vegetation, before outlining the hydrodynamic modelling and validation in Section 3.1.5 and 3.1.6. The workflow in Figure 6 shows three different method routes: Progressive Morphological Filtering, Image Classification, and combination, producing seven DTMs for all possible combinations of the

two methods. The seven DTM outputs are identified based on the method combination used to produce the DTM. Reference to specific tools and software are given for transparency and replicability, but the tools are based on generic operations. It is worth noting alternatives to these tools - particularly open-source options – are available. For example, Schreyer *et al.,* (2016) use open-source statistical programming software R packages “raster”, “mmand” and “rgdal” to conduct their Progressive Morphological Filtering method (R Core Team, 2018). Similar segmentation and Image Classification workflows can be utilized in open source software such as Ilastik (Available from: https://github.com/ilastik/ilastik).

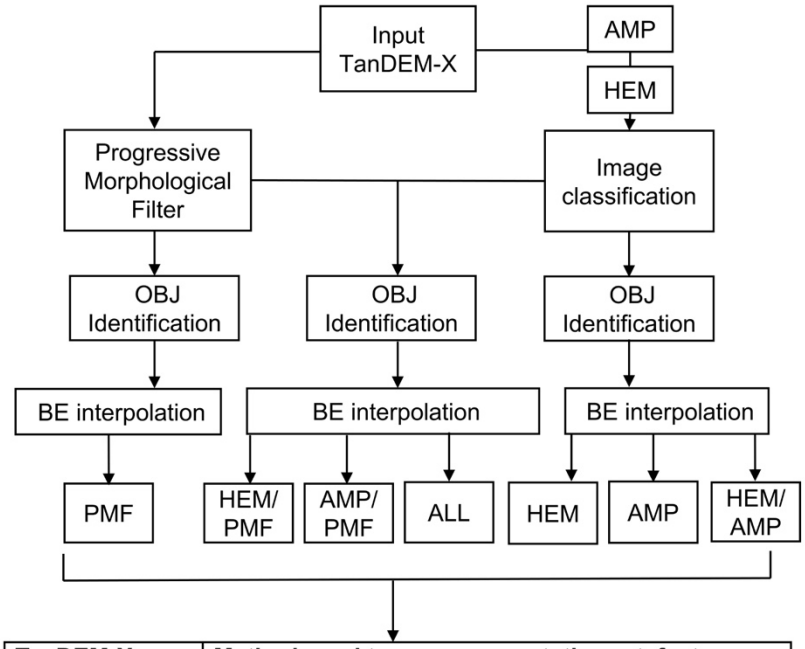

TanDEM-X Digital Terrain Model	**Method used to remove vegetation artefact**
PMF	Progressive Morphological Filtering
HEM	Image Classification of Height Error Map
AMP	Image Classification of Amplitude
HEM/PMF	Combination of Image Classification of the Height Error Map and Progressive Morphological Filtering
AMP/PMF	Combination of Image Classification of the Amplitude Map and Progressive Morphological Filtering
HEM/AMP	Combination of Image Classification of the Height Error Map and Amplitude
ALL	Combination of Image Classification of the Height Error Map and Amplitude and Progressive Morphological Filtering

Figure 6 - Diagram showing the methodology workflow for TanDEM-X processing and the names of the output DTMs created using each combination. 'OBJ' refers to objects and 'BE' refers to bare earth. HEM refers to the TanDEM-X Height Error Map, AMP to amplitude and PMF to Progressive Morphological Filtering. The output table shows the 7 different DTMs produced and which methods have been used to produce the DTM.

3.1.3 Progressive Morphological Filtering

Often used for LiDAR processing (Zhang *et al*., 2003), Progressive Morphological Filtering was utilized by Geiß *et al*., (2015) and Schreyer *et al*., (2016) to identify buildings and vegetation artefacts in the Intermediate-TanDEM-X DEM. A Progressive Morphological Filter conducts an iteration of opening operations on an image using a sequentially-increasing window size to identify artefacts of a defined smallest to largest size using two key operators: erosion and dilation (Zhang *et al*., 2003). The erosion operator (Equation 3) searches the pixels $(x_{p,}y_p)$ within the window size (B) to find the minimum elevation to assign the defined pixel (z_p). The dilation operator (Equation 4) searches for the maximum elevation height within the specified window using the same principle.

$$Erosion = \varepsilon_p = (x_{p,}y_p)^{min}_{\in B}(z_p) \text{ Equation 3}$$

$$Dilation = \delta_p = (x_{p,}y_p)^{max}_{\in B}(z_p) \text{ Equation 4}$$

An opening then sequentially applies an erosion (δ_p) and dilation (ε_p) filter to each pixel in the DEM (z_p) (Equation 5), lowering objects smaller than the window size (B) to the minimum height value through erosion, whilst preserving object structure through dilation (Zhang *et al*., 2003).

$$Opening = \gamma_p = \delta_p \circ \varepsilon_p(z_p) \text{ Equation 5}$$

The morphological opening filter was applied using the ENVI™ (v5.4) Convolutions and Morphology tool. The opening was first performed on the unprocessed TanDEM-X DSM using a minimum window size (B_{3x3}). Further openings were applied subsequently using an increasing window size of three pixels per iteration up to the maximum size (B_{15x15}), totalling five consecutive iterations. Minimum and maximum window sizes and thus the number of iterations necessary between the two were selected based on the smallest and largest object sizes present in the TanDEM-X through visual inspection of Google Earth™ imagery. The output of each iteration identified anomalous pixels in comparison to the other pixels within the window, identifying objects of increasing size. The height

difference (dh) between the output of the opening and the original DEM was established, and an elevation threshold (θ), ranging from 1-4m was applied to each height difference pixel (dh_p), classifying the pixel as an 'object' if above the threshold and 'bare earth' if below (Schreyer *et al*., 2016). This reduces over-flattening of the terrain to the minimum pixel value and is necessary when using highly-detailed terrain data (Zhang *et al*., 2003). Once all objects were identified, the corresponding pixels were removed from the unprocessed TanDEM-X DSM, with the remaining pixels considered 'bare earth'.

$$Bare\ earth = dh_p < \theta$$

$$Object = dh_p > \theta$$

Following Geiß *et al*., (2015) and Schreyer *et al*., (2016), an additional step was implemented before interpolating the 'bare earth' pixels to create a DTM to reduce omission (false negative) and commission errors (false positive). A segmentation, using the ENVI™ (v5.4) Segmentation Image tool, was performed on each output to identify additional 'object' pixels not identified during the opening, as omitted pixels will have the largest effect on the resulting DTM. The segmentation reclassifies 'bare earth' as an 'object' if a certain number of surrounding pixels within a defined neighbourhood have been identified as 'objects', improving homogeneity of 'object' regions. As this process results in the removal of pixels if not part of a defined region size, the 'objects' from the segmentation output were combined with the original 'objects' identified to retain the individual pixels identified such as isolated trees.

All identified 'object' pixels were removed from the DEM, as the opening does not provide adequate information on the height of the object. An Inverse-Distance-Weighting (IDW) interpolation is performed to estimate height values between remaining 'bare earth' pixels to create the PMF DTM (after Schreyer *et al*., 2016).

3.1.4 Image Classification

A second method was employed focusing on the removal of large dense areas of vegetation. Two auxiliary datasets that accompany the TanDEM-X data were utilized to identify 'objects' in this method: A Height Error Map and a map of Amplitude. The Height Error Map, which represents the height standard deviation, is derived using interferometric coherence (Wessel, 2016). The Amplitude map represents radar backscatter as a mean value for all the calibrated amplitudes between SAR images. These auxiliary datasets were chosen for two reasons. Firstly, both datasets provided the highest correspondence between high values and vegetated areas in the study area based on visual inspection of Google Earth™ imagery from the time period of TanDEM-X acquisition (see Figure 2). Secondly, Martone *et al*., (2018) suggest that areas of low interferometric coherence in the TanDEM-X data correlate with vegetated areas, due to an increase in volume decorrelation. As the Height Error Map is derived using interferometric coherence, this dataset is a suitable proxy in the absence of raw estimates of interferometric coherence.

An Image Classification method using the ENVI™ (v5.4) Supervised Image Classification workflow was used to classify the Height Error Map and Amplitude map to define large regions of vegetation. A supervised classification uses training data that is representative of a specific land use class to determine areas of the corresponding dataset that can be identified as the same class (Canty, 2014). Areas of (i) dense vegetation, (ii) mangrove and (iii) cropland, were identified and selected from Google Earth™ imagery to create the training data regions representative of each land use class. Cropland was used as a proxy for 'bare earth', instead of an airplane runway or another land use class, as this was the dominant land cover in the region, and other more suitable land use cover was not present in the domain. The corresponding pixels in these regions for each map were then used to classify the remaining pixels using a maximum likelihood classification based on the discriminant function by Richards (1999) in Equation 6. The class defined using the training data is (w_i), x refers to the dataset, where n is the number of bands, $p(w_i)$ refers to the probability that class (w_i) occurs

in the DEM, $\sum i$ is the determinant of the covariance matrix of the data in each class (w_i), and m_i the mean vector.

$$g_i(x) = 1n\, p(w_i) - \frac{1}{2}\, 1n\, |\sum i| - \frac{1}{2}(x - m_i)^T \sum_i -1\, (x - m_i) \quad \textit{Equation 6}$$

To determine the accuracy of the Image Classification, a confusion matrix was calculated for the Height Error Map and Amplitude classification outputs, using three alternative regions of interest to the regions used as training data for the classification, referred to as 'ground truth' regions (see Figure 7) (Congalton, 1991). The confusion matrices for both classifications are shown in Table 3, calculated using the ENVI™ (v5.4) post-classification Confusion Matrices Using Ground Truth ROIs tool, demonstrating the percentage of pixels classified and the producer and user accuracy of each class. Producer accuracy refers to the probability of correct classification and user accuracy refers to the probability that a given class classification is truly that class (Canty, 2014). Overall, the results demonstrate a 79.11% accuracy for the Height Error Map and a 78.17% accuracy for the Amplitude map by calculating correct pixels/total pixels. The Kappa Coefficient for both confusion matrices was 0.64, calculated to determine the agreement between the ground truth and classification values, whereby 1 equals complete agreement and 0 equals no agreement (Congalton, 1991). These results suggest good overall image classification accuracy, signifying that the 'objects' identified by the process are representative. Nonetheless, Table 3a shows limited capacity to classify between mangrove and forest in the Height Error Map classification, suggesting the height error values for both classes are similar, thus reducing the overall classification accuracy. Table 3b shows a relatively reduced capacity to distinguish between forest cover and cropland in the Amplitude map, although mangrove classification is superior, suggesting that amplitude values between forest and mangrove cover are dissimilar.

Table 3 - Confusion matrices using ground truth regions of interest to determine image classification accuracy of the a) TanDEM-X Height Error Map (HEM) and b) Amplitude map (AMP). Each matrix refers to percentages of pixels classified in each class, as well as overall producer and user accuracy in percent.

a)

HEM	Forest	Mangrove	Cropland	**User accuracy**
Forest	82.23	40.20	2.35	41.42
Mangrove	17.77	53.62	6.23	73.70
Cropland	0	6.17	91.42	96.69
Producer accuracy	82.23	53.62	91.42	

b)

AMP	Forest	Mangrove	Cropland	**User accuracy**
Forest	59.91	2.83	25.97	29.93
Mangrove	0	96.83	1.75	96.56
Cropland	40.09	0.34	72.28	90.03
Producer accuracy	59.91	96.83	72.28	

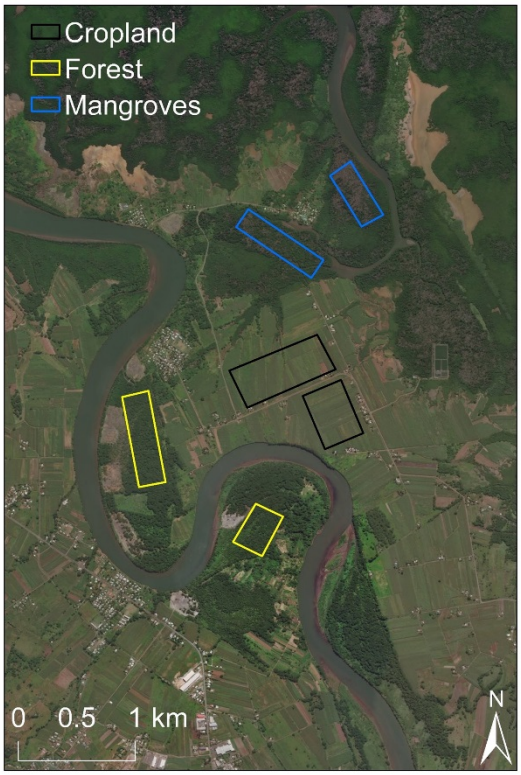

Figure 7 - Map demonstrating the regions of interest used to conduct the image classification, as well as the regions of interest used for ground truth comparison in the confusion matrices.

For the purpose of 'object' identification, a good classification between 'objects' (in this case forest or mangrove) and 'bare earth' (in this case cropland) is required. Despite the little difference in overall classification accuracy, the Height Error Map may have a higher capacity to accurately identify 'objects' in comparison to the Amplitude map due to the performance of the 'cropland' classification. Both the Height Error Map and Amplitude map have limited user accuracy for forest, suggesting forest classification has the most limited classification. Despite the good accuracy of the Image Classification, the external dataset 300m resolution Climate Change Initiative 2015 Land Cover Classification (Available from: https://www.esa-landcover-cci.org/) was used to further assess the general classification percentages for each land use to determine whether the data was likely to be representative of the floodplain land use (Arino and Ramoino, 2017). Overall, cropland was the dominant classification, showing good agreement (see Table 4). Vegetation classification in the

Height Error Map and Amplitude classification was higher than the Climate Change Initiative 2015 Land Cover Classification. This is likely due to the higher resolution, meaning smaller areas of vegetation are resolved in the TanDEM-X-derived datasets. Running an unsupervised classification showed <10 percentage point differences in land cover classification, identifying potential for automation in future work.

Table 4 - Table showing the percentage of pixels classified as cropland, vegetation and mangrove in the supervised image classification. The results are compared to the 300m Climate Change Initiative 2015 Land Cover Map pixel classification.

	Supervised classification pixels (%)		**CCI land use classification (%)**
	HEM	**AMP**	
Cropland	50.48	42.71	60.38
Vegetation	10.7	16.15	6.04
Mangroves	38.82	41.14	33.58

Once validated, the areas identified as forest or mangrove in the classification were identified as 'objects', and removed from the DEM. As the 'objects' identified in this method removed much larger areas than in the Progressive Morphological Filtering, the IDW interpolation was maintained for localized areas but an Elevation Void Filling function in ArcMap™ (v10.5) was used to interpolate larger areas using a plane fitting approach.

3.1.5 Hydrodynamic Modelling

As demonstrated in Figure 6, seven DTMs were produced using Progressive Morphological Filtering, the Height Error Map and Amplitude in isolation and combination. All seven DTMs, as well as the unprocessed TanDEM-X DSM, LiDAR, SRTM and MERIT DEMs were used as the topography input into the sub-grid variant of the hydrodynamic model LISFLOOD-FP (Neal *et al*., 2012a). The MERIT and SRTM 90m models were run in 0.67 minutes and SRTM 30m in 9.5 minutes. All other models were

run at the native TanDEM-X resolution (~12m) with an average run time of 140 minutes. The LiDAR model was run at the resolution of TanDEM-X, not at native resolution (~1m), as minimal improvement is shown with resolutions <50m at the cost of a large computational expense by an order of magnitude every time DEM resolution is reduced by half (Savage *et al*., 2016). This does mean that the other DEMs were compared to the coarsened LiDAR, but this was an acceptable limitation given these justifications. Key model inputs required by the hydrodynamic model include topography-derived variables and boundary conditions (Bates *et al*., 2013). The input variables to the model were identical except for the topography-derived variables (DEM, bank heights and bed elevation). Manning's coefficient friction was fixed at 0.035 for the channel and 0.040 for the floodplain in all models based on a typical agricultural floodplain in the absence of roughness estimates for the region. The sensitivity of the model to a range of coefficient values was not tested, despite the argument that this could lead to uncertainty regarding the impact of roughness on the friction slope and the resultant water surface elevation of the model output (Baugh *et al.,* 2013). Nonetheless, as the model outputs were used as an inter-comparison and not tested against an actual flood event, the uncertainty regarding friction sensitivity was acceptable.

The river channel in the sub-grid variant of LISFLOOD-FP is estimated using bank heights, bed heights and channel width information (Neal *et al*., 2012a). Bank heights were extracted along the perimeter of the river channel in the DEM. Due to the relatively small size of the river reach the widths were measured at a series of points along the river channel whose location was identified using Google Earth™ imagery. Bed elevation was estimated using bank height, river width and return period discharge estimates, such that the channel water level would closely match the banks height at a given return period flow (1 in 2 year in this case: Pickup and Warner, 1976). A binary channel mask (1=water and 0=data) was also employed to overlay the water-masked river channel in the unprocessed TanDEM-X DSM and DTMs, signalling to the model to start 2D floodplain flow at the channel boundary.

The LISFLOOD-FP model requires an input discharge at the upstream boundary and water surface elevation at the downstream boundary (Bates *et al*., 2013). The downstream boundary of the model was fixed at 0m, set at local mean sea level corresponding with the DEMs. The upstream boundary was located 21.72km upstream. Due to a lack of accurate and complete flow gauge data for the Ba river (Yeo *et al*., 2007), a historical flood event time-series could not be used to simulate discharge in the model. Thus, a Regional Flood Frequency Analysis outlined by Smith *et al*., (2015) was conducted to simulate peak discharge estimates (Table 5) at various return periods based on available flow data in hydrologically-similar catchments and rainfall data from the Fiji Meteorological Office.

Table 5 - Peak flow discharges for the modelled return period events estimated using Smith et al.'s (2015) Regional Flood Frequency Analysis method.

Return period event	**Estimated peak discharge (m^3s^{-1})**
50-year	5106
25-year	3544
10-year	2130

Hydrologically similar catchments were clustered by Köppen-Geiger region (tropical), catchment area and average annual rainfall, based on the argument that catchments with similar characteristics have comparable flow behaviour (Smith *et al.,* 2015). These variables were used to estimate peak flow for a particular return period by scaling the predicted mean annual flood using a growth curve model. As tropical catchments had a mean RMSE of 0.39 between modelled and observed events in Smith *et al.,* (2015) – with the second highest error after arid catchments (0.61) - the capacity to represent flow events may be poorer in tropical catchments. Despite these limitations, this method was also utilized in the Government of Fiji's (2017) Climate Vulnerability Assessment due to a lack of alternative flow information, but was found to have reduced predictive capacity for flow events in Fiji's flashy catchments. Therefore, an indicator of extreme rainfall (Q98) was included in the growth curve model to improve the estimation of peak flows in flashy catchments with high frequency

extreme rainfall events. Q98 represents the percentage of average annual rainfall falling within 2% of wet days, calculated using daily rainfall data for the Ba region as 18%.

A hydrograph was created using the Rational Method which takes the peak discharge estimates for the 50, 25 and 10-year return period events, and the catchment time to concentration of 5.43 hours to produce a hydrograph (see Table 5 and Figure 8). The total simulation duration was set at 48-hours following historical events in the region. Time to concentration was calculated using the velocity method detailed in Woodward *et al.*, (2010). This method calculates time to concentration by the sum of travel times from the most hydraulically distant point in the watershed to the downstream outlet, assuming three flow types: sheet flow, shallow concentrated flow and open channel flow. Three return-period events were simulated as larger 'valley-filling' floods can be less sensitive to floodplain dynamics and may therefore be less sensitive to DEM error (Schumann *et al.*, 2009).

Models using all eleven DEMs for the three return period events were simulated, and a maximum flood extent map was produced for each model run.

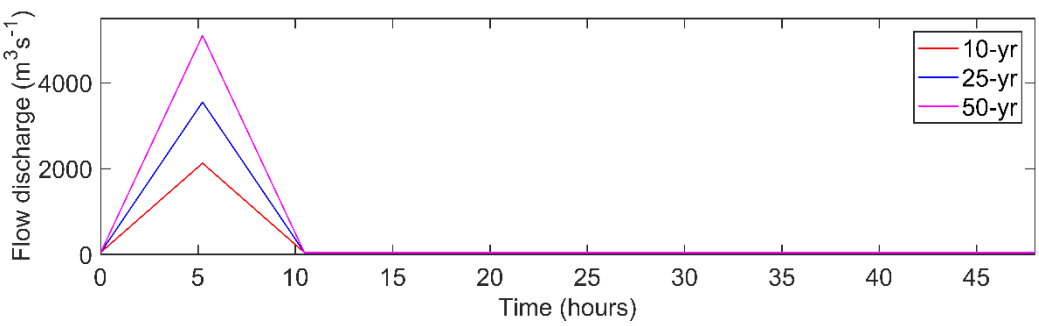

Figure 8 - Rational hydrograph for the 50, 25 and 10-year flood events, using peak flow estimations from the Regional Flood Frequency Analysis. The event simulated was 48 hours, with a time to concentration of 5.23 hours for the ascending and descending limb of the hydrograph.

3.1.6 Model Evaluation

The flood model outputs were evaluated using binary pattern-matching performance metrics based on a contingency table, commonly-used in flood modelling to validate model outputs (Hunter, 2005; Pappenberger *et al.*, 2007; Schumann *et al.*, 2009; Stephens *et al.*, 2014). As the LiDAR model is

considered as the 'truth' for the purposes of this study, the DEM that produces the flood extent and water surface elevation with the closest fit to the LiDAR model is considered the most successful candidate. The LiDAR model is not necessarily an exact representation of floodplain topography. Yet, for the purposes of DEM comparison, this was considered an acceptable limitation as the LiDAR data is likely to provide the most reliable benchmark available. A contingency table, as described in Stephens *et al*., (2014), was used to assess whether a pixel in the model is correctly/incorrectly identified as wet/dry (see Table 6). The metric was then calculated using the number of pixels in each category (A, B, C and D) to assess accuracy.

Table 6 - Contingency table (after Stephens et al., 2014).

	Present in observation	**Absent in Observation**
Present in model	A	B
Absent in model	C	D

Hunter (2005) and Stephens *et al*., (2014) stress the importance of calculating several binary metrics when assessing model performance, as individual metrics can present a bias to models under predicting, over predicting, or with large dry domains. Three binary metrics were calculated, as well as the Root Mean Square Error (RMSE) of the model water surface elevation, to determine the most successful model. The Critical Success Index, or $F^{<1>}$ score, is the most commonly-used binary metric when assessing flood model skill (Equation 7), and the $F^{<2>}$ and $F^{<3>}$ scores penalise under prediction and over prediction respectively (Equation 8 and 9) (Stephens *et al*., 2014). If a similar pattern is shown in all three metrics, then the Critical Success Index is unlikely to display bias towards over prediction in these models (Hunter, 2005).

$$CSI = \frac{A}{A+B+C} \quad \textit{Equation 7}$$

$$F^{<2>} = \frac{A-C}{A+B+C} \quad \textit{Equation 8}$$

$$F^{<3>} = \frac{A-B}{A+B+C} \quad \textit{Equation 9}$$

Stephens *et al*., (2014) suggest that calculating the RMSE of water surface elevation between a model and observation provides a useful metric to communicate the depth prediction skill of a model (Equation 10). The RMSE is a common statistical accuracy measure used to determine error between predicted and observed values (Wessel *et al*., 2018).

$$RMSE = \sqrt{\frac{\sum_{i=1}^{n}(P_i - O_i)^2}{n}} \quad \textit{Equation 10}$$

3.2 Results

The maximum flood extents for each model for the 50-year return period flood event are outlined for the ~12m models, followed by the metric results for all three return-period events.

3.2.1 How Well Does the Unprocessed TanDEM-X DSM Perform?

The maximum flood extents shown in Figure 9a demonstrate that the unprocessed TanDEM-X DSM has an improved capacity to model flooding in comparison to SRTM, suggesting improved DSM quality over SRTM. The metric scores outlined in Table 7 also indicate a marked improvement and are echoed by the $F^{<2>}$ and $F^{<3>}$ scores in Table 8.

The MERIT DTM has higher skill than both SRTM and TanDEM-X DSMs and SRTM 30m does not improve results significantly in comparison to SRTM at 90m, indicating the relative importance of a DTM over horizontal resolution. Two key areas that are flooded in the LiDAR model and the MERIT DTM but not TanDEM-X DSM and SRTM are the mangroves at the downstream boundary and the dense patches of vegetation along the river on the floodplain, demonstrating the impact of vegetation artefacts on model performance. The metrics were therefore calculated for the 50-year model including and excluding the mangroves at the downstream boundary and the 25 and 10-year models were calculated excluding mangroves, as the poor accuracy over mangrove areas reduces the ability to assess the DTMs upstream, which is of more interest in flood risk assessment. The mangroves provide a tough test case for an X-band InSAR such as TanDEM-X and are inherently difficult to model. Mangroves have a closed canopy meaning little ground return is available for the area (Mitchell *et al*., 2007), so the TanDEM-X DSM has a particularly difficult time measuring 'bare earth'. Furthermore, LiDAR ground truthing was not conducted by Thomas (2012) in the mangroves, so the authors cannot determine the accuracy of the LiDAR in this location. This creates a second justification for removal of mangroves in the analysis, as the benchmark LiDAR accuracy over these areas is unknown. This study does not suggest that the methods detailed can entirely remove mangrove regions, and the results show poorer accuracy in mangrove-covered areas. An artificial boundary either side of the mangroves at the downstream boundary is produced due to the constrained model domain (see Figure 3c), dictated by the LiDAR data coverage used as the

benchmark.

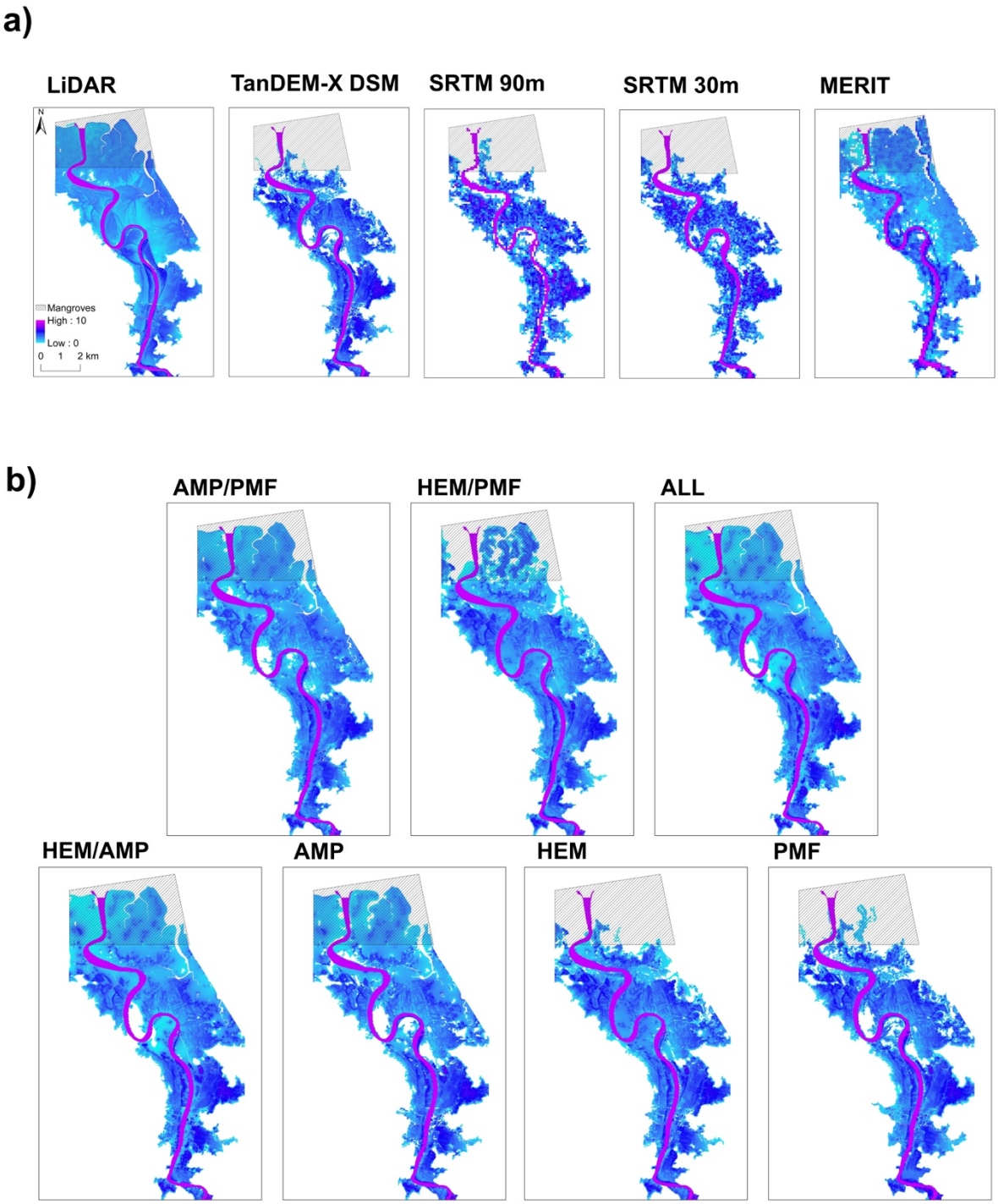

Figure 9 - a) Modelled flood extents for the LiDAR, TanDEM-X DSM, SRTM and MERIT DEMs for the 50-year return period event at ~12m resolution. b) Modelled flood extents for the 7 TanDEM-X DTMs for the 50-year return period event. Acronyms for the DTMs correspond with the method used: AMP describes use of TanDEM-X Amplitude map, HEM describes use of TanDEM-X Height Error Map and PMF Progressive Morphological Filtering.

3.2.2 TanDEM-X DTM Comparison Analysis

Figure 9b shows all seven TanDEM-X DTM model flood extents, produced using combinations of the Image Classification of the Height Error Map and Amplitude map and Progressive Morphological Filtering as described in Figure 6.

The PMF DTM, produced using only Progressive Morphological Filtering, is the worst performing TanDEM-X DTM when input into the hydrodynamic model, with the lowest agreement of the seven DTMs in maximum flood extent simulation and Critical Success Index (Table 7). The PMF DTM is also the worst-performing DTM created using one method.

The AMP/PMF is overall the most consistently superior DTM when visually comparing flood outputs as well as for overall model skill, despite the remaining presence of artefacts along the channel edge in the model output (see Figure 9b).

DTMs created using a combination of methods have higher agreement with the LiDAR model when visually comparing and assessing binary metric performance in comparison to DTMs created using one method. AMP/PMF is the most successful combination method. HEM/PMF has higher model skill than HEM/AMP and ALL, except for when mangroves are included in binary metric calculation for the 50-year event. There is little difference between HEM/AMP and ALL DTMs metric performance in Table 7 and the visual flood extents.

In general, when Progressive Morphological Filtering is combined with Image Classification of either the Height Error Map or Amplitude (AMP/PMF and HEM/PMF) the accuracy of the flood extent is improved in comparison to when the methods are used in isolation or in other combinations. This suggests that a combination of a coarse and fine processing methods produces the best-performing DTMs overall.

3.2.3 TanDEM-X DTM Selection

When analysing all 11 flood extents in Figure 9 and Table 7 and 8, AMP/PMF was the DTM selected as the most successful candidate for flood inundation and water surface estimation in comparison to the LiDAR model. This method is therefore considered the most suitable TanDEM-X processing method, creating a DTM with a higher capacity to model flooding in comparison to the other TanDEM-X DTMs and MERIT DTM, as well as the unprocessed TanDEM-X and SRTM DSMs.

The AMP/PMF DTM, as well as the other combination TanDEM-X DTMs, have a higher model skill than the MERIT DTM. As the MERIT DTM is currently most often used in data-sparse flood inundation modelling whereby LiDAR data is unavailable, it is important to directly compare the results of the AMP/PMF DTM to the MERIT DTM to consider the scale of improvement shown (see Figure 10). The AMP/PMF DTM has a Critical Success Index score of 12-14 percentage points higher than the MERIT DTM (Table 7) and performs consistently highest when tested for under and over prediction (Table 8), showing improved flood extent model skill. Water surface elevation prediction skill is also greater, with a RMSE of 0.11-0.21m lower than the MERIT DTM (Table 7).

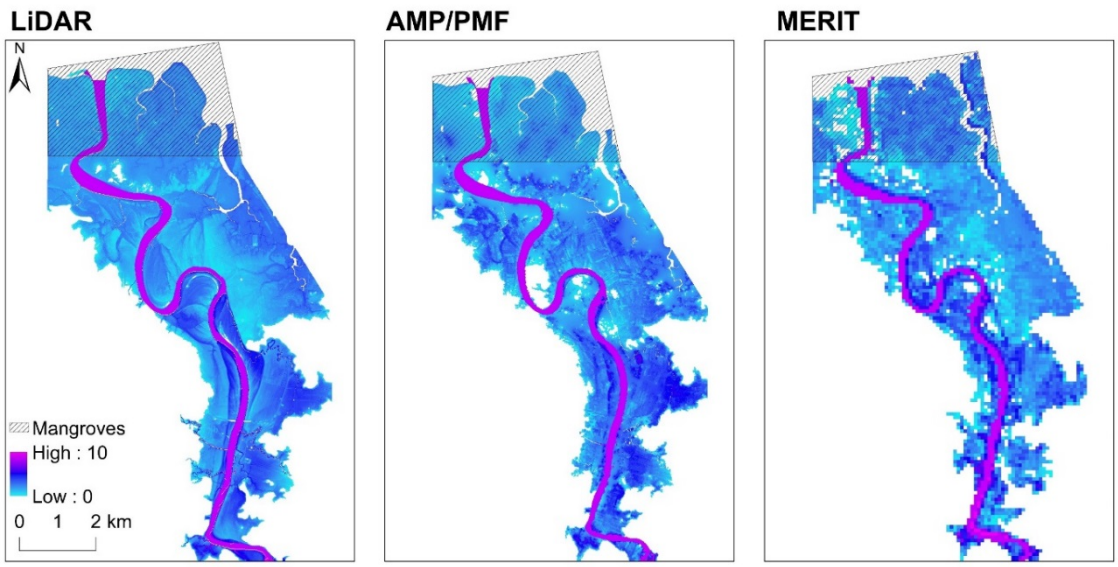

Figure 10 - Modelled flood extents of the two TanDEM-X DTMs AMP/PMF and MERIT in comparison to the LiDAR model for the 50-year return period event.

Table 7 – The left of the table shows the scores for each DEM for the Critical Success Index binary performance metric for each return period when compared to the LiDAR flood extent which is taken here as a benchmark. Scores range from 0 (no agreement) to 1 (total agreement). The right side of the table shows Root Square Mean Error (RMSE) between the water surface elevation of each DEM flood output and the LiDAR model. The higher the score the higher the error, reported in meters. The red highlighted boxes indicate the worst performing DEM in the category and the green highlighted boxes indicate the best performing DEM.

DEM	**Critical Success Index (0-1)**				**Water Surface Elevation RMSE (m)**			
	50-yr		***25-yr***	***10-yr***	***50-yr***		***25-yr***	***10-yr***
	Including mangroves	***Excluding mangroves***			***Including mangroves***	***Excluding mangroves***		
TanDEM-X DSM	0.61	0.75	0.70	0.57	0.72	0.75	0.65	0.50
SRTM 90m	0.58	0.69	0.63	0.48	0.88	0.95	0.84	0.66
SRTM 30m	0.58	0.71	0.65	0.51	0.85	0.91	0.81	0.65
MERIT	0.77	0.77	0.72	0.60	0.63	0.68	0.62	0.52
PMF	0.64	0.77	0.71	0.58	0.68	0.70	0.61	0.46
HEM	0.67	0.84	0.78	0.63	0.62	0.62	0.55	0.43
AMP	0.86	0.84	0.80	0.66	0.51	0.59	0.54	0.45
HEM/PMF	0.84	0.89	0.85	0.69	0.52	0.53	0.49	0.42
AMP/PMF	0.90	0.89	0.85	0.74	0.42	0.49	0.41	0.37
HEM/AMP	0.90	0.88	0.83	0.65	0.52	0.58	0.55	0.43
ALL	0.90	0.88	0.83	0.67	0.51	0.57	0.54	0.48

Table 8 - Scores for each DEM, ranging between -1 (no agreement) to 1 (total agreement). The 50-year return period scores are calculated including and excluding mangroves, and the 25 and 10-year event scores are calculated excluding mangroves. The red highlighted boxes indicate the worst performing DEM in the category and the green highlighted boxes indicate the best performing DEMs.

DEM	$F^{<2>}$ (-1 to 1)				$F^{<3>}$ (-1 to 1)			
	50-yr		***25-yr***	***10-yr***	***50-yr***		***25-yr***	***10-yr***
	Including mangroves	*Excluding mangroves*			*Including mangroves*	*Excluding mangroves*		
TanDEM-X DSM	0.56	0.69	0.64	0.47	0.28	0.57	0.46	0.24
SRTM 90m	0.49	0.59	0.52	0.34	0.24	0.48	0.36	0.1
SRTM 30m	0.22	0.48	0.37	0.12	0.53	0.65	0.58	0.40
MERIT	0.65	0.66	0.61	0.45	0.65	0.64	0.56	0.34
PMF	0.59	0.71	0.64	0.48	0.34	0.61	0.5	0.27
HEM	0.64	0.78	0.72	0.54	0.42	0.73	0.62	0.37
AMP	0.82	0.79	0.74	0.56	0.76	0.73	0.66	0.41
HEM/PMF	0.8	0.84	0.79	0.58	0.71	0.82	0.75	0.48
AMP/PMF	0.87	0.84	0.8	0.64	0.84	0.81	0.76	0.59
HEM/AMP	0.85	0.82	0.77	0.55	0.84	0.81	0.73	0.41
ALL	0.85	0.83	0.77	0.56	0.85	0.82	0.73	0.47

3.3 Discussion

Consistently for all four metrics, TanDEM-X DSM has a higher flood estimation accuracy than the SRTM DSM, but worse than the MERIT DTM and the TanDEM-X DTMs. Crucially, just because TanDEM-X has a higher resolution and higher average vertical accuracy, pre-processing to a DTM is still required to remove surface artefacts, aligning with previous review of SRTM and LiDAR in hydrodynamic modelling (Bates, 2004; 2012; Sampson *et al.*, 2016).

TanDEM-X has a higher accuracy than SRTM in comparison to LiDAR for three key reasons: (i) acquisition date (ii) spatial resolution (iii) vertical accuracy. As TanDEM-X was acquired between

2010-2015 (Rizzoli *et al*., 2017), and the LiDAR data was acquired in 2012 (Thomas, 2012), the characteristics of the floodplain captured are likely to be more similar in comparison to SRTM which was acquired in 2000 (Rabus *et al*., 2003), following changes in land use during the period (Yeo, 2015). Furthermore, as TanDEM-X has a higher spatial resolution and a higher specified vertical accuracy than the SRTM mission (Rizzoli *et al*., 2017; Wessel *et al.,* 2018), the finer-scale characteristics of the floodplain morphology will be better-represented than in the SRTM.

Although the MERIT DTM is an error-reduced SRTM product at 90m, the unprocessed TanDEM-X DSM has a lower flood prediction accuracy for flood extent and water surface elevation. It is apparent in Figure 9a that the main areas which remain dry in TanDEM-X but not in the LiDAR or MERIT DTMs are the mangroves at the downstream boundary and large patches of tall vegetation along the floodplain, leading to poorer flood extent prediction skill. Water surface elevation RMSE in the TanDEM-X DSM is also higher than the MERIT DTM, likely due to vegetation artefacts blocking key flow pathways across the floodplain surface (Mason *et al*., 2011). This highlights the pronounced presence of vegetation artefacts in the TanDEM-X, largely because the X-band SAR system has limited penetration of the canopy (Martone *et al*., 2018; Wessel *et al.,* 2018). Therefore, presence of mangroves strongly affects the overall results potentially masking the capability of the DEM in upstream areas. The skill of the model in these upstream areas is in fact more critical as these are the more populated areas and thus of more interest in flood risk assessment, especially considering the accuracy of the LiDAR benchmark in the mangrove area is also unknown. Although mangroves appear to have been removed in Yamazaki *et al*.'s (2017) MERIT DTM using height information indicated in the ~90m resolution global vegetation height map (Simard *et al*., 2011), the methods used to remove these are coarse-scale and thus not suitable for TanDEM-X. Therefore, further investigation is required to optimize mangrove-removal for TanDEM-X for the DEM to be applicable for hydrodynamic modelling at the global scale.

3.3.1 TanDEM-X DTM Processing: A Balance

The DTM produced using the AMP/PMF method is the most suitable candidate for modelling both flood extent and water surface elevation in comparison to the LiDAR model, followed by HEM/PMF. This underpins the argument that previously-established DEM processing methods used for both fine-resolution (<5m) LiDAR data (Zhang *et al*., 2003; Schreyer *et al*., 2016) or coarse-scale (>90m) InSAR data (Baugh *et al*., 2013; Yamazaki *et al*., 2017) cannot be directly applied to the TanDEM-X data in isolation, indicating the need for a balance between coarse and fine-scale processing. When the methods are used in isolation the resulting DTM still contains too many artefacts to provide a smooth representation of 'bare earth' topography, as shown in the binary metric performance for PMF, AMP and HEM DTMs in comparison to AMP/PMF, HEM/PMF, HEM/AMP and ALL DTMs (see Table 7 and 8). The results are also consistent with Geiß *et al*.'s (2015) argument that the spatial resolution of TanDEM-X still limits the use of Progressive Morphological Filtering in isolation, as even the smallest window size (3x3 pixels) is larger than individual trees or buildings, with the PMF DTM ranking as the worst-performing TanDEM-X DTM.

Initial assumptions would suggest that the more artefacts identified and removed from the DEM, the smoother and thus more representative the resulting DTM, justifying the iterative procedure (Geiß *et al*., 2015; Yamazaki *et al*., 2017). However, the AMP/PMF is clearly the most consistently-superior DTM across all metrics when compared against the other combination DTMs, despite using fewer methods to remove artefacts. Although the ALL DTM, whereby all three methods are combined, has particularly good skill for the 50-year return period event, this is likely influenced by the 'valley-filling' flood effect, whereby larger floods are less sensitive to floodplain error, meaning little difference in performance is identified using the binary metric assessment between the combination methods (see Table 7). The ALL DTM also shows superior performance when mangroves are included in binary metric calculation for the 50-year return period event, suggesting that the

capacity to flood the mangrove area may provide a bias in the results towards the ALL DTM in comparison to other DTMs, leading to an overestimation of model skill.

Results showing that HEM/AMP and ALL DTMs have little difference between metric results also reinforces the need for a balance between large and fine scale artefact removal, as the results indicate that adding another method to remove artefacts doesn't necessarily improve the output DTM. This is echoed by Baugh *et al*.'s (2013) comparison with Coe *et al*., (2008) and Paiva *et al*.'s (2011) SRTM vegetation removal studies, indicating that larger modification does not necessarily improve accuracy. Therefore, although a combination of methods improves TanDEM-X DTM flood prediction accuracy over methods in isolation, a delicate balance between fine and coarse scale processing is required to process TanDEM-X data, as the AMP/PMF DTM (and to a lesser-extent HEM/PMF DTM) demonstrate the best performance overall for the various-sized flood events, and particularly for the smaller events whereby DEM error is more influential (Schumann *et al*., 2009).

Despite the successful use of interferometric coherence estimates to detect vegetation in the TanDEM-X DSM by Martone *et al*., (2018) and the superior classification accuracy of the Height Error Map in comparison to the Amplitude map (see Table 3), the finding that AMP/PMF has a better flood prediction accuracy than when the Height Error Map – an error map created using interferometric coherence – is used to produce the output DTMs HEM, HEM/PMF and HEM/AMP suggests that interferometric coherence is not necessarily the most useful indicator for vegetation artefact at this site when compared to the Amplitude map. Perhaps because the Height Error Map is derived using interferometric coherence as opposed to being a direct indicator (Wessel, 2016), the capacity to remove vegetation artefact using the Height Error Map as opposed to true interferometric coherence estimates may be different. As AMP/PMF is the most suitable DTM candidate, the Amplitude map clearly has a good capacity to identify vegetation objects despite the Image Classification showing relatively lower accuracy between 'forest' and 'cropland' classification. Without information on suggested amplitude and interferometric coherence values for both 'forest'

and ‘mangrove’, explanation for this result is limited, so further investigation into the use of amplitude as an indicator of surface artefacts in the TanDEM-X DSM should be conducted.

3.3.2 Future Application

Overall, this study outlines the first results using TanDEM-X as an unprocessed DSM and a processed DTM in a hydrodynamic model. These results demonstrate that when TanDEM-X is processed to produce a DTM using a combination of methods, it greatly improves flood estimates in comparison to both SRTM and MERIT, signifying potential for use of higher resolution, globally-available TanDEM-X data for flood modelling. Specifically, the TanDEM-X AMP/PMF DTM greatly improves on the capacity to model both flood extent and water surface elevation.

However, this study only investigates the TanDEM-X DSM and DTMs in one catchment, despite the argument that model sensitivity to a DEM differs between catchments, which may lead to divergent conclusions when applied elsewhere. The method was not applied to another study area due to limited access to TanDEM-X data, meaning there are several ways TanDEM-X and the AMP/PMF method should be tested in other sites to validate the observations of TanDEM-X performance in this study. These include investigating the use of TanDEM-X for inundation prediction in other small data-sparse catchments within SIDS and elsewhere, urban catchments and larger river basins. Modelled flood extents using both the TanDEM-X DSM and AMP/PMF DTM should also be validated against Synthetic Aperture Radar flood observation images and other validation data to determine whether TanDEM-X has suitable predictive skill in comparison to actual flood events (Bates, 2012). Yet, despite these caveats, the accuracy metrics in this paper are concurrent with arguments in the literature i.e. the results show that having a DTM improves prediction over DSM (Bates, 2012) and higher resolution DTMs produce more accurate topographic representations and hence better flood estimates (Horritt and Bates, 2001; Sanders, 2007). Therefore, it is likely that TanDEM-X will have a capacity to improve flood estimates in other locations with similar characteristics, but additional

work is needed to verify this. Further processing is also likely to be required in urban catchments due to presence of building artefacts in the TanDEM-X DSM.

There are key barriers that are likely to reduce the use and further validation of this TanDEM-X AMP/PMF DTM approach globally, but also specifically in SIDS. The TanDEM-X data is not open-source, but available through the German Aerospace Center (DLR) following an application process for scientific use and a cost of ~€100/tile (Wessel, 2016). As it is much easier to access the open-source globally-available SRTM or MERIT, e.g. MERIT has been released free for non-commercial use by Yamazaki *et al*., (2017), a scientific community familiar with these datasets is likely to continue using these DEMs until access to TanDEM-X is easier and/or proved to be more effective (i.e. worth the additional effort to both get the data and apply new methods). This is specifically likely to hamper TanDEM-X application in SIDS due to the limited capacity or resources to implement new methodologies and datasets to existing flood risk assessment (Yeo, 2015). The fact that almost two years after the release of the TanDEM-X DEM (Moreira, 2017), there has been no study demonstrated the suitability of TanDEM-X for flood modelling until now, despite this being an obvious application area, is an indication of these access and capability issues.

It is worth noting that a suitable error-reduced DTM from SRTM was only produced 17 years after the SRTM DSM release despite the open-source availability of SRTM (Schumann *et al*., 2014). Without wider accessibility of TanDEM-X, the capabilities of TanDEM-X for flood modelling may be realized much more slowly than SRTM, and quality of DEM data will remain the key limitation to high-accuracy hydrodynamic modelling for years to come (Schumann *et al*., 2014; Sampson *et al*., 2016). This would be a significant limitation to future flood modelling in data-sparse areas, and specifically SIDS, whereby better flood risk assessment is urgently needed (Hay and Mimura, 2013; Nurse *et al*., 2014). The release of 90m TanDEM-X in October 2018 (DLR, 2018) may accelerate the uptake of the data for flood applications, although as was the case with SRTM the results in this

thesis suggest that a vegetation removal algorithm will be needed. Notably, Airbus (2019) have released a global DTM product WorldDEM™ from the TanDEM-X DSM, providing 'bare earth' elevation values at 12m resolution. Nonetheless, this data must be purchased privately at a significant cost of $20 per km^2 and a minimum purchasing order of $100km^2$, reducing the likelihood of uptake by economically-limited SIDS. No information has been published regarding the processing method used to produce WorldDEM™.

Thus, it is timely that this study provides an insight into the competency of TanDEM-X for flood modelling, highlighting key methodological approaches to process the data, and identifying gaps for further investigation. Continued exploration of other potential artefacts in the TanDEM-X DSM such as possible striping error causing a repetitive undulation in the elevation heights are necessary but were beyond the scope of this study. Following the analysis of TanDEM-X in Ba, Fiji, there is confidence that the results from this study will be broadly applicable to other floodplains that share similar characteristics. Nevertheless, the AMP/PMF method should be applied in other study sites to validate the results of this study.

3.4 Chapter Conclusion

The aim of this chapter was to identify whether an appropriate method can be used to process TanDEM-X for use in a hydrodynamic model, and whether this improves flood estimates in comparison to already-existing global DEMs SRTM and MERIT in a SIDS context. The unprocessed TanDEM-X DSM did improve flood estimates over the SRTM DSM when input into a hydrodynamic model, but not the MERIT DTM, emphasizing that although TanDEM-X has a higher resolution, this does not negate the need for surface artefact processing from a DSM to a DTM. This study also demonstrates the first application of a method to process the TanDEM-X DSM to a DTM for use in a hydrodynamic model. The results identified that the method combining the Image Classification of the TanDEM-X auxiliary Amplitude map and Progressive Morphological Filtering (AMP/PMF DTM) is the most appropriate vegetation-removal method for TanDEM-X. When using the AMP/PMF method

to produce a DTM, the Critical Success Index measuring flood extent accuracy relative to the LiDAR model is 12-14 percentage points higher than the MERIT DTM, and the water surface elevation RMSE is 0.11-0.21m lower than the MERIT DTM. This indicates that when TanDEM-X is processed using this method, flood estimates are greatly improved in comparison to already-existing DEMs used in flood modelling. This provides substantial promise for TanDEM-X in hydrodynamic modelling, specifically in SIDS whereby a high-resolution but comparatively less-expensive DEM is critical to improve flood risk assessment in relatively small catchments typical in the region, under both current and future extreme rainfall scenarios. The improved capabilities for flood modelling, along with suitable methods for processing data highlighted for the first time in this study, should provide stimulus for the application of this data and approach to a range of study sites to both validate and extend the use of TanDEM-X to improve future flood modelling.

Chapter 4 – Thesis Conclusion

A key conclusion of Chapter 2 was that although SIDS undoubtedly have an extraordinary risk to hydro-meteorological hazards, there is a mismatch between the level of risk and the capacity to estimate risk due to an inadequacy of available data. Previous estimates of flood hazard in SIDS have relied upon near-global and freely-available datasets such as the SRTM at ~90m (Albert *et al*., 2013). Such datasets facilitate the modelling of flood hazard but are limited by the high vertical error (~10m: Rodriguez *et al*., 2006) and relatively-coarse horizontal resolution (~90m) in relation to the scale required to adequately represent small SIDS catchments (<1000km^2). As a result, flood hazard estimates relying on these datasets are insufficient for the assessment of flood risk in SIDS, but to date have been the best-available option besides expensive LiDAR acquisition (Albert *et al*., 2013). Based on the argument that a highly accurate topographic dataset is a key input for improving accurate flood hazard estimation, this thesis aimed to address this deficit by focusing on whether the recently-released TanDEM-X DEM could improve flood estimates in comparison to frequently-used datasets SRTM and MERIT. However, as TanDEM-X is a DSM, firstly a method to process the TanDEM-X to a DTM was required. Chapter 2 summarised the different DEMs frequently used in flood modelling and identified the key ways these datasets have been processed to DTMs. Overall, it was determined that the methods used to process LiDAR at the fine-scale (<5m) and methods used to process SRTM (~90m) may not be applicable to the resolution of TanDEM-X (~12m) (Geiß *et al*., 2015, Schreyer *et al*., 2016), although indicators of amplitude and interferometric coherence available for TanDEM-X may be utilised to remove vegetation height from the DSM (Breidenbach *et al*., 2010; Martone *et al*., 2018).

Given this clear disparity between flood risk and sufficient data identified in Chapter 2 and calls to investigate whether TanDEM-X could be used as a suitable DEM for hydrodynamic models (e.g. Yan *et al*., 2015; Mason *et al*., 2016), Chapter 3 aimed to determine whether the newly-released

TanDEM-X could firstly be processed from a DSM to a DTM for input into a hydrodynamic model. Three methods were implemented to produce seven TanDEM-X DTMs using combinations of Progressive Morphological Filtering and Image Classification of Amplitude and Height Error Maps. This investigation was a necessary step in determining whether TanDEM-X has the capacity to improve flood estimates. A LiDAR model was developed as a benchmark along with flood extents produced using the SRTM DSM and SRTM-based MERIT DTM.

Relating back to the two research questions steering the investigation in this thesis as shown again below for reference, two conclusions were reached in Chapter 3.

1) How can artefacts be removed from TanDEM-X to create a suitable Digital Terrain Model for input into a hydrodynamic model?
2) Are flood estimates improved using TanDEM-X in comparison to SRTM and MERIT?

Firstly, although the TanDEM-X DSM has a horizontal resolution (~12m) and relative vertical accuracy (<2m in low slope (<20%) areas and <4m in high slope (>20%) areas: Rizzoli *et al*., 2017), it does not improve flood estimates over the ~90m MERIT DTM, demonstrating the importance of artefact removal for improved flood estimates regardless of horizontal resolution. This suggests that having a DTM of SIDS catchments is of greater importance for flood hazard simulation than horizontal resolution. TanDEM-X does improve estimates over the SRTM DSM however.

Secondly, the results of the DTM-processing methods showed that a balanced combination of methods produced elevation estimates that best fit the LiDAR model. The method combining the Image Classification of the TanDEM-X Amplitude map and Progressive Morphological Filtering produced the TanDEM-X DTM (AMP/PMF) considered as the most suitable candidate for improved flood hazard estimates in the Ba catchment. The research identified in Chapter 2 detailing the use of interferometric coherence and amplitude estimates for vegetation detection in the TanDEM-X are supported by the conclusions of Chapter 3, suggesting that estimates of these variables can be

utilised in a DTM-processing workflow to remove vegetated pixels from the unprocessed TanDEM-X DSM.

As a result, the methodology developed in Chapter 3 produced a DTM from the TanDEM-X DSM that has the capacity to improve flood estimates relative to the benchmark LiDAR model in comparison to commonly-used DEMs SRTM and MERIT, providing a sufficient conclusion to both research questions posed at the start of this thesis. Therefore, this thesis concludes that TanDEM-X has the capacity to improve flood hazard estimates in SIDS, offering a starting point for improving overall flood risk estimates under current and future extreme rainfall event scenarios. However, there are significant barriers to SIDS adopting the TanDEM-X DTM for flood hazard mapping as the TanDEM-X DEM is not open-access. The introduction of TanDEM-X in SIDS may therefore be slow, and thus a focus on providing the TanDEM-X data for SIDS should be prioritised to determine whether TanDEM-X can be used to improve flood hazard estimates in these locations.

4.1 Key Limitations

The method outlined in this thesis provided a TanDEM-X DTM which improved flood estimates over SRTM and MERIT. However, it is important to understand the limitations of the processes and assumptions made, which may affect the conclusions given.

Although the TanDEM-X DTMs were compared with a LiDAR model as a benchmark - in agreement with common practice amongst the literature (Yamazaki *et al*., 2012) - it is important to reiterate that while the LiDAR data has an extremely small vertical error (5-20cm: Baltsavias, 1999), the hydrodynamic model simulation does not necessarily represent the flood event because of uncertainties in other elements of the model structure, boundary conditions and parameters, but is likely the best simulation available. As topographic data is a key model input affecting the hydrodynamics of the flood model (Bates, 2012), the data with the highest vertical accuracy are

likely to produce the most reliable simulations (Mason *et al*., 2015). Thus, without information available for the actual flood events simulated (e.g. gauge data, flood extent and depth information for a historical event), there is a level of uncertainty as to whether the LiDAR model can replicate characteristics of a particular flood event. However, it is well-acknowledged in the literature that hydrodynamic model simulations using LiDAR have high accuracy (Marks and Bates, 2000; Schumann *et al*., 2009), and thus this uncertainty is acceptable for benchmark purposes when comparing other DEMs in the absence of other available validation data.

Evidently, with access to ground truth information such as GPS-related elevation data, or validation data such as Synthetic Aperture Radar imagery of a flood extent, the different DEMs could be additionally evaluated. Firstly, to validate the performance of the LiDAR model to determine whether it produces the most accurate flood output, and subsequently to validate overall model skill for each DEM. Future work should aim to incorporate this validation data, where available, for the catchment and utilise the data to validate the methodology in other test sites. Unfortunately, as is characteristic of many other data-sparse locations, these datasets were not available to the author's knowledge at the time of this project. Nevertheless, the open-access availability of Sentinel-1 Synthetic Aperture Radar imagery through the European Space Agency's Copernicus Open Access Hub (https://scihub.copernicus.eu/) may mean that future flood events across Fiji and other SIDS could be captured and utilised for validation purposes.

Furthermore, using a hydrodynamic model to understand the performance of different DEMs can introduce an element of uncertainty into the results. Pinel *et al*., (2015) criticised Baugh *et al*., (2013) for assessing their vegetation-removed SRTM using hydrodynamic model simulations. This is because although a model attempts to simulate the real world, it is not an exact representation, and therefore using a model to assess the performance of a dataset can introduce further uncertainty

(Pinel *et al*., 2015). As a result, many studies have assessed error within the DEM specifically (e.g. O'Loughlin *et al*., 2016; Hirt *et al*., 2018). Assessing vertical error within the DEM would allow one to determine the overall error of each TanDEM-X DTM in comparison to SRTM and MERIT against the LiDAR DEM. However, as one of the key aims of this thesis was to determine whether TanDEM-X can be used to improve estimates of flood hazard in SIDS, it was necessary to assess the different DTM performance within the hydrodynamic model, as this is the primary way flood hazard is assessed.

Regarding the TanDEM-X DTMs, one error likely introduced through manipulation of the data is during the interpolation of the 'bare earth' pixels to create a DTM surface. This is because interpolation assigns pixel values using the available data based on a set of parameters, and thus the resulting pixels are largely dependent on the quality of original data and the parameter selection (Weschler, 2007; Meng *et al*., 2010). Interpolation can also result in 'smoothness artefact' as identified by Hirt (2018), whereby the output DEM is over-smoothed in comparison to actual terrain. Nonetheless, little research has actively compared how interpolation affects an output DEM (Weschler, 2007), and thus the error is difficult to quantify. Results comparing interpolation methods used to create LiDAR surfaces by Bater and Coops (2009) suggest that there is little difference between interpolation methods when comparing RMSE of output DEMs, although natural neighbour interpolation was favoured due to its easy application and visual appearance of the results. IDW interpolation was specifically chosen for this thesis based on other studies that have created DTMs using Intermediate-TanDEM-X data (Geiß *et al*., 2015, Schreyer *et al*., 2016). Further research should be conducted into the specific error characteristics introduced to the TanDEM-X DTMs by different interpolation methods to determine the most suitable interpolation method for use on the TanDEM-X data.

Interpolation would not be necessary if vegetation heights could be removed from the elevation heights in the unprocessed TanDEM-X DSM, as is characteristic of methods used to remove vegetation from the SRTM (e.g. Coe *et al*., 2008, Paiva *et al*., 2011; Baugh *et al*., 2013). However, in the absence of vegetation height maps that are of high enough spatial resolution (<12m) to identify small patches of vegetation present in the TanDEM-X, this methodology is unlikely to remove all vegetation from the TanDEM-X data. The ~50m resolution Global Forest/Non-Forest Map detailed by Martone *et al*., (2018) may be suitable to remove large patches of vegetation from the TanDEM-X, and thus research should be conducted using this dataset when it is available to determine whether this method of vegetation-removal is suitable for TanDEM-X.

4.2 Recommendations for Further Work

The two main aims of this thesis were to determine whether the TanDEM-X DEM could be used to improve flood hazard estimates in SIDS - specifically focusing on the Ba catchment in Fiji – and to develop and test a method to suitably process the TanDEM-X DSM to a DTM for input into hydrodynamic model LISFLOOD-FP. The results demonstrated that when the DTM method combining Image Classification of the Amplitude map and Progressive Morphological Filtering was utilised to create a DTM, flood estimates were greatly improved over all other tested DSMs and DTMs in comparison to the LiDAR benchmark. Thus, the impetus should now focus on applying this method to other test sites in SIDS to determine whether similar results are obtained. This will better allow one to determine whether TanDEM-X has the capacity to improve flood hazard estimates across SIDS generally. It is expected that the results will be replicable in other catchments, as the study site selected in this thesis was specifically chosen to be a representative site for many agricultural catchments in SIDS. Alternative validation data sources such as ground truth information and Synthetic Aperture Radar images of flood extents should be utilised where possible to validate the results of the flood hazard simulation, although it is acknowledged that these data are rarely available in SIDS.

Further work should also be conducted to determine how building artefacts can be removed from the unprocessed TanDEM-X DSM, as vegetation removal in isolation may not be sufficient to produce a DTM, especially for flood model applications in urban areas whereby buildings will be more pronounced than the agricultural floodplain in this study site. It is likely that the methods described in Chapter 3 do remove some building artefacts, as the Progressive Morphological Filter is used to remove buildings from LiDAR and Intermediate-TanDEM-X data in Zhang *et al*., (2003) and Geiß *et al*., (2015). The image classification may have misclassified buildings as vegetation depending on the similarity of interferometric coherence and amplitude values, and thus this should also be investigated. This will likely be necessary for TanDEM-X to be applicable in urban catchments, as currently SRTM and MERIT are unable to provide enough detail to adequately model urban catchments (Yan *et al*., 2015).

Although the focus on flood hazard has dominated within this thesis, it is vital to reiterate the importance of considering flood risk as a function of hazard, exposure and vulnerability (UNISDR, 2015a). Beyond this thesis, research should also focus on the application of datasets providing better-resolved and more detailed estimates of exposure and vulnerability. This will be paramount to improve flood risk estimates alongside flood hazard. Global, low-cost datasets on exposure and vulnerability are necessary for SIDS applications and must provide a high-enough resolution to provide detailed estimates suitable for the small scale of SIDS. Only then will there be an improved capacity for policy makers to produce a detailed and holistic estimate of flood risk in SIDS.

References

Abrams, M., 2016, *ASTER Global DEM Version 3, and New ASTER Water Body Dataset,* ISPRS-International Archives of the Photogrammetry, Remote Sensing and Spatial Information Sciences, Prague, Czech Republic, 107-110

Adger, N.W., 2006, 'Vulnerability', *Global Environmental Change*, vol. 16, 268-281

Airbus, 2019, *WorldDEM™ - The New Standard of Global Elevation Models*, Airbus, https://www.intelligence-airbusds.com/elevation-models/#worlddem (accessed 30th January 2019)

Albert, S., Abernethy, K., Gibbes, B., Grinham, A., Tooler, N., Aswani, S., 2013, 'Cost-effective methods for accurate determination of sea level rise vulnerability: A Solomon Islands example', *Weather Climate and Society*, vol. 5, no. 4, 285-292

Alfieri, L., Bisselink, B., Dottori, F., Naumann, G., de Roo, A., Salamon, P., Wyser, K., Feyen, L., 2017, 'Global projections of river flood risk in a warmer world', *Earth's Future*, vol. 5, no. 2, 171-182

Apel, H., Aronica, G.T., Kreibich, H., Thieken, A.H., 2009, 'Flood risk analyses – how detailed do we need to be?', *Natural Hazards*, vol. 49, no. 1, 79-98

Arino, O., Ramoino, F., 2017, *Land Cover CCI Product User Guide Version 2.0*, http://maps.elie.ucl.ac.be/CCI/viewer/download/ESACCI-LC-Ph2-PUGv2_2.0.pdf (Accessed 4th June, 2018)

Arrell, K., Wise, S., Wood, J., Donoghue, D., 2008, 'Spectral filtering as a method of visualising and removing striping artefacts in digital elevation data', *Earth Surface Processes and Landforms*, vol. 33, no. 6, 943-961

Baade, J., Schmillius, C., 2016, 'TanDEM-X IDEM precision and accuracy assessment based on a large assembly of differential GNSS measurements in Kruger National Park, South Africa', *ISPRS Journal of Photogrammetry and Remote Sensing*, vol. 119, 496-508

Baltsavias, E.P., 1999, 'Airborne laser scanning: Basic relations and formulas', *ISRPRS J Photogramm*, vol. 54, 199-214

Bannari, A., Kadhem, G., Hameid, N., El-Battay, A., 2017, 'Small island DEMS and topographic attributes analysis: A comparative study among SRTM-V4.1, ASTER-V2.1, high topographic contours maps and DGPS', *Journal of Earth Science and Engineering*, vol. 7, 90-119

Barnes, R., Legman, C., Mulla, D., 2014, 'Priority-flood: An optimal depression-filling and watershed-labeling algorithm for digital elevation models', *Computers and Geosciences,* vol. 62, 117-127

Barnett, J., 2001, 'Adapting to climate change in Pacific Island countries: The problem of uncertainty', *World Development*, vol. 29, no. 6, 977-993

Barnett, J., Adger, N., 2003, 'Climate Dangers and Atoll Countries', *Climatic Change*, vol. 61, 321-337

Bates, P.D., 2004, 'Remote sensing and flood inundation modelling', *Hydrological Processes*, vol. 18, 2593–2597

Bates, P.D., 2012, 'Integrating remote sensing data with flood inundation models: How far have we got?' *Hydrological Processes*, vol. 26, no. 16, 2515-2521

Bates, P.D., De Roo*, A.P.J.,* 2000*,* 'A simple raster-based model for flood inundation simulation', *Journal of Hydrology*, vol. 236, no. 1-2, 54-77

Bates, P.D., Horritt, M.S., Fewtrell, J.T., 2010, 'A simple inertial formulation of the shallow water equations for efficient two-dimensional flood inundation modelling', *Journal of Hydrology*, vol. 387, no. 1–2, 33-45

Bates, P.D., Horritt, M.S., Hunter, N.M., Mason, D., Cobby, D., 2005, 'Numerical modelling of floodplain flow', In: Bates, P.D., Lane, S.N., Ferguson, R.I., (eds.), *Computational Fluid Dynamics: Applications in Environmental Hydraulics*, John Wiley and Sons, Chichester, 271-304

Bates, P.D., Neal, J.C., Alsdorf, D.E., Schumann, G.J.P., 2014, 'Observing global surface water flood dynamics', *Surveys in Geophysics*, vol. 35, no. 3, 839-852

Bates, P.D., Stewart, M.D., Desitter, A., Anderson, M.G., Renaud, J.-P., Smith, J.A., 2000, 'Numerical simulation of floodplain hydrology', *Water Resources Research*, vol. 36, 2517-2530

Bates, P.D., Trigg, M., Neal, J., Dabrowa, A., 2013, *LISFLOOD-FP User Manual: Version 2.0*, University of Bristol, Bristol

Bates, P.D., Wilson, M.D., Horritt, M.S., Mason, D.C., Holden, N., Currie, A., 2006, 'Reach scale floodplain inundation dynamics observed using airborne synthetic aperture radar imagery: Data analysis and modelling', *Journal of Hydrology*, vol. 328, no. 1–2, 306–318

Bater, C., Coops, N.C., 2009, 'Evaluating error associated with lidar-derived DEM interpolation', Computers and Geosciences, vol. 35, no. 2, 289-300

Baugh, C.A., Bates, P.D., Schumann, G., Trigg, M.A., 2013, 'STRM vegetation removal and hydrodynamic modeling accuracy', *Water Resources Research*, vol. 49, no. 9, 5276-5289

Berry, P.A.M., Garlick, J. D., Smith, R.G., 2007, 'Near-global validation of the SRTM DEM using satellite radar altimetry', *Remote Sensing and the Environment*, vol. 106, no. 1, 17–27

Bettencourt, S., Croad, R., Freeman, P., Hay, J., Jones, R., King, P., Lal, P., et al., 2006, *Not if but When: Adapting to Natural Hazards in the Pacific Islands Region,* World Bank, Washington DC, USA

Blaikie, P., Cannon, T., Davis, I., Wisner, B., 1994, *At Risk. Natural Hazards, People's Vulnerability and Disasters*, Routledge, London

Blöschl, G., Sivapalan, M., Wagener, T., Viglione, A., Savenije, H., (eds.), 2013, *Runoff Prediction in Ungauged Basins: Synthesis Across Processes, Places and Scales*, Cambridge University Press, Cambridge, United Kingdom

Borla-Tridon, D., Bachmann, M., Martone, M., Schulze, D., Zink, M., 2016, *The Future of TanDEM-X: Final DEM and Beyond,* Proc. of the European Conference on Synthetic Aperture Radar, Hamburg, Germany

Breidenbach, J., Ortiz, S., Reich, M., 2010, 'Forest monitoring with TerraSAR-X: First results', *European Journal of Forest Research*, vol. 129, 813-823

Briguglio, L., 1995, 'Small island developing states and their economic vulnerabilities', *World Development,* vol. 23, no. 9, 1615-1632

Brooks, N., 2003, *Vulnerability, risk and adaptation: A conceptual framework*, Tyndall Centre for Climate Change Research: Working Paper 38, Norwich, UK

Brown, C.G., Sarabandi, K., Pierce, L.E., 2010, 'Model-based estimation of forest canopy height in Red and Austrian Pine stands using Shuttle Radar Topography Mission and ancillary data: A proof-of-concept study', *IEEE Transactions on Geosciences and Remote Sensing*, vol. 48, no. 3, 1105-1118

Brown, P., Daigneault, A., Gawith, D., 2014, 'Climate change and the economic impacts of flooding on Fiji', *Climate and Development*, vol. 9, no. 6, 493-504

Buchele, B., Kreibich, H., Kron, A., Thieken, A., Ihringer, J., Oberle, P., Merz, B., Nestmann, F., 2006, 'Flood-risk mapping: contributions towards an enhanced assessment of extreme events and associated risks', *Nat. Hazards Earth Syst. Sci.,* vol. 6, 485–503

Bündis Entwicklung Hilft, 2017, *Indicators for the WorldRiskIndex*, Bündis Entwicklung Hilft, http://weltrisikobericht.de/wp-content/uploads/2017/11/Indicators-WorldRiskIndex.pdf (accessed 28th February, 2018)

Burn, D.H., 1990, 'An appraisal of the "region of influence" approach to flood frequency analysis', *Hydrological Sciences Journal*, vol. 35, 149-165

Callow, J.N., Van Niel, K.P., Boggs, G.S., 2007, 'How does modifying a DEM to reflect known hydrology affect subsequent terrain analysis?', *Journal of Hydrology*, vol. 332, no. 1-2, 30-39

Canty, M.J., 2014, *Image Analysis*, *Classification and Change Detection in Remote Sensing: With Algorithms for ENVI/IDL* (3rd ed.), CRC Press, Florida, USA

Cardona, O.D., van Aalst, M.K., Birkmann, J., Fordham, M., McGregor, G., Perez, R., Pulwarty, R.S., Schipper, E.L.F., Sinh, B.T., 2012, 'Determinants of risk: exposure and vulnerability' In: Intergovernmental Panel on Climate Change (eds.), *Managing the Risks of Extreme Events and Disasters to Advance Climate Change Adaptation. A Special Report of Working Groups I and II of the Intergovernmental Panel on Climate Change (IPCC),* Cambridge University Press, Cambridge, UK, 65-108

Carlisle, B.H., 2005, 'Modelling the spatial distribution of DEM error', *Transactions in GIS*, vol. 9, no. 4, 521-540

Castellarin, A., Di Baldassarre, G., Bates, P.D., Brath, A., 2009, 'Optimal cross-sectional spacing in Preissmann scheme 1D hydrodynamic models', *ASCE Journal of Hydraulic Engineering*, vol. 135, no. 2, 96-105

Chandler, R.E., Isham, V.S., Northrop, P.J., Wheater, H.S., Onof, C.J., Leith, N.A., 2014, 'Uncertainties in Rainfall Inputs', In: Beven, K., Hall, J., (eds.), 2014, *Applied Uncertainty Analysis for Flood Risk Analysis*, Imperial College Press, London, 101-152

Chen, Q., Gong, P., Baldocchi, D., Xin, G., 2007, 'Filtering airborne laser scanning data with morphological methods', *Photogrammetric Engineering and Remote Sensing*, vol. 73, no. 2, 175-185

Chirico, P.G., 2004, An Evaluation of SRTM, ASTER and Contour-Based DEMs in the Caribbean Region, Proceedings of the URISA 2nd Caribbean GIS Conference, Barbados, Caribbean, 209-219

Cisneros, J.B.E., Oki, T., Arnell, N.W., Benito, G., Cogley, J.G., Döll, P., Jiang, T., Mwakalila, S.S., 2014, 'Freshwater resources' In: Intergovernmental Panel on Climate Change (eds.)*, Climate Change 2014:*

Impacts, Adaptation, and Vulnerability. Part A: Global and Sectoral Aspects. Contribution of Working Group II to the Fifth Assessment Report of the Intergovernmental Panel on Climate Change, Cambridge University Press, Cambridge, United Kingdom, 229-269

Cobby, D.M., Mason, D.C., Davenport, I.J., 2001, 'Image processing of airborne scanning laser altimetry for improved river flood modelling', *ISPRS Journal of Photogrammetry and Remote Sensing,* vol. 56, no. 2, 121-138

Coe, M.T., Costa, M.H., Howard, E.A., 2008, 'Simulating the surface waters of the Amazon River basin: Impacts of new river geomorphic and flow parameterizations', *Hydrological Processes*, vol. 22, no. 14, 2542–2553

Congalton, R.G., 1991, 'A review of assessing the accuracy of classifications of remotely sensed data', *Remote Sensing of Environment*, vol. 37, no. 1, 35-46

Cunge, J.A., Holly, F.M., Verwey A., 1980, *Practical Aspects of Computational River Hydraulics*, Pitman Publishing, London

Cutter, S.L., 1996, Vulnerability to environmental hazards', *Progress in Human Geography*, vol. 20, no. 4, 529-539

Cutter, S.L., Boruff, B.J., Shirley, W.L., 2003, 'Social vulnerability to environmental hazards', *Social Science Quarterly*, vol. 84, no. 2, 242-261

Dalrymple, T., 1960, *Flood Frequency Analysis: Water Supply Paper 1543A*, US Geological Survey, Virginia, United States

Department of the Environment, Transport and the Regions (DETR), 2000, *Guidelines for Environmental Risk Assessment and Management*, Department of the Environment, Transport and the Regions, London, United Kingdom

Di Baldassarre, G., Schumann, G., Bates, P.D., 2009, 'Near real time satellite imagery to support and verify timely flood modelling', *Hydrological Processes*, vol. 23, 799-803

Di Baldassarre, G., Uhlenbrook, S., 2012, 'Is the current flood of data enough? A treatise on research needs for the improvement of flood modelling', *Hydrological Processes*, vol. 26, no. 1, 153-158

DLR (German Aerospace Center), 2018, *Global 3D Elevation Model from the TanDEM-X Mission Now Freely Available*, DLR, https://www.dlr.de/dlr/en/desktopdefault.aspx/tabid-10081/151_read-30139/#/gallery/32238 (accessed 18th October, 2018)

Eckstein, D., Kunzel, V., Schafer, L., 2017, *Global Climate Risk Index 2018: Who Suffers most from Extreme Weather Events? Weather-related Loss Events in 2016 and 1997 to 2016*, Germanwatch, Bonn, Germany

Egorova R., Van Noortwuk, J.M., Holterman, S.R., 2008, 'Uncertainty in flood damage estimation', *Int. J. River Basin Management*, vol. 6, no. 2, 139–148

European Union, 2017, *The EU Floods Directive: Requirements of the Directive,* European Union, http://ec.europa.eu/environment/water/flood_risk/implem.htm (accessed 2nd February, 2018)

Fabris, M., Pesci, A., 2005, 'Automated DEM extraction in digital aerial photogrammetry: Precisions and validation for mass movement monitoring', *Annals of Geophysics*, vol. 48, no. 6, 973-988

Falorni, G., Teles, V., Vivoni, E.R., Bras, R.L., Amaratunga, K.S., 2005, 'Analysis and characterization of the vertical accuracy of Digital Elevation Models from the Shuttle Radar Topography Mission', *Journal of Geophysical Research: Earth Surfaces*, vol. 112, no. F2

Farr, T.G., Caro, E., Crippen, R., Duren, R., Hensley, S., Kobrick, M., Paller, M., Rodriguez, E., Rosen, P., Roth, L., Seal, D., Shaffer, S., Shimada, J., Umland, J., Werner, M., Burbank, D., Oskin, M., Alsdorf, D., 2007, 'The Shuttle Radar Topography Mission', *Reviews of Geophysics*, vol. 45, no. 2, 1-33

Fernández, A., Najafi, M.R., Durand, M., Mark, B.G., Moritz, M., Jung, H.C., Neal, J.C., Shastry, A., Laborde, S., Phang, S.C., Hamilton, I.M., Xiao, N., 2016, 'Testing the skill of numerical hydraulic modelling to simulate spatiotemporal flooding patterns in the Logone floodplain, Cameroon', *Journal of Hydrology,* vol. 539, 265-280

Ferretti, A., Prati, C., Rocca, F., 2000, 'Nonlinear subsidence rate estimation using permanent scatterers in differential SAR interferometry', *IEEE Transactions on Geosciences and Remote Sensing*, vol. 38, 2202-2212

Fisher, P.F., Tate, N., 2006, 'Causes and consequences of error in digital elevation models', *Progress in Physical Geography*, vol. 30, no. 4, 467-489

French, J.R., 2003, 'Airborne LiDAR in support of geomorphological and hydraulic modelling', *Earth Surface Processes and Landforms,* vol. 28, no. 3, 321–335

Fujisada, H., Urai, M., Iwasaki, A., 2012, 'Technical Methodology for ASTER Global DEM', *IEEE Trans. Geosci. Remote Sens*, vol. 50, 3725–3736

Füssell, H-M., Klein, R.J.T., 2006, 'Climate change vulnerability assessments: An evolution of conceptual thinking', *Climatic Change*, vol. 75, 301-329

Gallant, 2011, 'Adaptive Smoothing for noisy DEMs', *Proc. Geomorphometry*, vol. 33, 7-9

Gallant, J., Read, A., Dowling, T., 2012, 'Removal of tree offsets from SRTM and other digital surface models', *The International Archives of the Photogrammetry, Remote Sensing and Spatial Information Sciences*, vol. 1, 275-280

Geiß, C., Wurm, M., Breunig, M., Felbier, A., Taubenböck, H., 2015, 'Normalization of TanDEM-X DSM data in urban environments with morphological filters', *IEEE Trans. Geosci. Remote Sens.,* vol. 53, no. 8, 4348–4362

Gesch, D.B., 2009, 'Analysis of Lidar elevation data for improved identification and delineation of lands vulnerable to sea-level rise', *Journal of Coastal Research: Special Issue*, vol. 53 49 – 58

Government of Fiji, 2016, *Post-Disaster Needs Assessment: Tropical Cyclone Winston*, Government of Fiji, Suva, Fiji

Government of Fiji, 2017, *Climate Vulnerability Assessment: Making Fiji Climate Resilient*, Government of Fiji, Suva, Fiji

Grimaldi, S., Nardi, F., Di Benedetto, F., Istanbulluoglu, E., Bras, R.L., 2007, 'A physically-based method for removing pits in digital elevation models', *Advances in Water Resources*, vol. 30, 2151-2158

Gruber, A., Wessel, B., Huber, M., Breunig, M., Wagenbrenner, S., Roth, A., 2012, *Quality Assessment of First TanDEM-X DEMs for Different Terrain Types*, 9th European Conference on Synthetic Aperture Radar Program, Nuremburg, Germany

Guha-Sapir, D., Hoyois, P.H., Wallemacq, P., Below, R., 2017, *Annual Disaster Statistical Review 2016; The Numbers and Trends*, Centre for the Research on the Epidemiology of Disasters (CRED), Brussels, Belgium

Gupta, V.K., Mesa, O.J., Dawdy, D.R., 1994, 'Multiscaling theory of flood peaks: Regional quantile analysis', *Water Resources Research*, vol. 30, 3405-3421

Hallegatte, St., Bangalore, M., Bonzanigo, L., Fay, M., Kane, T., Narloch, U., Rozenberg, J., Treguer, D., Vogt-Schilb, A., 2016, *Shock Waves: Managing the Impacts of Climate Change on Poverty. Climate Change and Development Series*, World Bank, Washington DC, USA

Hansen, M.C., Potapov, P.V., Moore, R., Hancher, M., Turubanova, S.A., Tyukavina, A., Thau, D., Stehman, S.V., Goetz, S.J., Loveland, T.R., Kommareddy, A., Egorov, A., Chini, L., C.O., Justice, J.R.G., Townshend, 2013, 'High-resolution global maps of 21st-century forest cover change', *Science*, vol. 342, no. 6160, 850-853

Harding, D.J., Lefsky, M.A., Parker, G.G., Blair, J.B., 2001, 'Laser altimeter canopy height profiles: Methods and validation for closed-canopy, broadleaf forests', Remote Sensing of Environment, vol. 76, no. 3, 283-297

Hay, J.E., Mimura, N., 2013, 'Vulnerability, risk and adaptation assessment methods in the Pacific Islands region: Past approaches and considerations for the future', *Sustain Sci*, vol. 8, 391-405

Hirt, C., 2018, 'Artefact detection in global digital elevation models (DEMs): The maximum slope approach and its application for complete screening of the SRTM v4.1 and MERIT DEMs', *Remote Sensing of Environment*, vol. 207, 27-41

Hirt, C., Filmer, M. S., Featherstone, W.E., 2010, 'Comparison and validation of the recent freely available ASTER-GDEM ver1, SRTM ver4.1 and GEODATA DEM-9S ver3 digital elevation models over Australia', *Aust. J. Earth Sci*. vol. 57, 337–347

Hofton, M., Dubayah, R., Blair, J.B., Rabine, D., 2006, 'Validation of SRTM elevations over vegetated and non-vegetated terrain using medium footprint lidar', *Photogrammetric Engineering and Remote Sensing*, vol. 72, no. 3, 279-285

Hohle, J., 2009, 'DEM generation using a digital large format frame camera', *Photogrammetric Engineering and Remote Sensing*, vol. 75, no. 1, 87-93

Holland, P., 2014, *Economic dimensions of improved meteorological services in the Pacific*, South Pacific Community, Suva, Fiji

Horritt, M.S., Bates, P.D., 2001, 'Effects of spatial resolution on a raster based model of flood flow', *Journal of Hydrology*, vol. 253, 239-249

Horritt, M.S., Bates, P.D., 2002, 'Evaluation of 1-D and 2-D numerical models for predicting river flood inundation', *Journal of Hydrology*, vol. 268, 87-99

Hunter, N.M., Bates, P.D., Horritt, M.S., Wilson, M.D., 2007, 'Simple spatially-distributed models for predicting flood inundation: A review', *Geomorphology*, vol. 90, 208-225

Hunter, N.M., Bates, P.D., Neelz, S., Pender, G., Villanueva, I., Wright, N.G., Liang, D., Falconer, R.A., Lin, B., Waller, S., Crossley, A.J., Mason, D.C., 2008, 'Benchmarking 2D hydraulic models for urban flooding', *Water Management*, vol. 161, no. WM1, 13-30

Ingham, D.B., Ma, L., 2005, 'Fundamental equations for CFD in river flow simulations', In: Bates, P.D., Lane, S.N., Ferguson, R.I., (eds.), *Computational Fluid Dynamics: Applications in Environmental Hydraulics*, John Wiley and Sons, Chichester, 19-50

Intergovernmental Panel on Climate Change (IPCC), 2012, 'Summary for Policymakers', In: Intergovernmental Panel on Climate Change (eds.), *Managing the Risks of Extreme Events and Disasters to Advance Climate Change Adaptation. A Special Report of Working Groups I and II of the Intergovernmental Panel on Climate Change*, Cambridge University Press, Cambridge, UK, 1-19

Jarihani, A.A., Callow, J.N., McVicar, T.R., Van Niel, T.G., Larsen, J.R., 2015, 'Satellite-derived Digital Elevation Model (DEM) selection, preparation and correction for hydrodynamic modelling in large, low-gradient and data-sparse catchments', *Journal of Hydrology*, vol. 524, 489–506

Jarvis, A., Rubiano, J., Nelson, A., Farrow, A., Mulligan, M., 2004, *Practical use of SRTM data in the tropics: Comparisons with digital elevation models generated from cartographic data*, Centro Internacional de Agricultura Tropical, Cali, Colombia

Jarvis, A., Reuter, H.I., Nelson, E., Guevara, E., 2008, *Hole-filled SRTM for the globe. Version 4.* CGIAR-CSI Database, http://srtm.csi.cgiar.org (Accessed 3rd October 2017)

Jenson, S.K., Domingue, J.O., 1988, 'Extracting topographic structure from digital elevation data for geographic information systems analysis', *Photogrammetric Engineering and Remote Sensing*, vol. 54, no. 11, 1593-1600

Jing, C., Shortridge, A., Lin, S., Wu, J., 2013, 'Comparison and validation of SRTM and ASTER GDEM for a subtropical landscape in Southeastern China', *Int. J. Digit. Earth,* vol. 7, 969–992

Jonkman, S.N., van Gelder, P.H.A.J.M., Vrijling, J.K., 2003, 'An overview of quantitative risk measures for loss of life and economic damage', *Journal of Hazardous Materials*, vol. 99, no. 1, 1-30

Jonkman, S.N., Bockarjova, M., Kok, M., Bernardini, P., 2008, 'Integrated hydrodynamic and economic modelling of flood damage in the Netherlands', *Ecol. Econ.,* 66, 77–90

Julca, A., Paddison, O., 2010, 'Vulnerabilities and migration in Small Island Developing States in the context of climate change', *Natural Hazards*, vol. 55, no. 3, 717–728

Kellndorfer, J., Walker, W., Pierce, L., Dobson, C., Fites, J.A., Hunsaker, C., Vona, J., Clutter, M., 2004, 'Vegetation height estimation from Shuttle Radar Topography Mission and national elevation data sets', *Remote Sensing of Environment*, vol. 93, no. 3, 339-358

Kenyi, L.W., Dubayah, R., Hofton, M., Schardt, M., 2009, 'Comparative analysis of SRTM-NED vegetation canopy height to LiDAR-derived vegetation canopy metrics', *International Journal of Remote Sensing,* vol. 30, no. 11, 2797-2811

Komi, K., Neal, J.C., Trigg, M.A., Diekkruger, B., 2017, 'Modelling of flood hazard extent in data sparse areas: A case study of the Oti River basin, West Africa', *Journal of Hydrology: Regional Studies*, vol. 10, 122-132

Kraus, K., Pfeifer, N., 1998, 'Determination of terrain models in wooded areas with airborne laser scanner data', *ISPRS Journal of Photogrammetry and Remote Sensing*, vol. 53, no. 4, 193-203

Krieger, G., Moreira, A., Fiedler, H., Hajnsek, I., Werner, M., Younis, M., Zink, M., Krieger, G., Moreira, A., Fiedler, H., Hajnsek, I., Werner, M., Younis, M., Zink, M., 2007, 'TanDEM-X: A satellite formation for high-resolution SAR Interferometry', *IEEE Transactions on Geoscience and Remote Sensing*, vol. 45, 3317–3341

Kron, W., 2005, 'Flood Risk = Hazard • Values • Vulnerability', *Water International*, vol. 30, no.1, 58-68

Laaha, G., Blöschl, G., 2006, 'A comparison of low flow regionalisation methods – catchment grouping', *Journal of Hydrology*, vol. 323, 193-214

LaLonde, T., Shortridge, A., Messina, J., 2010, 'The influence of land cover on Shuttle Radar Topography Mission (SRTM) elevations in low-relief areas', *Transactions in GIS*, vol. 14, no. 4

Lane, S.N., 2000, 'The measurement of river channel morphology using digital photogrammetry', *Photogrammetric Record*, vol. 16, no. 96, 937-961

Lane, S.N., Bradbrook, K.F., Richards, K.S., Biron, ., P.A., Roy, A.G., 1999, 'The application of computational fluid dynamics to natural river channels: Three-dimensional versus two-dimensional approaches', *Geomorphology*, vol. 29, no. 1–2, 1-20

Lee, H.S., Younan, N.H., 2003, 'DTM extraction of LiDAR returns via adaptive processing', *IEEE Transactions on Geoscience and Remote Sensing,* vol. 41, no. 9, 2063-2069

Lefsky, M.A., 2010, 'A global forest canopy height map from the Moderate Resolution Imaging Spectroradiometer and Geoscience Laser Altimeter System', *Geophysical Research Letters*, vol. 37, no. 15

Lehner, B., Verdin, K., Jarvis, A., 2008, 'New global hydrography derived from spaceborne elevation data', *EoS Transactions American Geophysical Union*, vol. 89, no. 10, 93-94

Liu, X., 2008, 'Airborne LiDAR for DEM generation: Some critical issues', *Progress in Physical Geography*, vol. 32, no. 1, 31-49

Lohmann, P., Koch, A., Schaeffer, M., 2000, 'Approaches to the filtering of laser scanner data', *International Archives of Photogrammetry and Remote Sensing*, vol. 33, no. B3/1, 540-547

Marks, K., Bates, P.D., 2000, 'Integration of high resolution topographic data with floodplain flow models', *Hydrological Processes*, vol. 14, 2109-2122

Martone, M., Bräutigam, B., Rizzoli, P., Gonzalez, C., Backmann, M., Krieger, G., 2012, 'Coherence evaluation of TanDEM-X interferometric data', *ISPRS Journal of Photogrammetry and Remote Sensing,* vol. 73, 21-29

Martone, M., Rizzoli, P., Wecklich, C., Gonzalez, C., Bueso-Bello, J-L., Valdo, P., Schulze, D., Zink, M., Krieger, G., Moreira, A., 2018, 'The global forest/non-forest map from TanDEM-X interferometric SAR data', *Remote Sensing of Environment*, vol. 205, 352-373

Mason, D.C., Cobby, D.M., Horritt, M.S., Bates, P.D., 2003, 'Floodplain friction parameterisation in two-dimensional river flood models using vegetation heights derived from airborne scanning laser altimetry', *Hydrological Processes*, vol. 17, no. 9, 1711-1732

Mason, D.C., Horritt, M.S., Hunter, N.M., Bates, P.D., 2007, 'Use of fused airborne scanning laser altimetry and digital map data for urban flood modelling', *Hydrological Processes*, vol. 21, 1426-1477

Mason, D.C., Schumann, G., Bates, P.D., 2011, 'Data utilization in flood inundation modelling', In: Pender, G., Faulkner, H., (eds.), *Flood Risk Science and Management*, Wiley-Blackwell, Hoboken, USA, 211-233

Mason, D.C., Garcia-Pintado, J., Cloke, H.L., Dance, S., 2015, 'The potential of flood forecasting using a variable-resolution global Digital Terrain Model and flood extents from Synthetic Aperture Radar images', *Frontiers in Earth Science,* vol. 3, no. 43, 1-14

Mason, D.C., Trigg,M., Garcia-Pintado, J., Cloke, H.L., Neal , J.C. Bates, P.D., 2016, 'Improving the TanDEM-X Digital Elevation Model for flood modelling using flood extents from Synthetic Aperture Radar images', *Remote Sensing of Environment*, vol. 173. 15-28

Mataki, M, Koshy K.C., Lal, M., 2006, 'Baseline climatology of Viti Levu (Fiji) and current climatic trends', *Pacific Science,* vol. 60, 49–68

McAneney, J., van den Honert, R., Yeo, S., 2017, 'Stationarity of major flood frequencies and heights on the Ba River, Fiji, over a 122-year record', *International Journal of Climatology*, vol. 37, 171–178

McGree, S., Yeo, S.W., Devi, S., 2010, 'Flooding in the Fiji Islands between 1840 and 2009', *Risk Frontiers*, Macquirie, Australia

Meigh, J.R., Farquharson, F.A.K., Sutcliffe, J.V., 1997, 'A worldwide comparison of regional flood estimation methods and climate', *Hydrological Sciences Journal*, vol. 42, 225-244

Meng, X., Currit, N., Zhao, K., 2010, 'Ground filtering algorithms for airborne LiDAR data: A review of critical issues', *Remote Sensing*, vol. 2, no. 3, 833-860

Merz, R., Blöschl, G., 2005, 'Flood frequency regionalisation-spatial proximity vs. catchment attributes', *Journal of Hydrology,* vol. 302, 283-306

Merz, B., Hall, J., Disse, M., Schumann, A., 2010a, 'Fluvial flood risk management in a changing world', *Natural Hazards and Earth System Science*s, vol. 10, 509-527

Merz, B., Kreibich, H., Schwarze, R., Thieken, A., 2010b, 'Review article "Assessment of economic flood damage"', *Natural Hazards and Earth System Sciences*, vol. 10, 1697-1724

Mileti, D.S., Gailus, J.L., 2005, 'Sustainable development and hazards mitigation in the United States: Disasters by design revisited', *Mitigation and Adaptation Strategies for Global Change*, vol. 10, 491-504

Montenari, A., 2012, 'Hydrology of the Po River: Looking for changing patterns in river discharge', *Hydrology and Earth System Sciences*, vol. 16, 3737-3747

Moreira, A., 2017, *The Tan-DEM-X Mission: A New Measurement of The Earth's Topography and Much More,* The 18th International Radar Symposium 2017, Prague

Munich Re, 2016, *NatCatSERVICE: Loss events worldwide 1980-2015*, Munich Re, https://www.munichre.com/site/touch-naturalhazards/get/documents_E-

1125431578/mr/assetpool.shared/Documents/5_Touch/_NatCatService/Focus_analyses/Loss_events_worldwide_1980-2015.pdf (accessed 30th November, 2017)

National Aeronautics and Space Administration (NASA), 2017, *NASA Damage Map Aids Puerto Rico Hurricane Response*, National Aeronautics and Space Administration, https://www.nasa.gov/feature/jpl/nasa-damage-map-aids-puerto-rico-hurricane-response (Accessed 1st June, 2018)

Nawai, J., Gusyev, M.A., Hasegawa, A., Takeuchi, K., 2015, *Flood and Drought Assessment with Dam Infrastructure: A Case Study of the Ba River basin, Fiji*, 21st International Congress on Modelling and Simulation, Golden Coast, Australia

Neal, J., Schumann, G., Bates, P., 2012a, 'A subgrid channel model for simulating river hydraulics and floodplain inundation over large and data sparse areas', *Water Resources Research*, vol. 48, no. 11

Neal, J., Villenueva, I., Wright, N., Willis, T., Fewtrell, T.J., Bates, P.D., 2012b, 'How much physical complexity is needed to model flood inundation?', *Hydrological Processes*, vol. 26, no. 15, 2264-2282

Neelz, S., Pender, G., 2013, *Benchmarking the Latest Generation of 2D Hydraulic Modelling Packages*, Environment Agency, Bristol

Nurse, L.A., McLean, R.F., Agard, J., Briguglio, L.P., Duvat-Magnan, V., Pelesikoti, N., Tompkins, E.L., Webb, A., 2014, 'Small islands', In: Intergovernmental Panel on Climate Change (eds.), *Climate Change 2014: Impacts, Adaptation, and Vulnerability. Part B: Regional Aspects. Contribution of Working Group II to the Fifth Assessment Report of the Intergovernmental Panel on Climate Change*, Cambridge University Press, Cambridge, United Kingdom, 1613-1654

O'Loughlin, F.E., Paiva, R.C.D., Durand, M., Alsdorf, D.E., Bates, P.D., 2016, 'A multi-sensor approach towards a global vegetation corrected SRTM DEM product', *Remote Sensing of Environment*, vol. 182, 49-59

Paiva, R.C.D., Collischonn, W., Tucci, C.E.M., 2011, 'Large scale hydrologic and hydrodynamic modeling using limited data and a GIS based approach', *Journal of Hydrology*, vol. 406, no. 3–4, 170–181

Pappenberger, F., Frodsham, K., Beven, K., Romanowicz, R., Matgen, P., 2007, 'Fuzzy set approach to calibrating distributed flood inundation models using remote sensing observations', *Hydrology and Earth System Sciences.*, vol. 11, 739–752

Pelling, M., Uitto, J., 2001, 'Small island developing states: Natural disaster vulnerability and global change', *Environmental Hazards*, vol. 3, no. 2, 49-62

Pickup, G., Warner, R., 1976, 'Effects of hydrologic regime on magnitude and frequency of dominant discharge', *Journal of Hydrology*, vol. 29, no. 1, 51-75

Pinel, S., Bonnet, M-P., Santos Da Silva, J., Moreira, D., Calmant, S., Saté, F., Seyler, F., 2015, 'Correction of interferometric and vegetation biases in the SRTMGL1 spaceborne DEM with hydrological conditioning towards improved hydrodynamics modelling in the Amazon basin', *Remote Sensing*, vol. 7, no. 12, 16108-16130

Pirotti, F., Tarolli, P., 2010, 'Suitability of LiDAR point density and derived landform curvature maps for channel network extraction', *Hydrological Processes*, vol. 24, 1187-1197

Plate, E.J., 2002, 'Flood risk and flood management', *Journal of Hydrology*, vol. 267, no. 1-2, 2-11

Pulighe, G., Fava, F., 2013, 'DEM extraction from archive aerial photos: Accuracy assessment in areas of complex topography', *European Journal of Remote Sensing*, vol. 46, no. 1, 262-278

Rabus, B., Eineder, M., Roth, A., Bamler, R., 2003, 'The Shuttle Radar Topography Mission – A new class of Digital Elevation Models acquired by spaceborne radar', *ISPRS J Photogramm*, vol. 57, 241-262

Radtke, K., Luther, S., Kirch, L., Prütz, R., 2017, 'WorldRiskIndex: A five-year perspective – Risk analysis 2012-2016', In: Bündis Entwicklung Hilft, *World Risk Report: Analysis and Prospects 2017*, Bündis Entwicklung Hilft, Aachen, Germany, 19-29

Raj, R., 2004, *Integrated Flood Management Case Study. Fiji Islands: Flood Management – Rewa River Basin*, WMO-GWP Associated Programme on Flood Management, Stockholm, Sweden

Rao, A.R., Srinivas, V.V., 2006, 'Regionalisation of watersheds by hybrid-cluster analysis', *Journal of Hydrology*, vol. 318, no. 1-4, 37-56

Rathnayake, U.S., Arachchi, S.M.A., 2015, *Flood Modelling in Waidina Tributary, Fiji Islands,* 3rd International Symposium on Advances in Civil and Environmental Engineering, Galle, Sri Lanka

R Core Team, 2018, *R: A Language and Environment for Statistical Computing version 3.5.1*, R Core Team, https://www.r-project.org/ (Accessed 16th September, 2018)

Reed, D., 2002, 'Reinforcing flood-risk estimation', *Philosophical Transactions of the Royal Society of London Part A*, vol. 360, 1373-1387

Rexer, M., Hirt, C., 2014, 'Comparison of free high resolution digital elevation data sets (ASTER GDEM2, SRTM v2.1/v4.1) and validation against accurate heights from the Australian National Gravity Database', *Aust. J. Earth Sci.*, vol. 61, 213–226

Rexer, M., Hirt, C., 2016, 'Evaluation of intermediate TanDEM-X digital elevation data products over Tasmania using other digital elevation models and accurate heights from the Australian National Gravity Database', *Australian Journal of Earth Sciences,* vol. 62, no. 5, 599-609

Richards, J., 1999, *Remote Sensing Digital Image Analysis*, Springer-Verlag, Berlin, Germany, 1-240

Rizzoli, P., Martone, M., Gonzalez, C., Wecklich, C., Borla-Tridon, D., Bräutigam, B., Bachmann, M., Schulze, D., Fritz, T., Huber, M., Wessel, B., Krieger, G., Zink, M., Moreira, A., 2017 'Generation and

performance Assessment of the global TanDEM-X Digital Elevation Model', *ISPRS Journal of Photogrammetry and Remote Sensing,* vol. 132, 119-139

Rodriguez, E., Morris, C.S., Belz, J.E., 2006, 'A global assessment of the SRTM performance', *Photogrammetric Engineering and Remote Sensing.,* vol. 72, no. 3, 249-260

Rosen, P.A., Hensley, S., Joughin, I.R., Li, F., Madsen, S.N., Rodriguez, E., Goldstein, R.N., 2000, 'Synthetic Aperture Radar Interferometry', *Proceedings of the IEEE,* vol. 88, no. 3, 333-382

Saksena, S., Merwade, V., 2015, 'Incorporating the effect of DEM resolution and accuracy for improved flood inundation mapping', *Journal of Hydrology*, vol. 530, 180-194

Salinas, J.L., Laaha, G., Rogger, M., Parajka, J., Viglione, A, Sivapalan, M., Blöschl, G., 2013, 'Comparative assessment of predictions in ungauged basins part 2: Flood and low flow studies', *Hydrology and Earth Systems Sciences*, vol. 17, 2637-2652

Sampson, C.C., Smith, A.M., Bates, P.D., Neal, J.C., Alfieri, L., Freer, J.E., 2015, 'A high-resolution global flood hazard model', *Water Resources Research*, vol. 51, no. 9, 7358-7381

Sampson, C.C., Smith, A.M., Bates, P.D., Neal, J.C., Trigg, M.A., 2016, 'Perspectives on open access high resolution Digital Elevation Models to produce global flood hazard layers', *Frontiers in Earth Science*, vol. 3, no. 85

Sanders, B.F., 2007, 'Evaluation of on-line DEMs for flood inundation modeling', *Adv. Water Resour.*, vol. 30, no. 8, 1831–1843

Savage, J.T.S., Bates, P., Freer, J., Neal, J., Aronica, G., 2016, 'When does spatial resolution become spurious in probabilistic flood inundation predictions', *Hydrological Processes*, vol. 30, no. 13, 2014-2032

Sayers, P.B., Hall, J.W., Meadowcroft, I.C., 2002, 'Towards risk-based flood hazard management in the UK', *Proceedings of ICE*, vol. 150, 36-42

Schlund, M., von Poncet, F., D.H., Hoekmann, Kuntz, S., Schmillius, C., 2014, 'Importance of bistatic SAR features from TanDEM-X for forest mapping and monitoring', *Remote Sensing of Environment*, vol. 151, 16-26

Schreyer, J., Geiß, C., Lakes, T., 2016, 'TanDEM-X for large-area modeling of urban vegetation height: Evidence from Berlin, Germany', *IEEE Journal of Selected Topics in Applied Earth Observations and Remote Sensing*, vol. 9, no. 5, 1876-1887

Schumann, G., Bates, P.D., Horritt, M.S., Matgen, P., Pappenberger, F., 2009, 'Progress in integration of remote sensing-derived flood extent and stage data and hydraulic models', *Reviews of Geophysics*, vol. 47, RG4001

Schumann, G.J.P., Bates, P.D., Neal, J.C., Andreadis, K.M., 2014, 'Technology: Fight floods on a global scale', *Nature*, vol. 507, 169

Schumann, G.J-P., Di Baldassarre, G., Alsdorf, D., Bates, P.D., 2010, 'Near real-time flood wave approximation on large rivers from space: Application to the River Po, Italy', *Water Resources Research*, vol. 46, no. 5, 1-8

Shaw, E.M., Beven, K.J., Chappel, N.A., Lamb, R., 2011, *Hydrology in Practice*, Spon Press, Oxford, United Kingdom

Shimada, M., Itoh, T., Motooka, T., Watanabe, M., Shiraishi, T., Thapa, R., Lucas, R., 2014, 'New global forest/non-forest maps from ALOS PALSAR data (2007-2010)', *Remote Sensing of Environment*, vol. 155, 13-31

Simard, M., Pinto, N., Fisher, J.B., Baccini, A., 2011, 'Mapping forest canopy height globally with spaceborne lidar' *J. Geophys. Res.*, vol. 116, G04021

Sithole, G., 2001, 'Filtering of laser altimetry data using a slope adaptive filter', *International Archives of Photogrammetry, Remote Sensing and Spatial Information Sciences*, vol. 34, no. 3/W4, 203-210

Slater, J.A., Garvey, G., Johnston, C., Haase, J., Heady, B., Kroenung, G., Little, J., 2006, 'The SRTM data "finishing" process and products', *Photogrammetric Engineering and Remote Sensing*, vol. 72, no. 3, 237-247

Smith, K., 2013, *Environmental Hazards. Assessing Risk and Reducing Disasters*, (6th ed.), Routledge, London

Smith, A., Sampson, C., Bates, P., 2015, 'Regional flood frequency analysis at the global scale', *Water Resources Research*, vol. 51, no. 1, 539-553

Smith, M.J., Edwards, E.P., Priestnall, G., Bates, P.D., 2006, 'Exploitation of new data types to create Digital Surface Models for flood inundation modelling', *Advances in Water Resources*, vol. 30, no.8, 1831-1843

Soille, P., Vogt, J.V., Colombo, R., 2003, 'Carving and adaptive drainage enforcement of grid digital elevation models', *Water Resources Research,* vol. 39, no. 12, 1366-1379

Stephens, E., Schumann, G., Bates, P.D., 2014, 'Problems with binary pattern measures for flood model evaluation', *Hydrological Processes*, vol. 28, 4928-4937

Stoesser, T., Wilson, C.A.M.E., Bates, P.D., Dittrich, A., 2003, 'Application of a 3D numerical model to a river with vegetated floodplains', *Journal of Hydroinformatics*, vol. 5, 99-112

SwissRe, 2018, *Sigma 1/2018: Natural Catastrophes and Man-made Disasters in 2017: A Year of Record-Breaking Losses*, SwissRe, Zurich, Switzerland

Tadono, T., Takaku, J., Tsutsui, K., Oda, F., Nagai, H., 2015, *Status of "ALOS World 3D (AW3D)" Global DSM Generation*, IEEE International Geoscience and Remote Sensing Symposium, Milan, Italy

Takeuchi, K., 2001, 'Increasing vulnerability to extreme floods and societal needs of hydrological forecasting', *Hydrological Sciences Journal*, vol. 46, no. 6, 869-881

Tarakegn, Savama, 2013, 'Correction of SRTM DEM artefacts by Fourier transform for flood inundation modeling', *Journal of Japan Society of Civil Engineers B3*, vol. 69, 193-198

Thieken, A.H., Muller, M., Kreibich, H., Merz, B., 2005, 'Flood damage and influencing factors: New insights from the August 2002 flood in Germany' *Water Resour. Res.,* vol. 41, no. 12, W12430

Thomas, B., 2012, *Nadi LiDAR Survey Report for the Secretariat of the South Pacific Community Applied Geoscience and Technology Division (SOPAC),* Network Mapping Aerial Laser Survey, Suva, Fiji

Toutin, T., 2008, 'ASTER DEMs for geomatic and geoscientific applications: A review'*, International Journal of Remote Sensing*, vol. 29, no. 7, 1855-1875

United Nations, 2015, *Small Island Developing States In Numbers: Climate Change Edition 2015*, UN Office of the High Representative of the Least Developed Countries and Small Island Developing States, Geneva

United Nations International Strategy for Disaster Reduction (UNISDR), 2012, *Reducing Vulnerability and Exposure to Disasters: The Asia-Pacific Report 2012*, United Nations International Strategy for Disaster Reduction, Bangkok, Thailand

United Nations International Strategy for Disaster Reduction (UNISDR), 2015a, *Global Assessment Report on Disaster Risk Reduction 2015*, United Nations International Strategy for Disaster Reduction, Geneva, Switzerland

United Nations International Strategy for Disaster Reduction (UNISDR), 2015b, *Sendai Framework for Disaster Risk Reduction 2015-2030*, United Nations International Strategy for Disaster Reduction, Sendai, Japan

United Nations International Strategy for Disaster Reduction (UNISDR), 2017, *Terminology on Disaster Risk Reduction*, United Nations International Strategy for Disaster Reduction, Geneva, Switzerland

United States Department of Agriculture, 1971, 'Section 16: Drainage of Agricultural Land' In: United States Department of Agriculture, 1971, *National Engineering Handbook*, United States Department of Agriculture, Washington DC, United States of America

Vosselman, G., 2000, 'Slope based filtering of laser altimetry data', International Archives of Photogrammetry, Remote Sensing and Spatial Information Sciences, vol. 33, no. B3/2, 935-943

Ward, P.J., Jongman, B., Salamon, P., Simpson, A., Bates, P.D., De Groeve, T., Muis, S., Coughlan de Perez, E., Rudari, R., Trigg, M.A., Winsemius, H.C., 2015, 'Usefulness and limitations of global flood risk models', *Nature Climate Change*, vol. 5, 712-715

Weschler, S.P., 2007, 'Uncertainties associated with digital elevation models for hydrologic applications: A review', *Hydrology and Earth System Sciences*, vol. 11, 1481-1500

Wessel, B., 2016, *TanDEM-X Ground Segment DEM Products Specification Document,* Earth Observation Center, DLR, Oberpfaffenhofen

Wessel, B., Huber, M., Wohlfart, C., Marschalk, U., Kosmann, D., Roth, A., 2018, 'Accuracy assessment of the global TanDEM-X Digital Elevation Model with GPS data', *ISPRS Journal of Photogrammetry and Remote Sensing*, vol. 129, 171-182

Wilson, M.C., Bates, P.D., Alsdorf, D., Forsberg, B., Horrit, M.S., Melack, J., Frappart, F., Famiglietti, J., 2007, 'Modelling large-scale inundation of Amazonian seasonally flooded wetlands', *Geophsyical Research Letters*, vol. 34, L15404

Willis, N.J., 2005, *Bistatic Radar* (2nd ed.), SciTech Publishing Inc, Raleigh, USA

Wise, S., 2000, 'Assessing the quality for hydrological applications of digital elevation models derived from contours', *Hydrological Processes*, vol. 14, 1909-1929

Woodward, D.E., Hoeft, C.C., Humpal, A., Cerrelli, G., 2010, 'Chapter 15: Time of Concentration', In: United States Department of Agriculture, 2010, *Part 630 – Hydrology: National Engineering Handbook*, Washington DC, United States of America

World Bank, 2017, *Enhancing Spatial Data for Flood Risk Management Project*, World Bank, http://projects.worldbank.org/P149629?lang=en (accessed 23rd August, 2018)

Yamazaki, D., Baugh, C.A., Bates, P.D., Kanae, S., Alsdorf, D.E., Oki, T., 2012, 'Adjustment of a spaceborne DEM for use in floodplain hydrodynamic modeling', *Journal of Hydrology*, vol. 436-437, 81-91

Yamazaki, D., O'Loughlin, F., Trigg, M.A., Miller, Z.F., Pavelsky, T., Bates, P.D., 2014, 'Development of the global width database for large rivers', *Water Resources Research*, vol. 50, no. 4, 3467-3480

Yamazaki, D., D. Ikeshima, R. Tawatari, T. Yamaguchi, F. O'Loughlin, J. C. Neal, C. C. Sampson, S. Kanae, and P. D. Bates (2017), A high-accuracy map of global terrain elevations, *Geophysical Research Letters*, vol. 44, 5844–5853

Yan, K., Di Baldassarre, G., Solomatine, D.P., Schumann, G.J.P., 2015, 'A review of low-cost space-borne data for flood modelling: Topography, flood extent and water level', *Hydrological Processes*, vol. 29, no. 15, 3368-3387

Yeo, S., 2015, *Refining the Historical Flood Series for Ba, Fiji*, Risk Frontiers Technical Report, Macquarie University, Australia

Yeo, S.W., Blong, R.J., McAneney, J., 2007, 'Flooding in Fiji: Findings from a 100-year historical series', *Hydrological Sciences*, vol. 52, no. 5, 1004-1015

Zaman, M.A., Rahman, A., Haddad, K., 2012, 'Regional flood frequency analysis in arid regions: A case study for Australia, *Journal of Hydrology*, vol. 475, 74-83

Zebker, H.A., Madsen, S.N., Martin, J., Wheeler, K.B., Miller, T., Lou, Y., Alberti, G., Vetrella, S., Cucci, A., 1992, 'The TOPSAR interferometric Radar Topographic Mapping Instrument," *IEEE Trans. Geosci, Remote Sens*., vol. 30, no. 5, 933-940

Zhang, J., Chen, S.H., Whitmann, D., Shyu, M-L., Zhang, C., 2003, 'A progressive morphological filter for removing non-ground measurements from airborne LIDAR data', *IEEE Transactions on Geoscience and Remote Sensing*, vol. 41, no. 4, 872-882